



## QSIDE

### REPORT

<b>Title</b>	<b>Action 2: Estimation of parameters in the global propagation</b>
<b>Status</b>	<b>Revision 5</b>
<b>Editors</b>	<b>Dick Botteldooren, Weigang Wei</b>
<b>Authors/contributors</b>	<b>Weigang Wei, Maarten Hornikx, Jens Forssén, Dick Botteldooren, Timothy van Renterghem , Mikael Ögren, Erik Salomons</b>
<b>Date</b>	<b>12 aug 2013</b>

### PROJECT

<b>Acronym</b>	QSIDE		
<b>Project title</b>	The positive effects of quiet facades and quiet urban areas on traffic noise annoyance and sleep disturbance		
<b>Project start date</b>	1 September 2010		
<b>Duration of the project</b>	36 months		
<b>Coordinating partner</b>	TNO Delft	TNO	NL
<b>Other partners</b>	Universiteit Gent	UGENT	BE
	Chalmers Teknsika Högskola AB	CUT	SE
	University of Gothenburg	UGOT	SE
	VTI, Statens väg- och transportforskningsinstitut	VTI	SE
	Gemeente Amsterdam	AMS	NL
	City of Gothenburg	GOT	SE



### FUNDING

<b>Funding</b>	Project funded by the European Commission
<b>Funding program</b>	LIFE+ program Environment and Eco-innovation
<b>Project number</b>	LIFE09 ENV/NL/000423





## Contents

1. Engineering model: outline .....	3
2. Validating approximations made in the engineering model.....	5
3. The engineering model without turbulence .....	6
4. Turbulence scattering .....	9
5. Conclusions and future work .....	11
Appendix A .....	
Appendix B .....	
Appendix C .....	
Appendix D .....	
Appendix E .....	

## 1. Engineering model: outline

The focus of QSIDE is on quiet sides and quiet areas. Classical noise mapping primarily aims at mapping the noise level at the most exposed façade of buildings accurately, which is a different focus. The QSIDE engineering model is expected to counter some shortcomings of classical noise mapping models such as ISO 9613, the Dutch “rekenmethode 2” or the French NMPB when it comes to mapping shielded areas: (1) taking into account multiple reflections in street canyons requires a lot of CPU time and is therefore neglected, resulting in reduced accuracy of the noise levels in shielded areas; (2) long distance propagation over urban areas also requires too much CPU time and is therefore neglected, yet it is known that distant sources contribute to the noise level in quiet areas and quiet sides. Therefore Action 2 of QSIDE aims at designing a new engineering noise mapping model.

Prerequisites for the engineering model:

- The model should have a very low computational demand, lower than ISO 9613-2 with multiple reflections.
- The implementation in GIS based software should be kept in mind, that is, it should be avoided to calculate input parameters that cannot easily be obtained, e.g. the length of a street canyon.
- Many noise maps in European cities are already available. Therefore it is important that the proposed model can be used to add information to these maps rather than to replace the models used. A city can then implement its national standard method and add “background level” in shielded areas if needed for a particular application.

With these prerequisites in mind, it was decided to opt for a 2.5D model. For every path connecting source to receiver in a horizontal 2D ray tracing, propagation effects in 2D vertical cross sections are added. Secondly, it was judged advantageous to express all attenuations for point sources in line with the ISO9613-2 method. Line segments are very useful for calculating the direct field but less crucial for determining the diffracted and reflected field in shielded areas.

The suggested procedure for calculating the noise level at the shielded location reads:

$$L_{pb} = L_{pdb} \oplus L_{p,scat}$$

$$L_{pdb} = L_w - A_{free} - A_{diff} - A_{inter}$$

$$A_{diff} = -10 \log_{10} (10^{-A_{bar}/10} + 10^{-A_{can}/10} )$$

where  $\oplus$  is a logarithmic sum and

- $L_{pb}$  = the “background” sound level excluding the diffraction and reflections around the vertical edges and excluding the diffraction over conventional noise barriers [dB].
- $L_{pdb}$  = the contribution to the “background” level in still homogeneous atmosphere [dB].
- $L_w$  = sound power level per octave band of a point source representing part of the road, no directivity is taken into account since multiple sources will contribute to the shielded level as well as multiple reflections from various directions [dB].
- $A_{diff}$  = the total shielding attenuation limited by diffraction over the building roof [dB].
- $A_{free}$  = 3D free field divergence [dB].
- $A_{bar}$  = the attenuation by the building(s) cutting the direct path between source and receiver limited by diffraction over the building roof, including the effect of the ground. Only the direct diffraction path without reflections in the canyon is considered [dB].

$A_{can}$  = the attenuation of the sound following a path between source and receiver including at least one reflection in the source and/or receiver canyon. If canyons are present, this term often is smaller than  $A_{bar}$  and thus determines  $A_{diff}$  [dB].

$A_{inter}$  = additional attenuation caused by the diffraction at intermediate canyons [dB].

$L_{p,scat}$  = the contribution to the background sound level caused by scattering from atmospheric turbulence [dB].

Suitable approximate formulas for the attenuations  $A$  are derived and fitted on an extensive database of detailed FDTD simulations. This implies that the formulas will be applicable only in the range of situations modeled, including the typical façade roughness and impedance, height of the sources and receivers, roof shapes, etc. In **Appendix B** the distribution of width and height of buildings and street canyons are shown for a typical old European city. They are used for constructing the database of FDTD simulations. **Appendix D** shows the façade geometry assumed in the detailed FDTD calculations.

In particular the model is not suitable for thin barriers where “thin” could be defined on the basis of street canyon decoupling as illustrated in **Appendix A**. Classical traffic noise barriers need to be included in the direct sound field calculation.

## 2. Validating approximations made in the engineering model

The proposed improved engineering method for urban areas shielded from direct exposure to traffic noise include terms that account for multiple reflections of the built environment in the source and receiver area. These separate terms,  $A_{\text{can},s}$  and  $A_{\text{can},r}$ , rely on 2D source-receiver propagation calculations using a wave-based acoustic propagation method. In **Appendix A**, the validity of this approach has been investigated. For this purpose, calculations with a wave-based calculation model have been carried out. First, an analysis for 2D configurations was examined. For source-receiver distances exceeding  $2W$ , where  $W$  is the canyon width, results support to split  $A_{\text{can},2D}$  into distance independent terms  $A_{\text{can},s,2D}$  and  $A_{\text{can},r,2D}$ , and additional analytical expressions to account for distance dependence which stem from equivalent free field analogies. Equivalent source and receiver positions for these analogies have been found for various urban configurations. It can also be concluded that, when averaging over various receiver positions in a shielded canyon environment, the terms  $A_{\text{can},s,2D}$  and  $A_{\text{can},r,2D}$  may be used independent from each other for canyon-to-canyon distances exceeding  $2W$ . For shorter distances, the effects of the source and receiver environment should be computed as a single term  $A_{\text{can},2D}$ .

The 2D results are extended by an analysis for a 3D configuration, with a street of infinite length. Conclusions for this 3D configuration are similar as for the 2D configuration, but  $A_{\text{can},s}$  and  $A_{\text{can},r}$  exhibit a stronger distance dependence in 3D and different positions of the equivalent sources and receivers have been found. For source-receiver distances exceeding  $2W$ , and propagation angles normal to street façades, attenuation terms averaged over various receiver positions are very similar in 2D and 3D, supporting the use of 2D calculations. For source-receiver propagation angles deviating from the normal to the axis of the infinitely long street canyon and below  $70^\circ$ ,  $A_{\text{can},s}$  is rather independent on the angle, and the similarity between 2D and 3D attenuation terms may be used here too. For propagation angles exceeding  $70^\circ$ , 2D results start to deviate from the 3D results. Calculations also identify that for wave propagation with oblique incidence to street façades, the edge diffraction calculation assuming that street façades are normal to the source-receiver direction, as common in engineering methods, leads to too low levels. By computing  $A_{\text{can},s}$  and  $A_{\text{can},r}$  based on 2D calculations, this error is not corrected for. Calculations of  $A_{\text{can},s}(\theta)$  for a street with finite length with cross streets shows that its value on average is significantly lower than results from the infinite street configuration. For engineering purposes,  $A_{\text{can},s}$  and  $A_{\text{can},r}$  could therefore be adjusted when calculated from a 2D model. In the proposed model we opted for a 2.5D approach that accounts for finite length of the street canyon in a slightly different way.  $A_{\text{can}}$  is reduced significantly for those source-receiver paths that cut a cross street or canyon opening. Finally,  $A_{\text{can},r}(\theta)$  is investigated for the configuration of a receiver position in a closed courtyard. Results exhibit low angle dependence and it is proposed to use results from a 2D model for all angles in a courtyard situation. The suggested 2.5D model in this configuration would also predict low angle dependence.

When interpreting the feasibility analysis for the proposed approach presented in **Appendix A**, the reader should keep in mind that the QSIDE background noise model is derived for road traffic situations and therefore all sources will be line sources. This averages out many of the angle dependent effects.

### 3. The engineering model without turbulence

**Appendix B** contains a detailed report on the development of expressions for the different terms in the formula for  $L_{pbd}$ . The geometric quantities that need to be extracted for every 2D cross section are defined in Figure 1.

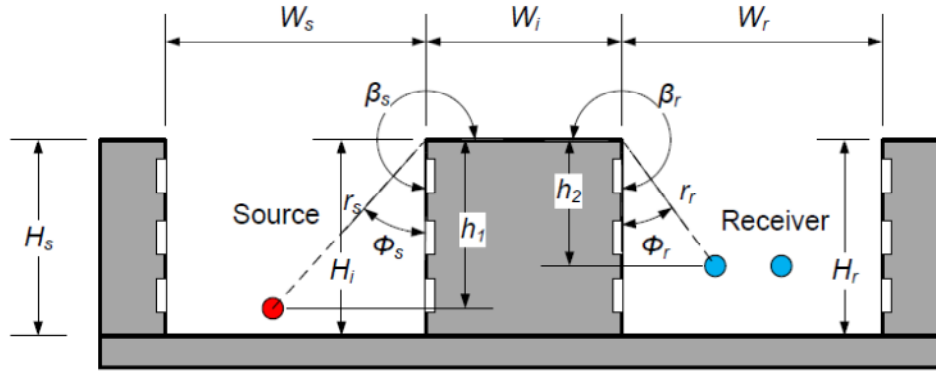


**Figure 1. Definition of the geometrical parameters that need to be extracted for every 2D cross section when applying the model**

The formulas for the different attenuation terms in the engineering model extracted in this appendix read:

For  $A_{bar}$ , several analytic formulas are compared. For simplicity the flat roof attenuation  $A_{bar}^f$  is first considered and afterwards corrected with a tilted roof effect  $A_{bar,roof}$ . The ISO 9613-2 underestimates the effect of thick barriers compared to FDTD simulations. The general theory of diffraction matches FDTD results better but includes Fresnel integrals that are computationally expensive. A simple approximation for these integrals works well for the typical configuration encountered when sound diffracts over a house. In absence of ground and for a flat roof, the approximation reads:

$$A_{bar,0}^f = -10 \log_{10} \left( \frac{0.37}{X_1 + 0.37} \right)^2 \left( \frac{0.37}{X_2 + 0.37} \right)^2$$

where the subscript 0 refers to the direct path without ground reflection and where  $X_1 = Y_s$  and  $X_2 = BY_r$ , when  $Y_s > Y_r$ ;  $X_1 = BY_s$  and  $X_2 = Y_r$ , when  $Y_s < Y_r$ . and  $Y_s$  is defined by (and a similar equation holds for  $Y_r$ )

$$Y_s = \gamma_s M_{vs} (\beta_s - \phi_s)$$

$$\gamma_s = \sqrt{2r_s(r_r + w) / (\lambda L)}$$

$$M_{vs}(\theta) = \frac{\cos(v\pi) - \cos(v\theta)}{v \sin(v\pi)}$$

$L$  is the shortest distance between source and receiver over the buildings,  $W_i$  is the width of the screening building block, and the angles and distances are defined in Figure 1 and **Appendix B**. To account for ground reflections, the contribution of the four image source and image receiver combinations is included. Note that  $A_{bar}^f$  does not contain fitted parameters.

The effect of non-flat roofs is approximated as:

$$A_{bar,roof} = q_0 A_{bar}^f + q_1$$

where  $q_0$  and  $q_1$  are fitting coefficients that can be found in Appendix B.

An analytic approximation for the effects of multiple reflections in canyons is based on explicit summing of contributions of multiple image sources and the requirement that the approximation has suitable limit behavior outside the region of simulated cases. A formula that fits the numerical simulations well is:

$$A_{can}^f \approx -F(0) 10 \log_{10} \left[ \begin{array}{l} F(1) \frac{C_{1s} \alpha^2 R^2}{(C_{3s} + W_s)^2} 10^{0.1L_{hs}} + F(2) \frac{C_{1r} \beta^2 R^2}{(C_{3r} + W_r)^2} 10^{0.1L_{hr}} \\ + F(3) \frac{\alpha^2 \beta^2 R^2}{(3.31h_1/\sqrt{\lambda} + C)(3.31h_2/\sqrt{\lambda} + C)} 10^{0.1L_{hs}} 10^{0.1L_{hr}} \end{array} \right]$$

where

$$C_{1s} = \left( \frac{0.37}{\sqrt{\frac{2r_r}{\lambda} \frac{\sqrt{3}}{2}} \cos \phi_r + 0.37} \right)^2$$

$$C_{3s} = \frac{3.31h_1}{\sqrt{\lambda}} + 0.5W_s + r_r + W_i$$

$$C_{1r} = \left( \frac{0.37}{\sqrt{\frac{2r_s}{\lambda} \frac{\sqrt{3}}{2}} \cos \phi_s + 0.37} \right)^2$$

$$C_{3r} = \frac{3.31h_2}{\sqrt{\lambda}} + 0.5W_r + r_s + W_i$$

$$C = 1.5W_s + W_i + 1.5W_r$$

and  $\alpha$  and  $\beta$  are the equivalent reflection coefficients in the source and receiver canyon respectively.  $F(0)$ ,  $F(1)$ ,  $F(2)$ , and  $F(3)$  are coefficients obtained by fitting the analytical result on FDTD simulations of canyon to canyon propagation (see **Appendix B** for numerical value). As expected  $F(0)$  is very close to 1. The three terms in the sum reflect propagation including multiple reflections in respectively the source canyon, the receiver canyon, and both canyons.  $R$  is the straight line distance between source and receiver.

$L_{hs}$  and  $L_{hr}$  account for the situation where the source and receiver canyon flanking buildings are smaller than the intermediate building.

$$L_{hs} = \begin{cases} -\infty, & \frac{H_s - h_s}{H_i - h_s} < \frac{1}{3} \\ -6.17 \left( 1 - \frac{H_s - h_s}{H_i - h_s} \right) \left[ 1 - 1.37 \log_{10} \left( \frac{\sqrt{\lambda W_s}}{W_i} \right) \right], & \frac{3}{5} < \frac{H_s - h_s}{H_i - h_s} \leq 1 \\ 1, & \frac{H_s - h_s}{H_i - h_s} > 1 \end{cases}$$

$$L_{hr} = \begin{cases} -\infty, & \frac{H_r - h_r}{H_i - h_r} < \frac{1}{3} \\ -6.17 \left(1 - \frac{H_r - h_r}{H_i - h_r}\right) \left[1 - 1.37 \log_{10} \left(\frac{\sqrt{\lambda W_r}}{W_i}\right)\right], & \frac{3}{5} < \frac{H_r - h_r}{H_i - h_r} \leq 1 \\ 1, & \frac{H_r - h_r}{H_i - h_r} > 1 \end{cases}$$

With  $h_s$  is the source height from the ground;  $h_r$  is the receiver height from the ground.

When  $\frac{1}{3} < \frac{H_s - h_s}{H_i - h_s} \leq \frac{3}{5}$ , only the first image source contributes. In this situation the contribution can be calculated by  $A_{bar}^f$ , with the “source position” being at the first image source on the façade away from the intermittent canyon. Similar case could be applied to the receiver canyon. In a special case,  $H_i = h_r$ , the canyon effect is neglected as well.

Again, the effect of a non-flat roof is included as a correction  $A_{can;roof}$ . This effect depends strongly on the roof shape and the geometrical configuration of the buildings and canyons. In the proposed model,  $A_{can;roof}$  is quantified from literature.  $A_{can;roof} = 5\text{dB}$  if both source and receiver canyons exist;  $A_{can;roof} = 2.5\text{dB}$  if only one canyon exists. Details can be found in **Appendix B**.

Finally an expression for  $A_{inter}$  is suggested. This term is rather strongly dependent on meteorological conditions and will be affected by relative height of intermediate buildings. It still needs further attention but based on typical canyon number, PE calculations, and FDTD simulations, an additional attenuation of 1 dB/100m is suggested but with a limitation to 5 dBA. This approximation should account for mild downward refraction.

**Appendix B** also contains a validation of the resulting engineering model against measurements collected during several months in the city of Gent, Belgium.

## 4. Turbulence scattering

**Appendix C** derives an engineering model for the contribution to the sound level in shielded areas due to scattering of sound by atmospheric turbulence,  $L_{p,scat}$ . In the absence of a canyon, the scattered noise level is approximated as:

$$L_{p,scat,no\ canyon} = L_W - A_{free} + b_1 + b_2 \log_{10} \frac{h}{d_0} + b_3 \log_{10} \left[ \left( \frac{h^2}{d_S d_R} \right) + \varepsilon \right] + \frac{10}{3} \log_{10} \frac{f}{f_0} d$$

where  $b_1$ ,  $b_2$ , and  $b_3$  are fitted coefficients, the reference distance  $d_0=10$  m and the reference frequency  $f_0=1000$  Hz. The quantity  $h$  is the virtual height of the barrier, the orthogonal distance from the crossing of the lines connecting the source and receiver to the barrier edge to the source receiver line,  $d_S$  and  $d_R$  represent the distance from the source and receiver to the virtual barrier measured along the source-receiver line. The small quantity  $\varepsilon$  (0.0012) is added to assure that the scattered field saturates at large distances. See Figure 2 and **Appendix C** for a more detailed definition of these geometrical parameters.

This model is expected to accurately represent the detailed numerical calculations to within a standard deviation of 2 dB.

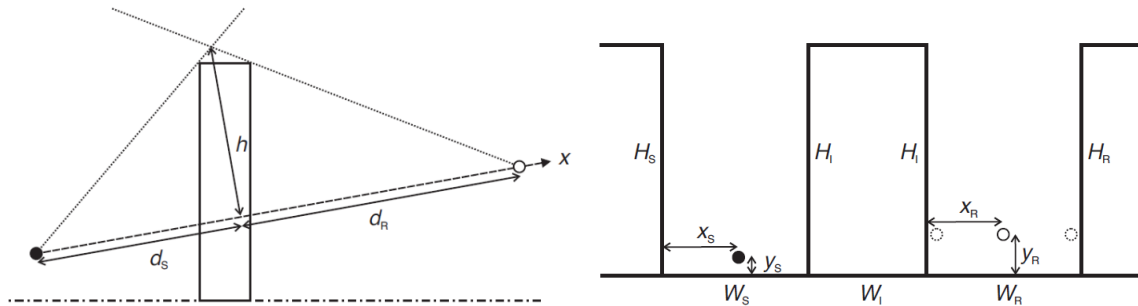


**Figure 2. Definition of the geometrical parameters used in the engineering model used turbulence scattering**

When canyons are present the model is extended with an additional term:

$$L_{p,scat,canyon} = L_{p,scat,no\ canyon} + \Delta L_\gamma$$

where

$$\Delta L_\gamma = \gamma_1 + \gamma_2 \log_{10} \frac{H_I}{H_0},$$

$$\gamma_1 = \begin{cases} 7, & \text{if single canyon} \\ 14, & \text{if double canyon} \end{cases}$$

$$\gamma_2 = \begin{cases} \frac{2H_I}{W_S}, & \text{if single canyon, on source side} \\ \frac{2H_I}{W_R}, & \text{if double canyon, on receiver side} \\ 2H_I(1/W_S + 1/W_R), & \text{if double canyon} \end{cases}$$

and  $H_0 = 10$ m.  $W_S$  and  $W_R$  are the source and receiver canyon widths;  $H_I$  is the height of the intermediate barrier.



This model is expected to accurately represent the detailed numerical calculations to within a standard deviation of 6 dB.

**Appendix E** contains a detailed experimental study on the effect of turbulence on the sound level in the deep shadow zone of a building and validates the proposed engineering model for turbulence scattering for this case.



## 5. Conclusions and future work

An engineering model is presented that allows calculating the noise levels in urban areas shielded from surface traffic sources by at least one row of buildings. This model complements current practice in noise mapping by replacing computationally intensive multiple reflections between buildings by simple formulas. To illustrate the efficiency of the model, we mention that the background levels in a 200 000 person city using a 1 m grid around all the buildings can be calculated within 24h cpu time on a single processor of a modern computer.

The hypotheses behind the proposed model have been tested using 2D and 3D FDTD as well as analytical formulations. Model coefficients were extracted from hundreds of numerically simulated cases. The overall model was validated by comparing the model results to long term (several months) noise measurements at several shielded locations in a typical old European city. Some additional work will be needed to fine tune the engineering model. Intermediate canyon effects need further care particularly with respect to meteorological influences. Future work also includes extending the validation to other cities.



## **Appendix A**

This is the author's version of a manuscript submitted to Acta Acustica united with Acustica

# Urban background noise mapping: the multiple-reflection correction term

Short title: multiple-reflection correction term in noise mapping

Maarten Hornikx<sup>1)</sup>, Jens Forssén<sup>2)</sup>, Dick Botteldooren<sup>3)</sup>, Timothy van Renterghem<sup>3)</sup>, Weigang Wei<sup>3)</sup>, Mikael Ögren<sup>4)</sup> and Erik Salomons<sup>5)</sup>

<sup>1)</sup>Building Physics and Services, Eindhoven University of Technology, P.O. box 513, 5600 MB Eindhoven, the Netherlands. m.c.j.hornikx@tue.nl  
0031-(0)402472297

<sup>2)</sup>Applied Acoustics, Chalmers University of Technology, Göteborg, Sweden.

<sup>3)</sup>Department of Information Technology, Ghent University, Ghent, Belgium

<sup>4)</sup>Department of Environmental and Traffic Analysis, VTI, Gothenburg, Sweden

<sup>5)</sup>TNO Urban Environment and Health, Delft, The Netherlands.

## Abstract

Mapping of road traffic noise in urban areas according to standardized engineering calculation methods systematically results in an underestimation of noise levels at areas shielded from direct exposure to noise, such as inner yards. In most engineering methods, road traffic lanes are represented by point sources and noise levels are computed utilizing point-to-point propagation paths. For a better prediction of noise levels in shielded urban areas, an extension of engineering methods by an attenuation term  $A_{can}$  has been proposed, including multiple reflections of the urban environment both in the source and in the receiver area. The present work has two main contributions for the ease of computing  $A_{can}$ . Firstly, it is shown by numerical calculations that  $A_{can}$  may be divided into independent source and receiver environment terms,  $A_S$  and  $A_R$ . Based on an equivalent free field analogy, the distance dependence of these terms may moreover be expressed analytically. Secondly, an analytical expression is proposed to compute  $A_S$  and  $A_R$  for 3D configurations from using 2D configurations only. The expression includes dependence of the street width-to-height ratio, the difference in building heights and the percentage of façade openings in the horizontal plane. For the expression to be valid, the source should be separated from the receiver environment by at least four times the street width.

## 1 Introduction

According to the European Noise Directive (END) 2002/49/EC, European cities have to produce road traffic noise maps for major roads, railways and airports and exposure distributions based

on noise levels at the façades of dwellings [1]. In addition, the END indicates that cities should quantify how many persons have access to a quiet façade, and that quiet urban areas should be protected. Current engineering methods for computing these noise maps work well for the areas directly exposed to noise, but have been shown to underestimate the levels at areas shielded from direct exposure – such as quiet façades and quiet urban areas – due to including a limited number of reflections [2, 3]. As a result, noise mapping might lead to a too optimistic picture of the urban noise situation. Therefore, an acoustic calculation model for road traffic noise that is more suitable to predict noise levels for quiet façades has recently been proposed [4]. At the same time, this method should be suitable for engineering use. The proposed method therefore extends existing engineering formulae for receiver positions shielded from direct exposure. For every contributing source the suggested procedure for calculating the noise level at a shielded receiver location  $\vec{x}_r$  per octave band reads:

$$L_{pb}(\vec{x}_r) = 10 \log_{10} \left( 10^{0.1L_{pdb}} + 10^{0.1L_{p,scatter}} \right), \quad (1)$$

$$L_{pdb}(\vec{x}_r) = L_W - A_{free} - A_{diffr} - A_{inter}, \quad (2)$$

$$A_{diffr} = -10 \log_{10} \left( 10^{-0.1A_{bar}} + 10^{-0.1A_{can}} \right), \quad (3)$$

$$A_{can} = A_s + A_r \quad \text{for} \quad |\vec{x}_{r,\perp} - \vec{x}_{s,\perp}| > x_{unc}, \quad (4)$$

where,

- $L_{pb}$  = the “background” noise level excluding the diffractions and reflections around the vertical edges and excluding the diffraction over conventional noise barriers [dB].
- $L_{pdb}$  = the contribution to the “background” level in still homogeneous atmosphere [dB].
- $L_W$  = the sound power level per octave band of a point source representing part of the road [dB].
- $A_{diffr}$  = the total shielding attenuation by diffraction over the building roof [dB].
- $A_{free} = 3D$  free field divergence [dB].
- $A_{bar}$  = the attenuation by the building(s) cutting the direct path between source and receiver limited by diffraction over the building roof, including the effect of the ground. Only the direct diffraction path without reflections in the source and receiver environments is considered [dB].
- $A_{can}$  = the attenuation of the sound following a path between source and receiver representing multiple reflections in the source and receiver environment [dB].

- $A_s$  = the attenuation of the sound following a path between source and receiver representing multiple reflections in the source environment [dB].
- $A_r$  = the attenuation of the sound following a path between source and receiver representing multiple reflections in the receiver environment [dB].
- $A_{\text{inter}}$  = additional attenuation caused by the diffraction at intermediate canyons [dB].
- $L_{p,\text{scatter}}$  = the contribution to the background sound level caused by scattering from atmospheric turbulence [5] [dB].
- $\vec{x}_s = (x_s, y_s, z_s)$  = source coordinates [m].  
 $\vec{x}_r = (x_r, y_r, z_r)$  = receiver coordinates [m].  
 $\vec{x}_{s,\perp} = (x_s, y_s)$  = source coordinates in the horizontal plane [m].  
 $\vec{x}_{r,\perp} = (x_r, y_r)$  = receiver coordinates in the horizontal plane [m].  
 $x_{\text{unc}}$  = distance of uncoupling [m].

In this paper, all terms related to 2D configurations are denoted by subscript 2D, e.g.  $A_{\text{can},2\text{D}}$ . Atmospheric absorption is not explicitly included in this model but is implicit in the  $A_{\text{bar}}$  and  $A_{\text{can}}$  terms. In the absence of multiple reflections in the source and receiver environment,  $A_{\text{can}} \gg A_{\text{bar}}$  and  $A_{\text{bar}}$  determines  $A_{\text{diffr}}$ . For multiple reflections in both source and receiver environments  $A_{\text{can}} \ll A_{\text{bar}}$  and  $A_{\text{can}}$  determines  $A_{\text{diffr}}$ . An expression has been derived to compute  $A_{\text{can}}$  [4], including various coefficients. For deriving these coefficients in  $A_{\text{can}}$  from a range of urban configurations, detailed point-to-point calculations using a wave-based sound propagation method have been proposed [4]. However, two problems arise using  $A_{\text{can}}$ , which are addressed in this paper. Firstly, it is favourable in point-to-point calculations to use the uncoupled terms  $A_s$  and  $A_r$  instead of  $A_{\text{can}}$ . Then,  $A_s$  and  $A_r$  can be assigned to source and receiver positions independently, and can be used for multiple source-receiver paths. For this, the distance of uncoupling  $x_{\text{unc}}$  needs to be found. Furthermore, it is preferable to express the distance dependence of the terms  $A_s$  and  $A_r$  analytically. The second problem relates to the used assumptions for computing  $A_{\text{can}}$  in [4], being that the sound propagation in 3D can be calculated by a 2D cross-section. Whereas 2D calculations have been made for the sake of efficiency, a relation between the 2D and full 3D expressions for  $A_{\text{can}}$ , and thus the independent terms  $A_s$  and  $A_r$ , should be available, preferably in an analytical form. Another purpose of this paper is therefore to find an analytical relation between  $A_s$  and  $A_{s,2\text{D}}$ , the latter being the 2D result of  $A_s$ , and  $A_r$  and  $A_{r,2\text{D}}$ , for various urban configurations.

The aimed expressions will be found through numerical computations for 2D and 3D urban configurations by means of the pseudo-spectral time-domain method (PSTD) [6, 7]. The paper is organized as follows. In Section 2, the studied urban configurations are presented. Also, the numerical modelling approach as taken in this work is mentioned in this Section. Section 3 is

devoted to examine the distance dependence of  $A_s$  and  $A_r$ , as well as the conditions for equation (4) to hold. The analysis is made for both 2D as well as 3D configurations. The analytical expression of the 3D coefficients  $A_s$  and  $A_r$  as a function of their 2D counterparts is proposed in Section 4. For that purpose, 3D calculations for various typical urban configurations have been carried out. Conclusions are drawn in Section 5. The paper includes an Appendix on the accuracy of the adopted numerical approach.

## 2 Configurations of study and modelling approach

Figure 1 shows the 2D configurations studied in this paper. Urban configurations are considered, with source and receivers located in street canyons. Configuration *diffr* represents the canyon-to-canyon configuration with road traffic represented by a single noise source in one street canyon and receiver positions in another canyon. All façades are considered to be equal and have six depressions, corresponding to window surfaces. The other façade parts represent brickwork. Window and brickwork materials are modelled by a real normalized impedance of  $Z_n=77$  and  $Z_n=10$  respectively. All other surfaces are acoustically rigid. The current work is restricted to a fixed canyon height of  $H=19.2$  m (see Figure 1). For all calculations in this work, a homogeneous and non-moving medium is assumed. Using equation (3), the term  $A_{\text{can},2\text{D}}$  is computed as:

$$A_{\text{can},2\text{D}} = -10 \log_{10} \left( 10^{-0.1A_{\text{diffr},2\text{D}}} - 10^{-0.1A_{\text{bar},2\text{D}}} \right) \quad (5)$$

with  $A_{\text{diffr},2\text{D}} = 20 \log_{10} \left| \frac{p_{\text{free},2\text{D}}}{p_{\text{diffr},2\text{D}}} \right|$ , with  $p_{\text{free},2\text{D}}$  the sound pressure computed in free field at distance  $R_{\text{free}} = Q + W$ , with  $Q$  the separation between streets and  $W$  the street width (see Figure 1a). Further  $p_{\text{diffr},2\text{D}}$  is the sound pressure computed for the 2D configuration *diffr*. The single barrier configuration, for which  $A_{\text{bar},2\text{D}}$  is computed, is also shown in Figure 1 indicated by configuration *bar*. As such,  $A_{\text{can},2\text{D}}$  only includes contributions from source to receiver including at least one façade reflection. Further, in order to investigate whether source and receiver environment effects may be treated as being uncoupled, configurations *diffr,s*, *diffr,r*, *bar,r* and *bar,s* as shown in Figure 1 are modelled to compute  $A_{\text{diffr},s,2\text{D}}$ ,  $A_{\text{diffr},r,2\text{D}}$ ,  $A_{\text{bar},s,2\text{D}}$  and  $A_{\text{bar},r,2\text{D}}$ , which are used similar to equation (5) to compute the attenuation terms  $A_{s,2\text{D}}$  and  $A_{r,2\text{D}}$ :

$$\begin{aligned} A_{s,2\text{D}} &= -10 \log_{10} \left( 10^{-0.1A_{\text{diffr},s,2\text{D}}} - 10^{-0.1A_{\text{bar},s,2\text{D}}} \right), \\ A_{r,2\text{D}} &= -10 \log_{10} \left( 10^{-0.1A_{\text{diffr},r,2\text{D}}} - 10^{-0.1A_{\text{bar},r,2\text{D}}} \right). \end{aligned} \quad (6)$$

In current engineering methods,  $A_{\text{bar}}$  is computed by an approximate diffraction method, see e.g. reference [8]. To comply with these engineering methods, the configurations of Figure 1(b) should be computed by the same diffraction method. In this work, the 3D model to compute diffraction around a wedge, based on the Hadden and Pierce model for a single wedge [9], has

been used for this purpose [10]. For the solution of the configurations in 2D, the equivalence of the diffracted sound pressure level relative to the free field level between a coherent line source and a point source, as proposed in reference [11], is used here to derive 2D solutions from 3D solutions. We note that by the used model for the barrier configurations, façades are treated as flat and rigid, see Figures 1(b). A full-wave numerical method is used to compute sound pressure levels for the configurations of Figure 1(a), i.e. the PSTD method [6]. Within this method, reflection-free boundaries have been modelled by including a perfectly matched layer (PML). For some of the calculations, a hybrid computational approach is adopted for efficiency reasons. This approach divides the computational domain in a part where a numerical solution is needed and a part where an analytical solution of the wave equation is available. The accuracy of this hybrid approach is discussed in the Appendix.

Full 3D configurations of (interrupted) street canyons and courtyards are considered to relate the source and receiver environment effects to results from a 2D configuration approach. Figure 2 shows the modelled situations. The 3D results for the uninterrupted street configuration of Figures 2 (a,b) are obtained by a 2.5D transform as in [13], an approach based on the 2D calculations for the configurations of Figure 1(a). To evaluate the interrupted street canyon of finite length and courtyard configurations of Figures 2(c,d) and 2(e,f), a 3D PSTD model is used. The building heights and façade properties are identical to the 2D configurations. Because of symmetry, only  $\frac{1}{4}$  of the interrupted street configurations has actually been modelled and only  $\frac{1}{2}$  of the courtyard configurations has been modelled, see Figures 2(c,d) and 2(e,f). The interrupted street is mainly of interest for a configuration with a source in the street and receiver outside the street. The courtyard case is mainly of interest for a configuration with a receiver in the courtyard and a source outside the courtyard.

In previous work, it was found that the frequency range of interest as concerns noise from road traffic in geometrically shielded urban areas may be limited to an upper 1/3 octave band of 1.6 kHz [14]. For the 2D calculations, this upper limit has here been used. Due to numerical overhead of the computational model, the 3D results are evaluated with an upper 1/3 octave band of 1 kHz. Levels in the 1/3 octave bands have been computed from 20 logarithmically spaced frequencies per band. When broadband results are presented, an *A*-weighted sound power spectrum representing urban road traffic has been used, i.e. the values of  $L_w = 63, 75, 87, 95, 97, 104$  dB have been used for the octave bands 32-1000 Hz. These values have been calculated with the Dutch standard traffic noise model for typical urban traffic noise situations.

### 3 Distance dependence and additivity of $A_s$ and $A_r$

A first step toward the analytical expression of  $A_s = A_s(A_{s,2D})$  and  $A_r = A_r(A_{r,2D})$  is to find relations of analytical distance dependence for the separate terms  $A_{s,2D}$ ,  $A_{r,2D}$ ,  $A_s$  and  $A_r$ . These dependencies are sought in this section, both for 2D as well as for 3D configurations of

Figure 1. Also, the independence of the source and receiver terms is verified, i.e.  $A_{\text{can},2\text{D}} = A_{s,2\text{D}} + A_{r,2\text{D}}$  and  $A_{\text{can}} = A_s + A_r$ . In particular, the distance of uncoupling for which these relations are valid is searched for.

### 3.1 Two-dimensional results

#### 3.1.1 Distance dependence of $A_{s,2\text{D}}$ and $A_{r,2\text{D}}$

To express the distance dependence in  $A_{s,2\text{D}}$  analytically, we project  $A_{s,2\text{D}}$  onto an equivalent free field situation, i.e. a source-receiver configuration in free field, see Figure 1(c). This approach assumes a distance independent part,  $A'_{s,2\text{D}}$ , and a distance dependent part. We write for  $A'_{s,2\text{D}}$  and similarly  $A'_{r,2\text{D}}$ :

$$A_{s,2\text{D}}(\vec{x}_r) = A'_{s,2\text{D}} + 10 \log_{10} \left( \frac{x_r - x_{\text{es},2\text{D}}}{x_r} \right). \quad (7)$$

$$A_{r,2\text{D}}(\vec{x}_r) = A'_{r,2\text{D}} + 10 \log_{10} \left( \frac{x_{\text{er},2\text{D}}}{x_r} \right). \quad (8)$$

Although  $A'_{s,2\text{D}}$  and  $A'_{r,2\text{D}}$  are considered to be distance independent, they might depend on the location of the source and receiver in the street, which is discussed in [4]. Optimal values of the equivalent source position  $x_{\text{es},2\text{D}}$  have been found by the minimizing the error  $\epsilon$ , which reads for  $x_{\text{es},2\text{D}}$ :

$$\epsilon(x_{\text{es},2\text{D}}) = \sum_{n=2}^{N-1} \left| \left( A_{s,2\text{D}}(Q_n) - A_{s,2\text{D}}(Q_N) + 10 \log_{10} \left( \frac{x_{r,n} (x_{r,N} - x_{\text{es},2\text{D}})}{x_{r,N} (x_{r,n} - x_{\text{es},2\text{D}})} \right) \right) \right|, \quad (9)$$

with  $A_{s,2\text{D}}$  the broadband level, computed from using equation (6) and using the spectral distribution of  $L_w$ ,  $x_{r,n} = (nQ + W)/2$  and  $N=19$ . For  $\epsilon(x_{\text{es},2\text{D}}) = 0$ ,  $x_{\text{es},2\text{D}}$  is found for which the distance dependence of  $A_{s,2\text{D}}$  is purely analytical. It may be expected that  $x_{\text{es},2\text{D}}$  depends on the  $W/H$  ratio as well as on the height of the left building relative to the right building. Results for  $x_{\text{es},2\text{D}}$  are plotted in Figure 3(a) as a function of the  $W/H$  ratio. It is clear that the  $W/H$  ratio has a small influence on the location of the equivalent source position. The location of  $x_{\text{es},2\text{D}}$  as a function of the height of the left building  $H_{\text{left}}$  is computed for  $W/H=1$ , and results are shown in Figure 3(b). The results from Figure 3 can now be used to construct an analytical expression to compute  $x_{\text{es},2\text{D}}$  as a function of the  $W/H$  ratio and the left building height  $H_{\text{left}}$ . We write for  $x_{\text{es},2\text{D}}$  and  $x_{\text{er},2\text{D}}$

$$\begin{aligned} x_{\text{es},2\text{D}} &= \frac{W}{2} \left( 1 - \frac{3}{4} \left( \frac{H_{\text{left}}}{H} \right)^4 \right), \\ x_{\text{er},2\text{D}} &= \frac{Q + W}{2} - x_{\text{es},2\text{D}}, \end{aligned} \quad (10)$$

where the coordinate origin of Figure 1(a) is respected. The relations from equations (10) are plotted in Figure 3 too by the dashed lines. Figure 4(a) shows  $\Delta A_{s,2\text{D}}(Q) = A_{s,2\text{D}}(Q) -$

$A_{s,2D}(Q = 20W)$  and  $\Delta A'_{s,2D}(Q)$  as a function of  $Q$ . It illustrates that the source environment attenuation term  $A_{s,2D}$  approaches a constant value for larger distances and shows that  $A'_{s,2D}$  is rather distance independent. Figure 4(b) shows  $\Delta A'_{s,2D}$  as a function of  $Q$  as well as 1/3 octave bands. When considering 0.5 dB as an acceptable error bound, we may conclude from the results that the distance dependence of  $A_{s,2D}$  can be described analytically for the 1/3 octave bands above 63 Hz and  $Q/W \geq 2$ .

For  $A_{r,2D}$ , a similar equivalent free field approach as for  $A_{s,2D}$  has been followed, i.e. with a single equivalent receiver position  $x_{er,2D}$  that replaces all receiver positions, see Figure 1(c) config.  $r$ . The source positions are equal to  $x = 0$  and  $A_{r,2D}$  is written in equation (8), with  $x_{er,2D}$  from equation (10). Figure 5(a) shows the broadband values of  $\Delta A_{r,2D}$  and  $\Delta A'_{r,2D}$ . The plotted results have arithmetically been averaged over all receiver positions and are very similar to the results in Figure 4(a). The results for  $\Delta A'_{r,2D}(Q = 2W)$ , are plotted in Figure 5(b), showing only deviations above 0.5 dB for the lowest and highest frequencies.

In summary, the proposed free field representations expressed in equations (7) and (8) for the source and receiver configuration return expressions for the correction terms  $A_{s,2D}$  and  $A_{r,2D}$ , which are analytically independent on the distance for  $Q/W \geq 2$ .

### 3.1.2 Additivity of $A_{s,2D}$ and $A_{r,2D}$

As for the separate terms  $A'_{s,2D}$  and  $A'_{r,2D}$  of Section 3.1.1,  $A'_{can,2D}$  may be expressed by an equivalent free field analogy, with equivalent source and receiver, see Figure 1(c). For  $A_{can,2D}$ , we write:

$$A_{can,2D}(\vec{x}_r) = A'_{can,2D} + 10 \log_{10} \left( \frac{x_{er,can,2D} - x_{es,can,2D}}{x_r} \right), \quad (11)$$

with  $x_{es,can,2D} = x_{es,2D}$ ,  $x_{er,can,2D} = (Q + W) - x_{es,2D}$  and  $x_r = Q + W$ . To verify the additivity of  $A_{s,2D}$  and  $A_{r,2D}$ , the broadband difference  $(A'_{s,2D} + A'_{r,2D}) - A'_{can,2D}$  is computed from equations (7), (8), and (11) and is plotted in Figure 6(a) as a function of  $Q$ . The results have arithmetically been averaged over all receiver positions. We notice an agreement within 0.5 dB(A) for  $Q/W \geq 2$ . Assuming that  $A'_{can,2D} = A'_{s,2D} + A'_{r,2D}$ ,  $A_{can,2D}$  can be computed from  $(A_{s,2D} + A_{r,2D})$  and analytical distance dependent terms as:

$$A_{can,2D}(\vec{x}_r) = \left( A_{s,2D} \left( \frac{\vec{x}_r}{2} \right) + A_{r,2D} \left( \frac{\vec{x}_r}{2} \right) \right) + 10 \log_{10} \left( \frac{x_{er,can,2D} - x_{es,can,2D}}{x_r} \right) + 6 \quad (12)$$

for  $Q \geq 2W$ ,

where we have added 6 dB(A) due to a double count of the reflection at the roof level in  $(A_{s,2D} + A_{r,2D})$ . Figure 6(b) shows the spectral agreement of  $(A'_{s,2D} + A'_{r,2D})$  and  $A'_{can,2D}$  for  $Q = 20W$ . The result of  $(A'_{bar,s,2D} + A'_{bar,r,2D})$  and  $A'_{bar,2D}$  are also shown, illustrating the dominance of  $A'_{can,2D}$  regarding the  $A'_{diff,2D}$  term.

In summary, for the 2D configurations,  $Q \geq 2W$  seems to be a good choice for  $x_{unc}$  of equation (4).

### 3.2 Three-dimensional results

#### 3.2.1 Distance dependence of $A_s$ and $A_r$

A similar analysis as for the 2D configurations is undertaken for the 3D configuration of an uninterrupted street, i.e. the configurations of Figure 1 where streets have an infinite length as depicted in Figures 2(a,b). We here limit the study to  $y_s = y_r = 0$ . For  $A_s$  and  $A_r$ , we write:

$$A_s(\vec{x}_r) = A'_s + 20 \log_{10} \left( \frac{x_r - x_{es}}{x_r} \right), \quad (13)$$

$$A_r(\vec{x}_r) = A'_r + 20 \log_{10} \left( \frac{x_{er}}{x_r} \right). \quad (14)$$

Similar to the 2D configuration, the optimal values of the equivalent source positions are computed and are shown in Figure 7. As concerns the  $W/H$ -dependence and the dependence on  $H_{\text{left}}$ , the similarity between the 2D results of Figure 3 is obvious. The location of the equivalent sources is however different from the locations in 2D, with smaller values of  $x_{es}$  compared to its 2D counterparts. A relation for  $x_{es}$  and  $x_{er}$  is derived from the numerical results of Figure 7:

$$\begin{aligned} x_{es} &= \frac{W}{3} \left( 1 - \frac{4}{5} \left( \frac{H}{W} \right) \right) - \frac{7}{5} \left( \frac{H_{\text{left}}}{H} \right)^{3/2}, \\ x_{er} &= \frac{Q + W}{2} - x_{es}, \end{aligned} \quad (15)$$

and is shown by the lines in Figure 7. The attenuation terms  $\Delta A_s$  and  $\Delta A'_s$  are plotted in Figure 8(a), and  $\Delta A'_s$  is plotted as a function of frequency and distance  $Q$  in Figure 8(b). For the receiver environment, the values of  $\Delta A_r$  and  $\Delta A'_r$  are plotted in Figure 9(a). The importance of splitting the attenuation terms  $A_s$  and  $A_r$  into a distance dependent and distant independent term is highlighted by the Figures: whereas  $A_s$  and  $A_r$  slowly converge with distance, the terms  $A'_s$  and  $A'_r$  show to be distance independent for  $Q/W \geq 4$  within the 0.5 dB(A) error. Figure 9(b) shows  $\Delta A'_r(4Q)$ , showing that in contrast to the 2D configuration however, a higher receiver position dependence of  $\Delta A'_r$  is noticeable.

The proposed free field representation expressed in equation (13) and (14) thus return an expressions for the correction terms  $A_s$  and  $A_r$ , which are analytically dependent on the distance for  $Q/W \geq 4$ .

#### 3.2.2 Additivity of $A_s$ and $A_r$

To verify the additivity of  $A_s$  and  $A_r$  in the 3D configuration of uninterrupted streets, an analogue analysis as for the 2D configuration has been carried out. In Figure 10(a), broadband results are shown for the differences  $(A'_s + A'_r) - A'_{\text{can}}$  and  $(A_s + A_r) - A_{\text{can}}$ . An agreement within 0.5 dB(A) for the primed numbers is found for  $Q/W \geq 2$ . For higher numbers of  $Q$ ,

results exceed 0.5 dB(A). This offset can also be seen to a smaller account in the 2D result of Figure 6(a). The reason is linked to the difference in the lower frequencies, see Figures 6(b) and 10(b). This difference can be attributed to the discrepancy between results from the Hadden and Pierce model and PSTD model for these frequencies: from an analysis for the  $A'_{\text{diff},r}$  term, these differences were not encountered as  $(A'_{\text{diff},s} + A'_{\text{diff},r}) - A'_{\text{diff},r} < 0.5$  dB(A) for all  $Q/W \geq 2$ . Figure 10(b) also shows the dominance of  $A'_{\text{can}}$  over  $A'_{\text{bar}}$ . From the equality of the primed numbers, we now can compute  $A_{\text{can}}$  as:

$$A_{\text{can}}(\vec{x}_r) = \left( A_s \left( \frac{\vec{x}_r}{2} \right) + A_r \left( \frac{\vec{x}_r}{2} \right) \right) + 20 \log_{10} \left( \frac{x_{\text{er,can}} - x_{\text{es,can}}}{x_r} \right) + 6 \quad (16)$$

for  $Q \geq 2W$ .

## 4 2D versus 3D approach

In Section 3, we have found distance dependence expressions for  $A_{s,2D}$ ,  $A_{r,2D}$ ,  $A_s$  and  $A_r$  and the conditions for which they are valid. Also, the expressions for  $A_{\text{can},2D}$  as well  $A_{\text{can}}$  based on the separate source and receiver environment terms have been derived. The objective of this section is to find expressions for the 3D attenuation terms as a function of their 2D counterpart. The analysis is based on three types of configurations: 1) an uninterrupted street of infinite length of Figures 2(a,b), 2) a finite-length street interrupted by a cross street, see Figures 2(c,d), and 3) a courtyard, see Figures 2(e,f). As road traffic is subdivided into point sources along the street, the effect of a horizontal directionality of attenuation terms  $A_s$  and  $A_r$  is low when including contributions from all sources in the street. The here adopted approach is therefore to use attenuation terms that are angular averaged values in the horizontal plane, further denoted by  $\bar{A}_s$  and  $\bar{A}_r$ . In this section, we thus search for the relations  $\bar{A}_s = \bar{A}_s(A_{s,2D})$  and  $\bar{A}_r = \bar{A}_r(A_{r,2D})$ .

### 4.1 Uninterrupted Street

For the uninterrupted street of Figures 2(a,b), we first examine the equivalence between 2D and 3D results where  $y_s = y_r = 0$ . We exploit the hypothesis that the 2D and 3D expressions only deviate through distance dependence, and that the distance independent coefficient are equal, i.e.  $A'_r \approx A'_{r,2D}$ ,  $A'_s \approx A'_{s,2D}$  and  $A'_{\text{can}} \approx A'_{\text{can},2D}$ . To verify this hypothesis, Figure 11 shows results of the broadband differences between 2D and 3D terms, averaged over the receiver positions. All results are consistent in showing clear deviations and a slow convergence with distance for the unprimed numbers, and deviations smaller than 0.5 dB(A) for the primed numbers for all distances above  $Q/W \geq 3$ , which supports the equalities  $A'_r = A'_{r,2D}$ ,  $A'_s = A'_{s,2D}$  and  $A'_{\text{can}} = A'_{\text{can},2D}$  for  $Q/W \geq 3$ . To verify whether  $\bar{A}'_s = A'_{s,2D}$  holds for the uninterrupted street, the configurations with  $y_r \neq 0$ ,  $y_s = 0$  are now investigated. Figure 12 shows the broadband attenuation terms  $A'_{s,2D}$  and  $A'_s(\theta)$  results for  $Q=19W$  as a function of the angle  $\theta$ , with equivalent sources according to equations (10) and (15). The 3D results for the barrier

configuration have been computed with a Hadden and Pierce model where the diffraction edge is perpendicular to the source-receiver direction, which is according to the approach in standard engineering methods [8]. Results show a decrease in attenuation term  $A'_s$  with increasing angle  $\theta$ , i.e. a lower shielding. The equality  $\bar{A}'_s = A'_{s,2D}$ , with  $\bar{A}'_s = 1/85 \int_0^{85} A'_s(\theta) d\theta$ , is clearly not valid and should be altered into  $\bar{A}'_s = B_s A'_{s,2D}$ . An expression for  $B_s$  will be derived in the following Section 4.2.

## 4.2 Interrupted street

Streets have a finite length and most streets are interrupted by cross streets or openings. The value of the coefficient  $B_s$  in  $\bar{A}'_s = B_s A'_{s,2D}$  is expected to deviate from 1. The studied configuration of interrupted streets is shown in Figures 2(c,d). We aim to derive an expression for  $B_s$  for these cases. Three locations of the cross street with respect to the main street, denoted by  $U$ , and two cross street widths, denoted by  $C$ , are investigated. The broadband results  $A'_s$  (up to the 1 kHz 1/3 octave band) are plotted as a function of the angle in Figure 13, along with the results for the barrier attenuation term  $A'_{bar,s}$ , and results for the uninterrupted infinitely long street of the former,  $A'_{s,2D}$  and  $A'_s$ . Equations (10) and (15) have been used to determine the equivalent source positions. For angles above  $70^\circ$ , Figure 13 shows that all values of  $A'_s$  increase for the finite street configuration, with large deviations from the results for the uninterrupted infinitely long street. The impact of the cross street increases with increasing cross street width, and with decreasing distance of the cross street to the source position. The configuration denoted as  $C2U1$ , i.e.  $C = W$  and  $U = W/2$  indeed shows largest deviations from the uninterrupted street. For this  $C2U1$  case, results between  $20^\circ$  and  $55^\circ$  do show values of  $A'_s \approx A'_{bar,s}$ , implying a slight effect compared to the single diffraction case. To quantify the effect of openings in the façades, the relative number  $S = \left( A'_{bar,s}(\theta = 0^\circ) - \bar{A}'_s \right) / \left( A'_{bar,s}(\theta = 0^\circ) - A'_{s,2D} \right)$  is plotted in Figure 14 for the various interrupted street configurations of Figures 2(c,d), with  $\bar{A}'_s$  the averaged value of  $A'_s$  over angles  $0^\circ$ – $85^\circ$ .  $S$  indicates the value of the  $\bar{A}'_s$ , relative to  $A'_{bar,s}(\theta = 0^\circ)$  and  $A'_{s,2D}$ : a value of  $S = 0$  implies that  $\bar{A}'_s = A'_{bar,s}(\theta = 0^\circ)$  and a value of  $S = 1$  means  $\bar{A}'_s = A'_{s,2D}$ . A clear trend is visible of a decreasing value of  $S$  with an increasing value of  $p$ , the angular fraction of open façades in the horizontal plane as seen from the source. A relationship of  $S = C_1 * (1 - p^{C_2})$  is derived from numerical data, with  $C_1 = 1.26$ ,  $C_2 = 0.6$ . Utilizing this expression for  $S$ , we find for the coefficient  $B_s$ :

$$B_s = \frac{A'_{bar,s}(\theta = 0^\circ)}{A'_{s,2D}}(1 - S) + S,$$

with

$$S = C_1 * (1 - p^{C_2}). \quad (17)$$

The sought relations  $\bar{A}_s = \bar{A}_s(A_{s,2D})$  and  $\bar{A}_r = \bar{A}_r(A_{r,2D})$  can now be written as:

$$\begin{aligned}
\bar{A}_s(\vec{x}_r) &= B_s A'_{s,2D} + 20 \log_{10} \left( \frac{|\vec{x}_{r,\perp}| - x_{es}}{|\vec{x}_{r,\perp}|} \right), \\
&= B_s \underbrace{\left( A_{s,2D} - 10 \log_{10} \left( \frac{|\vec{x}_{r,\perp}| - x_{es,2D}}{|\vec{x}_{r,\perp}|} \right) \right)}_{A'_{s,2D} \approx A'_s} + 20 \log_{10} \left( \frac{|\vec{x}_{r,\perp}| - x_{es}}{|\vec{x}_{r,\perp}|} \right), \tag{18}
\end{aligned}$$

$$\begin{aligned}
\bar{A}_r(\vec{x}_r) &= B_r A'_{r,2D} + 20 \log_{10} \left( \frac{|\vec{x}_{r,\perp}| - x_{es}}{|\vec{x}_{r,\perp}|} \right), \\
&= B_r \underbrace{\left( A_{r,2D} - 10 \log_{10} \left( \frac{|\vec{x}_{r,\perp}| - x_{es,2D}}{|\vec{x}_{r,\perp}|} \right) \right)}_{A'_{r,2D} \approx A'_r} + 20 \log_{10} \left( \frac{|\vec{x}_{r,\perp}| - x_{es}}{|\vec{x}_{r,\perp}|} \right). \tag{19}
\end{aligned}$$

### 4.3 Courtyard

The value of  $B$  is finally verified for a typical configuration of the receiver environment: a closed courtyard configuration as depicted in Figures 2(e,f). This configuration represents a situation with an angular fraction of open façades in the horizontal plane equal to  $p = 0$ . A single receiver is positioned at a height of 4.7 m in the middle of the courtyard. Equations (15) has been used to determine the equivalent receiver positions. Figure 15 shows broadband angular dependent results of  $A'_r(\theta)$  at  $Q = 40W$  for the two courtyard configurations, along with the 2D results  $B_r A'_{r,2D}$  for the cross-section where  $\theta = 0^\circ$ , with  $B = 1$  and  $B = 0.64$ , the latter being computed for from equation (17). The angular dependency for the courtyard cases is rather weak. The angular averaged values  $\bar{A}'_r$  are 8.0 dB(A) and 7.1 dB(A) for courtyard configurations with  $T = W/2$  and  $T = 3W/2$  respectively. These values are closer to the 2D results with  $B_r = 1$  than to  $B_r = 0.64$ , implying that the courtyard situations lead to a stronger attenuation term  $\bar{A}'_r$  than the infinitely long street case. Clearly, with increasing  $T$  the  $\bar{A}'_r = 0.64 A'_{r,2D}$  would apply here too.

## 5 Conclusions

A recently proposed improved engineering method for urban areas shielded from direct exposure to traffic noise includes  $A_{can}$ , a term that accounts for multiple reflections of the built environment in the source and receiver area. The proposed term relies point-to-point calculations using a wave-based acoustic propagation method for 2D urban canyon geometries, and may be split in a term accounting for reflections in the source environment  $A_s$ , and a term accounting for reflections in the receiver environment,  $A_r$ . In this work, an expression is derived to compute the full 3D  $A_{can}$  term from the 2D results, further relying on analytical terms only. For this purpose, 2D and 3D calculations with a wave-based calculation model have been carried out for various

urban configurations. First, expressions have been derived to compute the 2D and 3D attenuation terms of the source and receiver environment –  $A_{s,2D}$ ,  $A_{r,2D}$ ,  $A_s$  and  $A_r$  – into a distance independent term and a analytical term for the distance dependence. These expressions rely on equivalent free field analogies. The expressions were shown to be valid for source-to-receiver environment distances exceeding twice the street canyon width ( $Q=2W$ ) in 2D, i.e. and exceeding 4 times the street canyon width in 3D. Furthermore, it indeed was shown to be possible to compute  $A_{can}$  and  $A_{can,2D}$  from these separate source and receiver environment terms, when correcting for the distance dependence using analytical expressions. To express the 3D attenuation term by the 2D terms, we have proposed 3D term that represent an averaged value over the horizontal angles. The final equations, i.e. equations (18) and (19), enable to compute the 3D attenuation term for multiple reflections, from the 2D attenuation term, including analytical terms for distance dependence. For application to a wider range of configurations, the difference between the width-to-height ratio of the streets and height of the left building are incorporated in the equation, as well as the angular fraction of street openings. The model is also suitable for closed courtyards. The results of this work rely on values averaged of the receiver positions, and does not reflect the local differences between receiver positions. The latter is incorporated in the distance independent coefficients, which is subject of another paper.

## Acknowledgements

Part of this work was made possible by financial support by the Life+ program of the European Community (project QSIDE, LIFE09 ENV/NL/000423).

## A Accuracy of the Kirchhoff-Helmholtz integral approach

Far field sound propagation for calculation of the configurations  $diff;r,s$  and  $diff;r,r$  of Figure 1 are in this work computed using the Kirchhoff-Helmholtz (KH) integral technique as depicted in Figure 16 for the configuration  $diff;r,s$ . The PSTD method is used to solve the wave equation in the left part of Figure 16(b), and pressure and normal velocity components are stored at the vertical line at  $x = W/2 + 2$  m. Then, the solution in the latter part is computed by applying the Kirchhoff-Helmholtz (KH) integral method to the vertical line at  $x = W/2 + 2$  m, as depicted in Fig. 16(b). The KH method is described e.g. by Pierce [12]. This integral method relies on Green's functions, which are known at the right side of the vertical line at  $x = W/2 + 2$  m. With this hybrid approach, a higher numerical efficiency is obtained compared to applying the PSTD method to the complete domain. The 3D results for the uninterrupted street configuration of Figures 2 (a,b) are obtained by a 2.5D transform as in [13], an approach based on 2D calculations. A three step approach is then adopted: 1) a 2D PSTD calculation, 2) the KH-integral approach for far field results, 3) the 2.5D transform to obtain 3D results. For

the 3D configurations of Figure 2(c,e), far field results are also obtained by integrating over the solution at the KH-planes. For the interrupted street case, the KH-planes vertically range from  $H$  to  $H + z_{\text{KH}}$  and we assume a single hard ground surface outside the KH-planes.

The accuracy of the KH-approach is here investigated for an analytical case of a source over a rigid ground surface for 2D and 3D configurations, see Figures 17(a,b,e,f), with horizontal dimensions of the configurations according to the 2D configuration *diff,r,s*, the 3D interrupted street configuration of Figures 2(c,d) and the courtyard configuration with  $T = 3W/2$  of Figures 2(e,f). The solution at the KH-plane  $x_{\text{KH}}$ , computed with PSTD, is tapered near the top by a super-Gaussian window to avoid diffraction from the edge when integrating over the KH-plane, i.e. for the pressure in the 2D configuration:

$$p(x_{\text{KH}}, z) = \begin{cases} G(x_{\text{KH}}, z|0, 0)e^{-\alpha(z-z_0)^6} & \text{for } z_0 < z < z_{\text{KH}} \\ G(x_{\text{KH}}, z|0, 0) & \text{for } 0 < z < z_0, \end{cases} \quad (20)$$

with  $G(x_{\text{KH}}, z|0, 0)$  the 2D Green's function from the source to the KH-plane and  $z_0 = 0.7z_{\text{KH}}$ . We evaluate the KH-integral with 10 points per wavelength. Since the PSTD calculations have a spatial resolution of 2 points per smallest wavelength, spectral interpolation has been applied at the KH-plane prior to evaluation of the far field results. For the 2D configuration, Figures 17(c,d) show the error as a function of the 1/3 octave band with  $z_{\text{KH}} = 30$  m, for  $W = 19.2$  m and  $W = 19.2 / \cos(\theta = 80^\circ)$  respectively. The latter corresponds to projected street width for the uninterrupted street case configuration of Figure 12, with  $\theta = 80^\circ$ . For  $W = 19.2$  m, errors are below 0.5 dB for all distances and 1/3 octave bands. For  $W = 19.2 / \cos(80)$ , a larger error is retrieved for the lower 1/3 octave bands. As most results in this paper rely on broadband values, and since the  $A$ -weighted power spectrum is dominant for the highest 1/3 octave band, the broadband error will be small for  $\theta = 80^\circ$  too.

For the 3D configurations, results are shown in Figures 17(g,h) for the interrupted street and courtyard configurations respectively as a function of the 1/3 octave band and as a function of the angle  $\theta$  for  $x_{r,\perp} = 20W$ , with  $W = H$ . For both the street and the courtyard configuration, the error increases with angle, since  $y_{\text{KH}} > x_{\text{KH}}$ . Similar remarks as for the 2D error hold.

The value of  $z_{\text{KH}} = 30$  m has been used for all calculations in this paper.

## References

- [1] Directive 2002/49/EC of the European Parliament and of the Council relating to the assessment and management of environmental noise (2002).
- [2] M. Ögren, M., W. Kropp: Road traffic noise propagation between two dimensional city canyons using an equivalent source approach. *Acta Acust. United Ac.* **90** (2004) 293-300.

- [3] T. Kihlman, M. Ögren, W. Kropp: Prediction of urban traffic noise in shielded courtyards. Proceedings of The International Congress and Exposition on Noise Control Engineering, Dearborn, MI, USA, (2002).
- [4] W. Wei, T. Van Renterghem, D. Botteldooren, M. Hornikx, J. Forssén, E. Salomons, M. Ögren: Urban background noise mapping: the general model. Manuscript in preparation for submission to *Acta Acust. United Ac.* (2013).
- [5] J. Forssén, M. Hornikx, T. Van Renterghem, W. Wei, D. Botteldooren, M. Ögren.:Urban background noise mapping: the turbulence scattering model. *Manuscript in preparation for submission to Acta Acust. United Ac.*, 2013.
- [6] M. Hornikx, R. Waxler, J. Forssén: The extended Fourier pseudospectral time-domain method for atmospheric sound propagation. *J. Acoust. Soc. Am.* **128** (2010) 297-319.
- [7] M. Hornikx, J. Forssen: Modelling of sound propagation to three-dimensional urban courtyards using the extended Fourier PSTD method. *Appl. Acoust.* **72** (2011) 665-676.
- [8] E. Salomons, D. van Maercke, J. Defrance, F. de Roo: The Harmonoise Sound Propagation Model. *Acta Acust. United Ac.* **97** 2011 62-74.
- [9] J.D. Hadden, A.D. Pierce: Sound diffraction around screens and wedges for arbitrary point source locations. *J. Acoust. Soc. Am.* **69** (1981) 1266-1276. Erratum, *J. Acoust. Soc. Am.* **71** (1982) 1290.
- [10] E. Salomons: Sound propagation in complex outdoor situations with a non-refracting atmosphere: Model based on analytical solutions for diffraction and reflection. *Acta Acust. United Ac.* **83** (1997) 436-454.
- [11] T. Van Renterghem, E. Salomons, D. Botteldooren: Efficient FDTD-PE model for sound propagation in situations with complex obstacles and wind profiles. *Acta Acust. United Ac.* **91** (2005) 671-679.
- [12] A.D. Pierce: *Acoustics, an introduction to its physical principles and applications.* The Acoustical Society of America, Melville, NY, USA (1981).
- [13] M. Hornikx, J. Forssén: The 2.5-dimensional equivalent sources method for directly exposed and shielded urban canyons. *J. Acoust. Soc. Am.* **122** (2007) 2532-2541.
- [14] T. Van Renterghem, D. Botteldooren: The importance of roof shape for road traffic noise shielding in the urban environment. *J. Sound and Vibration* **329** (2010) 1422-1434.

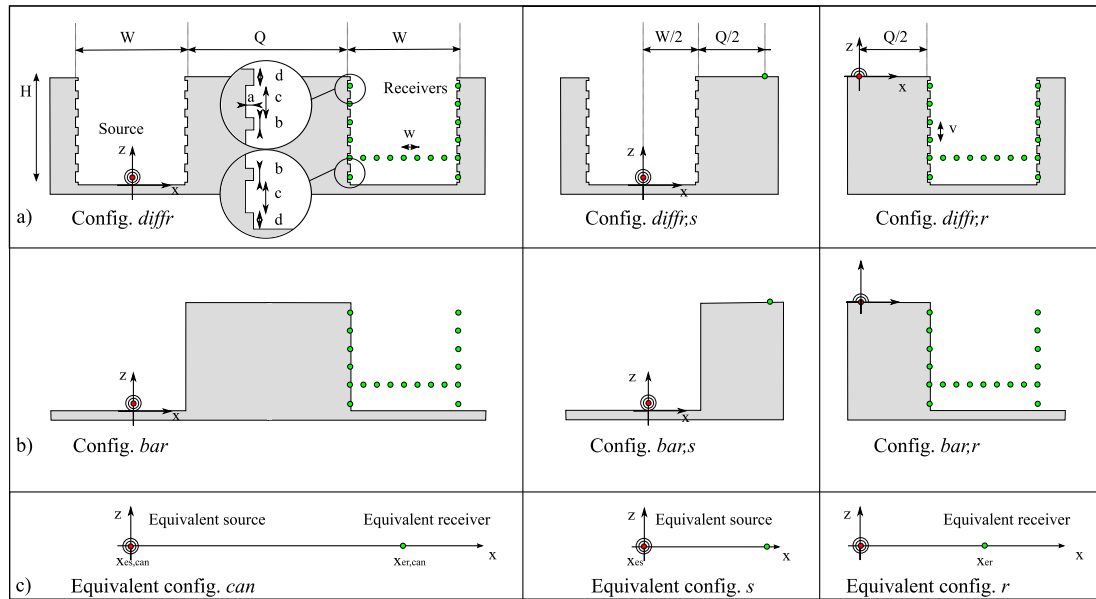


Figure 1: Configurations studied with numerical parameters  $a = 0.16$  m,  $b = 0.64$  m,  $c = 1.92$  m,  $d = 1.28$  m,  $v = c + d = 3.2$  m,  $w = 1.6$  m,  $z_s = 0.5$  m,  $W = 19.2$  m,  $H = 19.2$  m,  $Q$  is variable. (a) configurations for which the shielding attenuation terms  $A_{diffr}$ ,  $A_{diffr,s}$  and  $A_{diffr,r}$  are applicable, (b) configurations for which the barrier attenuation terms  $A_{bar}$ ,  $A_{bar,s}$  and  $A_{bar,r}$  are applicable, (c) equivalent configurations for which the shielding attenuation terms  $A_{can}$ ,  $A_s$  and  $A_r$  are applicable.

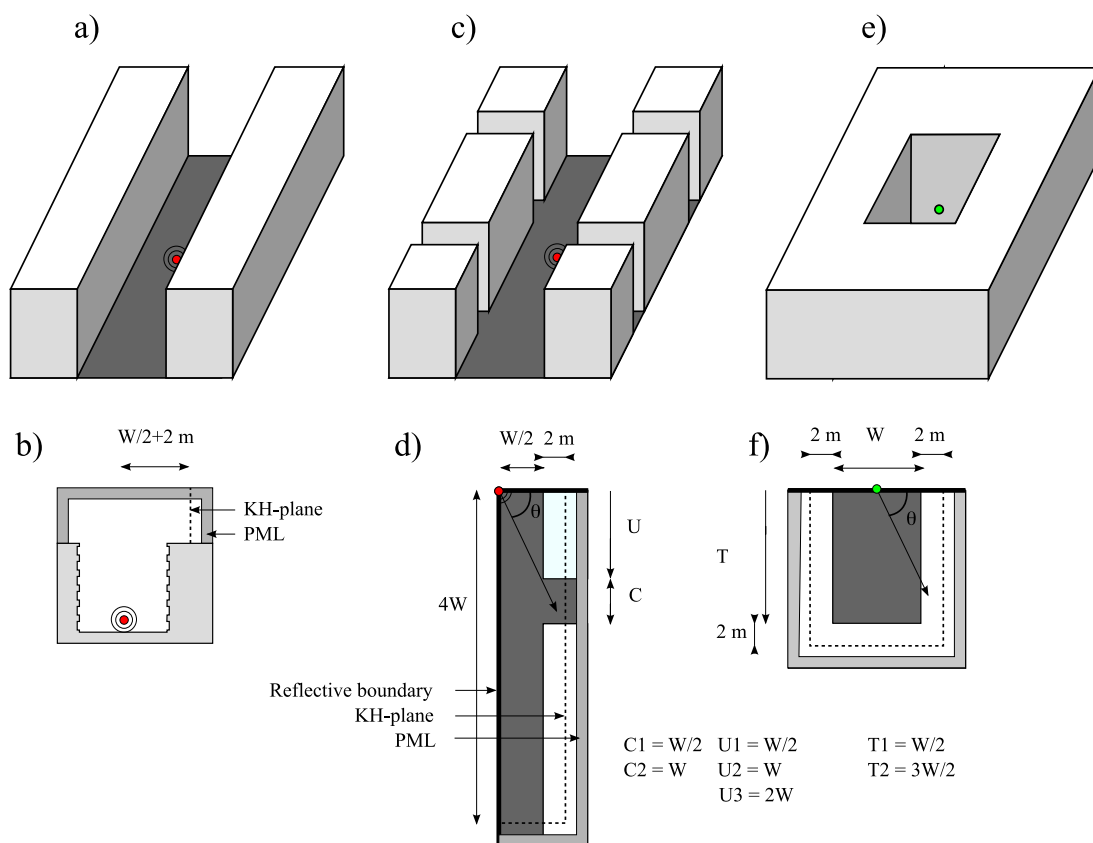


Figure 2: 3D configurations studied, a) Graphical representation infinite street, b) Computational approach shown by cross section at  $y = 0$ . A 2.5 D transform is applied to the 2D results obtain by computing the 2D problem of the cross section. c) Graphical representation of finite street with cross streets, d) Computational approach shown by top view, e) Graphical representation of courtyard, f) Computational approach shown by top view.

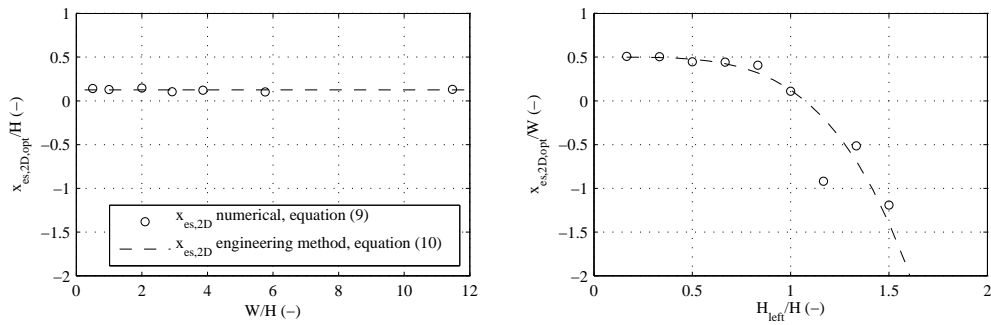


Figure 3: Optimal values of the equivalent source position  $x_{es,2D}$  for attenuation term  $A'_{s,2D}$ , a) as a function of the canyon width  $W$  with  $H = 19.2$  m, b) as a function of the left building height  $H_{left}$  with  $W = 19.2$  m.

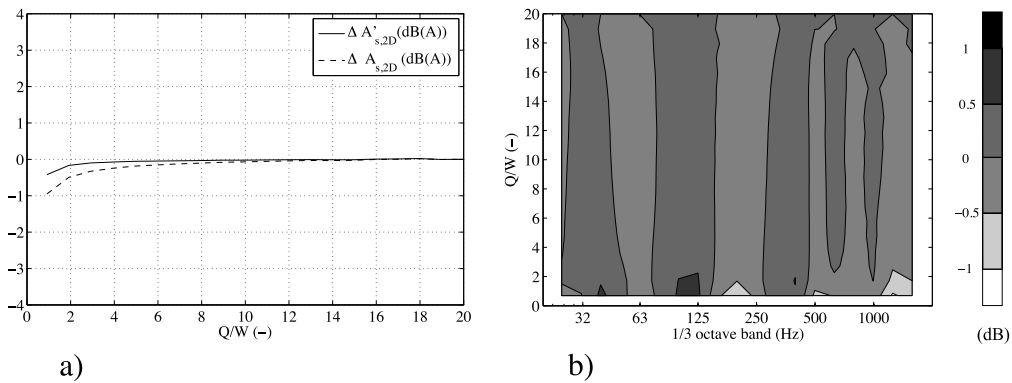


Figure 4: Attenuation terms computed from configurations *diffr,s* and *bar,s* of Figure 1, a)  $\Delta A_{s,2D}$  and  $\Delta A'_{s,2D}$  in dB(A), b)  $\Delta A'_{s,2D}$ .

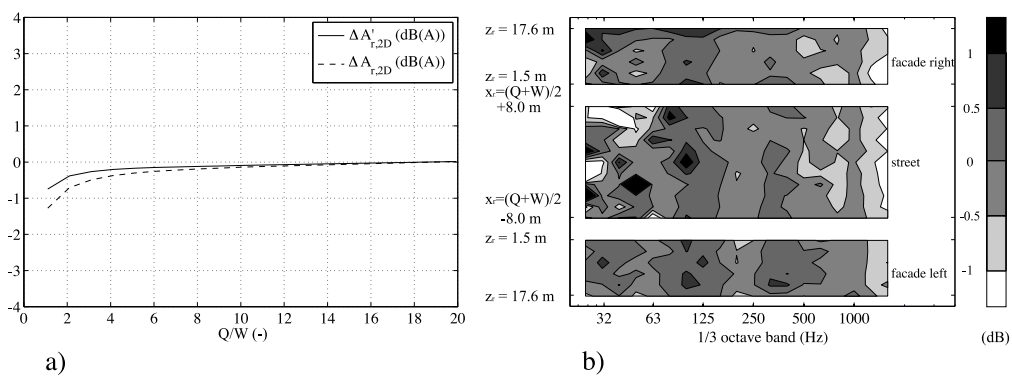


Figure 5: Attenuation terms computed from configurations *diffr,r* and *bar,r* of Figure 1, a)  $\Delta A'_{r,2D}$  and  $\Delta A_{r,2D}$ , averaged over all receiver positions, b)  $\Delta A'_{r,2D}$  ( $Q = 2W$ ) as a function of the receiver position and third octave bands.

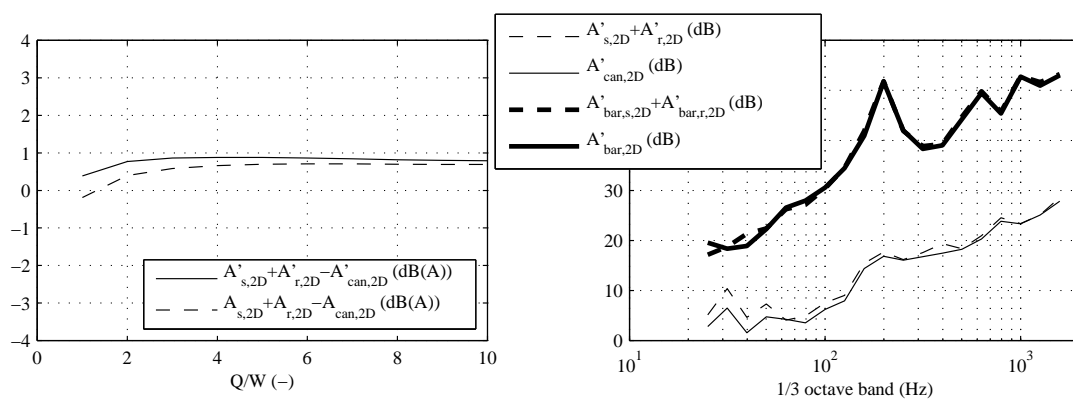


Figure 6: a) Broadband error of splitting the attenuation term  $A'_{can,2D}$  into  $A'_{s,2D} + A'_{r,2D}$  and  $A_{can,2D}$  into  $A_{s,2D} + A_{r,2D}$ . Results have been averaged over all receiver positions, b) Results at  $Q = 10W$  averaged over all receiver positions.

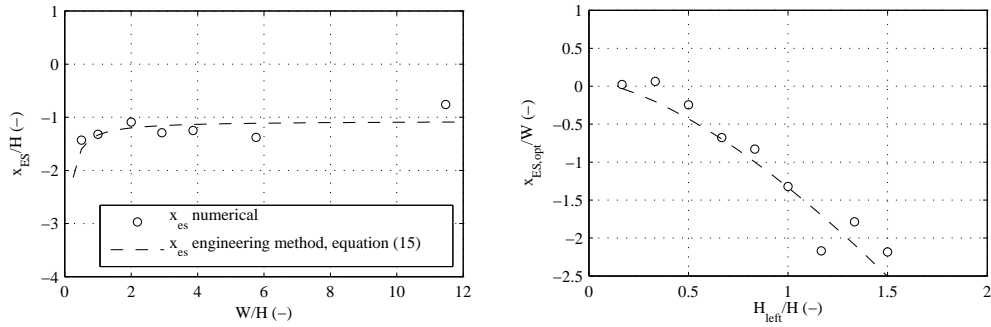


Figure 7: Optimal values of the equivalent source position  $x_{es}$  for 3D attenuation term  $A'_s$  for configuration (a) of Figure 2 and  $y_r=0$  m, as a function of the canyon width  $W$  with  $H = 19.2$  m, b) as a function of the left building height  $H_{left}$  with  $W = 19.2$  m.

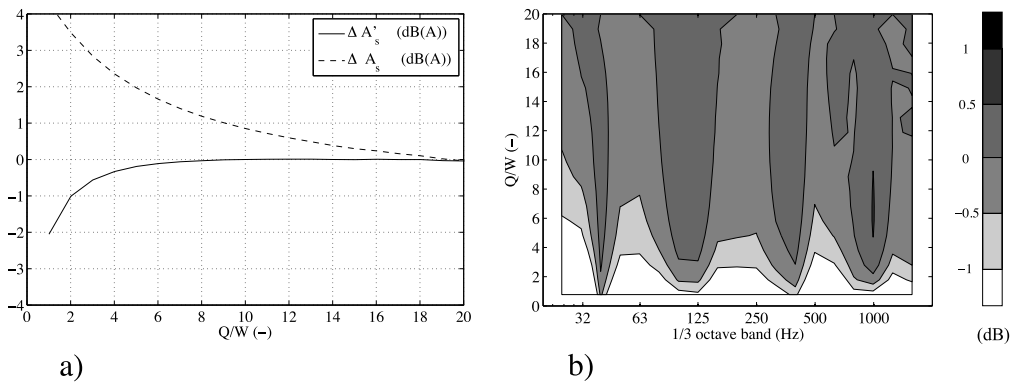


Figure 8: Attenuation terms computed from configurations *diffr,s* and *bar,s* of Figure 1, a)  $\Delta A_s$  and  $\Delta A'_s$  in dB(A), b)  $\Delta A'_s$ .

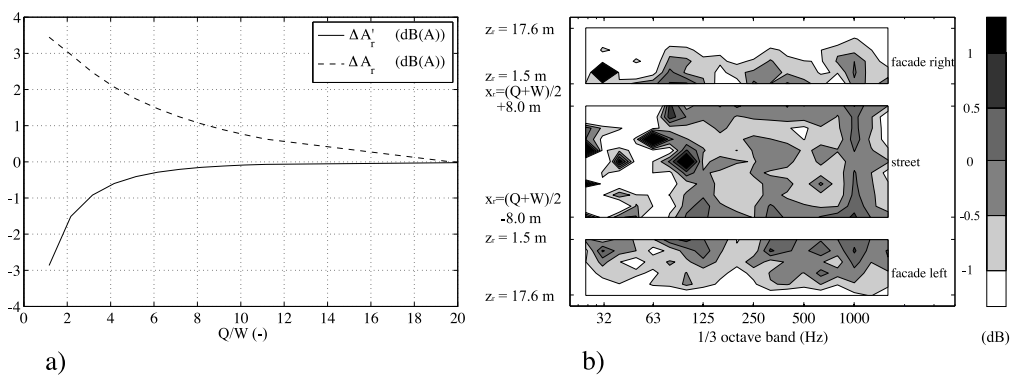


Figure 9: Attenuation terms computed from configurations *diffr,r* and *bar,r* of Figure 1, a)  $\Delta A'_r$  and  $\Delta A_r$ , averaged over all receiver positions, b)  $\Delta A'_r(Q = 4W)$  as a function of the receiver position and third octave bands.

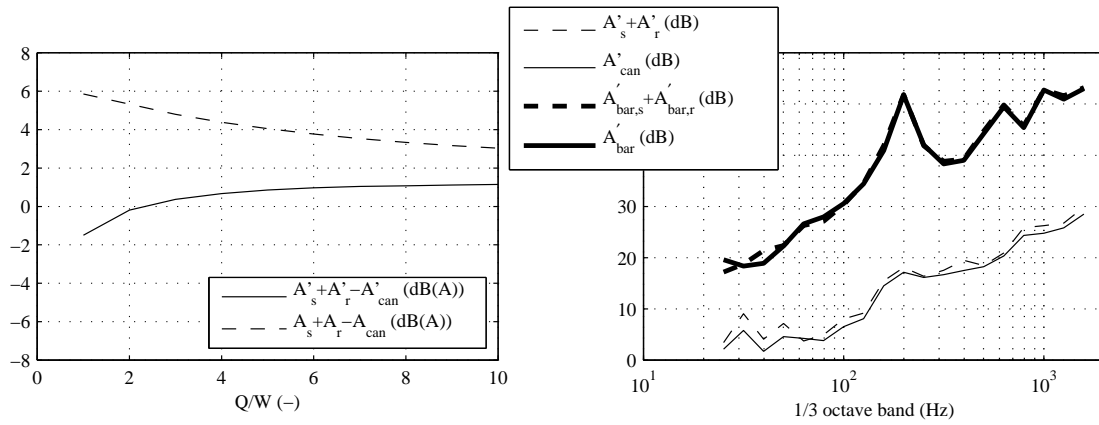


Figure 10: a) Broadband error of splitting the attenuation term  $A'_{can}$  into  $A'_s + A'_r$ , and  $A_{can}$  into  $A_s + A_r$ . Results have been averaged over all receiver positions, b) Results at  $Q = (10W)$  averaged over all receiver positions.

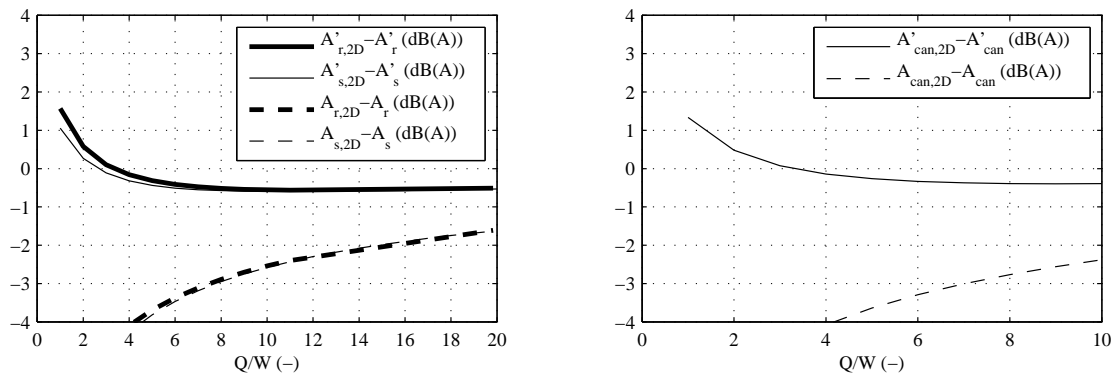


Figure 11: Broadband difference between 2D and 3D attenuation terms. Results have been averaged over all receiver positions, a) separate source and receiver environment terms, b) total canyon term.

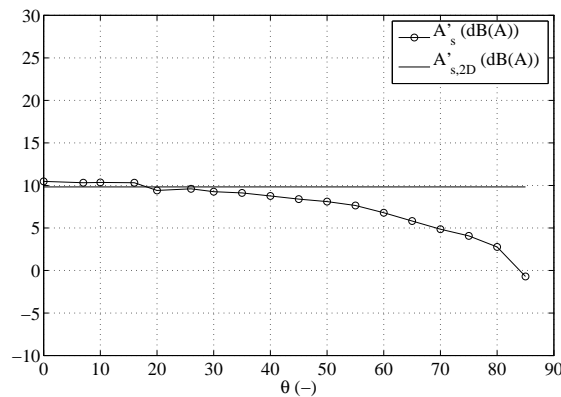


Figure 12: Broadband results of  $A'$  at  $Q = 19W$  up to 1.6 kHz for configuration of Figure 2(a).

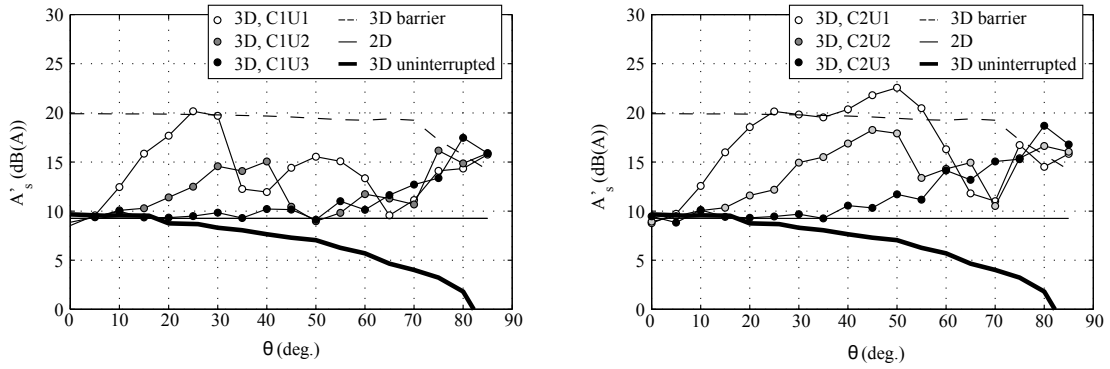


Figure 13: Broadband values up to 1 kHz at  $Q = 40W$  for configurations (a) and (c) as depicted in Figure 2.

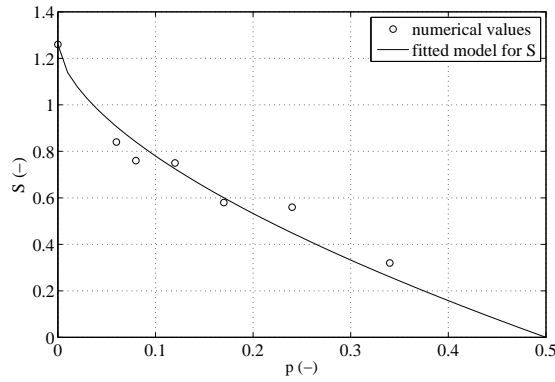


Figure 14: Angular averaged values of  $S = \left( A'_{\text{bar},s}(\theta = 0^\circ) - \bar{A}'_s \right) / \left( A'_{\text{bar},s}(\theta = 0^\circ) - A'_{s,2D} \right)$  for the various interrupted street configurations and the infinite street,  $p$  is the angular fraction of façades openings in the horizontal plane as seen from the source.

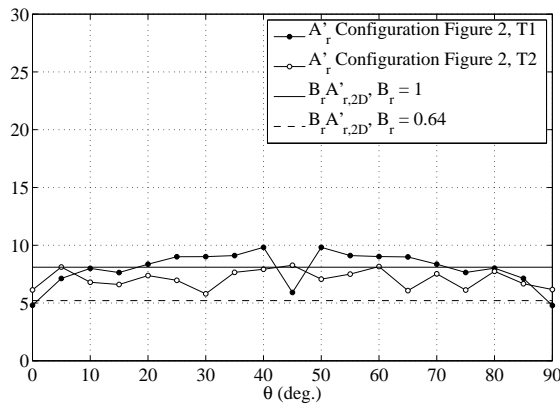


Figure 15: Broadband  $A'_r(\theta)$  values up to 1 kHz with source position at  $Q = 40 W$  for configuration (e) as depicted in Figure 2, and 2D result for  $\theta = 0^\circ$ .

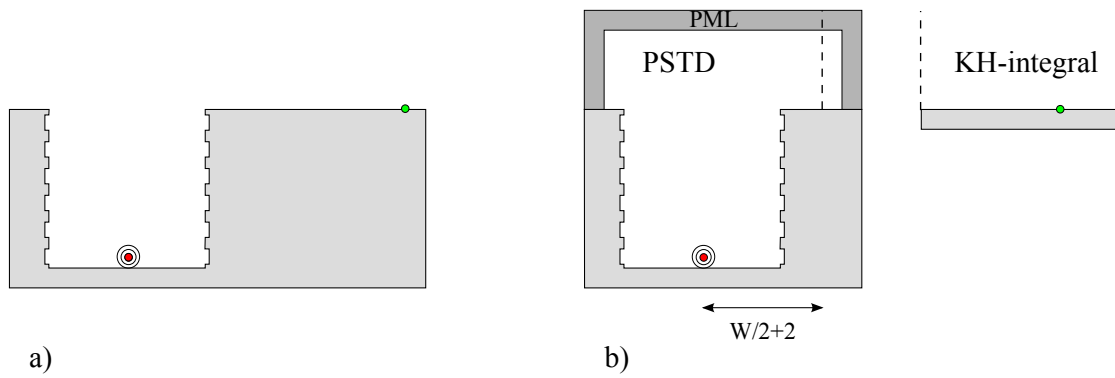


Figure 16: Two-step numerical approach to solve configuration of a), b) Application of PSTD method to solve source region part, and evaluation of the KH-integral equation to solve the region over roof level height.

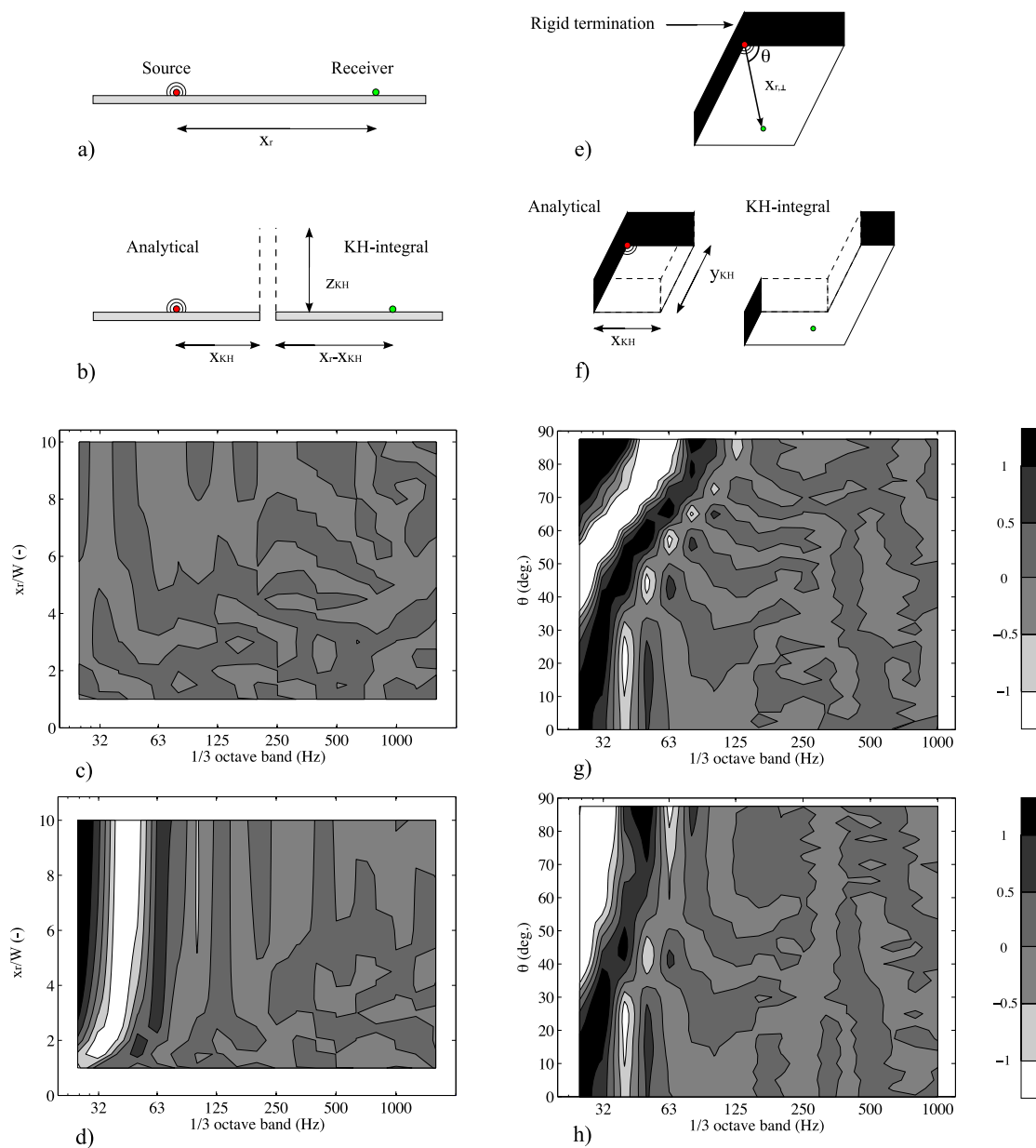


Figure 17: a) 2D configuration studied, b) Two-stage computational approach with analytical results at  $x_{KH}$  and KH-integral approach from  $x_{KH} = W/2 + 2$  m to receiver at  $x_r$ . c) Error of the KH-integral approach for  $z_{KH} = 30$  m for  $W = 19.2$  m, d) Error of the KH-integral approach for  $z_{KH} = 30$  m for  $W = 19.2 / \cos(\theta)$  m and  $\theta = 80$  deg., e) 3D configuration studied, f) Two-stage computational approach with analytical results at  $x_{KH} = W/2 + 2$  m and KH-integral approach to receiver at  $x_{r,\perp} = 20W$ ,  $W = 19.2$  m, g) Error of the KH-integral approach for  $z_{KH} = 30$  m for  $y_{KH} = 4W$  according to configurations (c,d) of Figure 2. h) Error of the KH-integral approach for  $z_{KH} = 30$  m for  $y_{KH} = 3W/2 + 2$  m according to configurations (e,f) of Figure 2 with  $T = 3W/2$ . Errors in dB.



## Appendix B

This is the author's version of a manuscript submitted to Acta Acustica united with Acustica

# Urban background noise mapping: the general model

W. Wei<sup>1</sup>, D. Botteldooren<sup>1</sup>, T. Van Renterghem<sup>1</sup>, M. Hornikx<sup>2,5</sup>, J. Forssén<sup>2</sup>, E. Salomons<sup>3</sup>,  
and M. Ögren<sup>4</sup>

<sup>1</sup>Department of Information Technology, Ghent University, Sint-pietersnieuwstraat 41, 9000 Ghent, Belgium, weigang@intec.ugent.be

<sup>2</sup>Department of Civil and Environmental Engineering, Chalmers University of Technology, Gothenburg, Sweden,

<sup>3</sup>TNO Urban Environment and Health, Delft, The Netherlands,

<sup>4</sup>Department of Environmental and Traffic Analysis, VTI, Gothenburg, Sweden,

<sup>5</sup>Building Physics and Services, Eindhoven University of Technology, Eindhoven, the Netherlands.

## Abstract

Surveys show that inhabitants of dwellings exposed to high noise levels benefit from having access to a quiet side. However, current practice in noise predicting often underestimates the noise levels at a shielded façade. Multiple reflections between façades in street canyons are commonly neglected and façades are approximated as perfectly flat surfaces yielding only specular reflection. In addition, sources at distances much larger than normally taken into account in noise maps might in some cases still contribute significantly. Since one of the main reasons for this poor approximation is computational burden, an efficient engineering model for the diffraction of the sound propagating over the roof tops is proposed, which considers multiple reflections, variation in building height, canyon width, building roughness and different roof shapes. The model is fitted on an extensive set of full-wave numerical calculations of canyon-to-canyon sound propagation with configurations matching the distribution of streets and buildings geometries in a typical historically grown European city. This model allows calculating the background noise in the shielded areas of a city, which could then be efficiently used to improve existing noise mapping calculations. The model was validated by comparison to long-term measurements at 9 building façades in the city of Ghent, Belgium. At shielded façades, a strong improvement in prediction accuracy is obtained.

## 1 Introduction

Several researchers found that inhabitants of dwellings exposed to road traffic noise levels can benefit from having access to a quiet side [1, 2, 3, 4]. The European Environmental Noise Directive specifies that a quiet side is present when the noise level at the shielded façades is at least 20 dBA lower than the noise level at the most exposed façades of the dwelling (Directive 2002/49/EC of the European Parliament and Council of 25 June 2002 Relating to the Assessment and Management of Environmental Noise) [5]. However, there is still some debate about accurately defining a quiet

side [6]. In typical European cities, many enclosed shielded courtyards and parks exist that can provide such quiet areas. Notwithstanding the lack of a good definition, research on quiet sides and its implementation in urban planning also suffers from a lack of accuracy in commonly used noise mapping when it comes to predicting noise levels in urban shielded areas. The EU is currently renewing its guidelines for methods to be used in noise mapping [7], yet the lack of accuracy of noise mapping in shielded areas is mainly due to the choices made during implementation and application of the methods. Typically, the underestimation of the noise level at such shielded places, is caused by limiting the number of reflections in streets and by neglecting contributions of distant sources that could become dominant. To solve these problems, simplified theoretical models, such as the “flat city model” and the “equivalent source model(ESM)”, were recently developed to predict the noise level in shielded courtyards [8, 9]. However, these models need further improvement. For example, the coupling between the sound field inside a street canyon and the propagation above the roofs can depend on the difference in height of the buildings forming the street canyon. The ESM, e.g., is computationally too costly to cover a whole city. In this paper, an efficient engineering model for background noise mapping is proposed that is inspired by the concept of the “flat city model” and a new approximation to more advanced diffraction formulas. The coefficients of the proposed engineering model are fitted on an extensive set of 2-D finite-difference-time-domain (FDTD) simulations [10, 11] of canyon-to-canyon sound propagation. The effect of multiple reflections, variation in building height, canyon width, building façade roughness, finite impedance and roof shape is taken into account. The proposed engineering model is designed to complement 2.5D calculation methodologies. The direct field, reflection in the horizontal plane as well as diffraction around vertical edges is assumed to be accounted for by the “parent” model (e.g. following the CNOSSOS methodology [7]). The proposed extension calculates the contribution to the noise level caused by all sources that are shielded by at least one building. In this, a building is a construction of at least 4m high and at least 5m wide; conventional noise barriers are expected to be correctly included in the “parent” model. The resulting “background” noise level should be added to a contribution obtain using standard noise mapping techniques, ignoring the contribution diffraction over buildings. With this approach the national and international standard methods currently in use can still be applied. For every contributing source the suggested procedure for calculating the “background” noise level at the shielded location reads:

$$L_{pb} = 10 \log_{10} (10^{0.1L_{pdb}} + 10^{0.1L_{p,scatter}}) \quad (1)$$

$$L_{pdb} = L_W - A_{free} - A_{diffr} - A_{inter} \quad (2)$$

$$A_{diffr} = -10 \log_{10} (10^{-0.1A_{bar}} + 10^{-0.1A_{can}}) \quad (3)$$

where,

- $L_{pb}$  = the “background” sound level excluding the diffraction and reflections around the vertical edges and excluding the diffraction over conventional noise barriers [dB].
- $L_{pdb}$  = the contribution to the “background” level in still, homogeneous atmosphere [dB].
- $L_W$  = sound power level per octave band of a point source representing part of the road, no

directivity is taken into account since multiple sources will contribute to the shielded level as well as multiple reflections from various directions [dB].

- $A_{diff_r}$  = the total shielding attenuation limited by diffraction over the building roof [dB].
- $A_{free}$  = 3D free field divergence [dB].
- $A_{bar}$  = the attenuation by the building(s) cutting the direct path between source and receiver limited by diffraction over the building roof, including the effect of the ground. Only the direct diffraction path without reflections in the canyon is considered [dB].
- $A_{can}$  = the attenuation of the sound following a path between source and receiver including at least one reflection in the source and/or receiver canyon. If canyons are present, this term quickly dominates  $A_{bar}$  and thus determines  $A_{diff_r}$  [dB].
- $A_{inter}$  = additional attenuation caused by the diffraction at intermediate canyons [dB].
- $L_{p,scatter}$  = the contribution to the background sound level caused by scattering from atmospheric turbulence [12].

Atmospheric absorption is not included explicitly in this model but is implicit in the fitting of  $A_{can}$  terms. One of the major assumptions for the model is that the sound propagation in 3D can be calculated by the summation of many 2D sections. This so called 2.5D approach is quite common, it also forms the basis of the Harmonoise reference model [13] and the CNOSSOS methodology [7]. Also the full wave numerical model used to extract the coefficients in the proposed equations cannot be used for 3D simulations due to CPU-time limitations. Therefore, also for the reference calculation, the line sources are split into many emission points and all contributions are summed. In this approach, facades are “twisted” so their faces become normal to the line connecting source-receiver [14]. Numerical simulations showed that when the twisted angle was less than 70 degree, the relative error between the 2D and 3D calculation is less than 1.5 dB [15]. A correction for 3D free field spreading of the contributions of reflections is taken into account. A second important assumption is that wind and temperature gradients do not affect the  $A_{bar}$  and  $A_{can}$  terms. For the  $A_{inter}$  term meteorological effects (except scattering) are considered implicitly since downwind refraction over larger distances may have a noticeable effect.

This paper is organized as follows: in section 2, the configurations and setups of the simulations that are used for fitting the engineering model are introduced; in section 3, the attenuation terms (A-terms) are studied in detail; in section 4, the calculated background noise levels are compared to long-term measurements at 9 locations in the city of Ghent, Belgium. The latter comparison includes the contribution from turbulence scattering, but the derivation and validation of the equations is given in a companion paper [12].

## 2 Simulation configurations and setups

The simulations cover different widths of source canyons, receiver canyons and intermediate buildings, as well as different building heights. Distributions of these parameters for a typical historically grown European city, are extracted from a GIS-building layer for the city of Ghent. The distribution of the projected canyon and building widths along each source-receiver line is shown in figure (1). Note that the width is defined along a line that is not necessarily orthogonal to the building façade, which

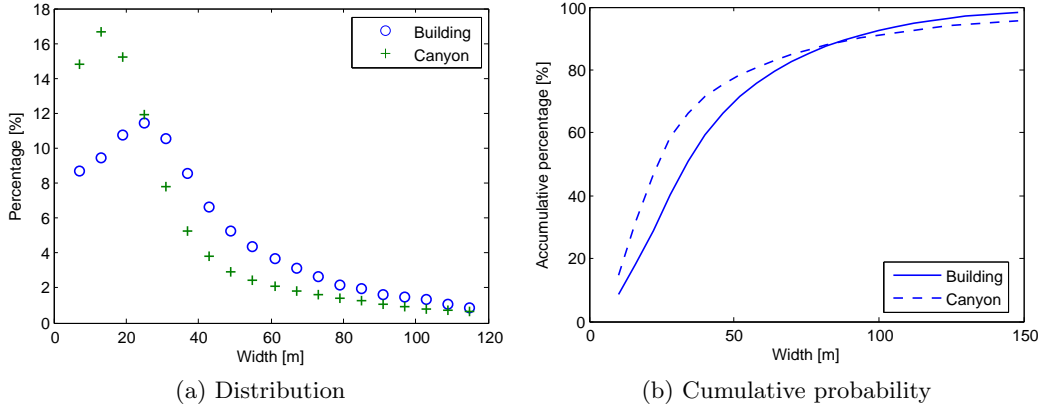


Figure 1: Distribution of the projected building and canyon width in the city of Ghent, Belgium

is compatible with the point-to-point model that is proposed. 72% of the projected buildings widths and 78% of the canyons are less than 50m wide. Besides, the most frequent projected widths of the buildings and canyons are 24m and 12m, respectively. The full wave numerical simulations on which the engineering model is based are limited to canyon and building widths between 4.8m and 38.2m. The heights of the buildings are varied from 0 to 16m. The building facades are modeled in a realistic way by assigning different materials and making the façade surface irregular to allow for the build-up of a diffuse sound field in the city canyons. The road surface is modelled as perfectly reflecting both in source and receiver canyon. In these simulations, the specific acoustic impedance of windows and brick walls are taken as  $Z_n = 77$  and  $Z_n = 10$  [16]. Receivers are located along the façade and across the canyons. A typical simulation configuration is shown in figure (2), where,  $W_s$ ,  $W_i$ ,  $W_r$  are the width of the source canyon, intermediate building and receiver canyon respectively.  $H_i$  is the height of the building in the direct sound path, and  $H_s$ ,  $H_r$  are the heights of the buildings flanking the source and receiver canyon respectively. Since the sound waves travel a longer distance because of multiple reflections, the air could absorb more sound energy than during direct propagation between source and receiver. The effect of the air absorption, with  $T = 10^\circ\text{C}$  and Humidity= 70%, is added to the simulated impulse response using the approach proposed in references [17, 18].

The multiple reflection effect will change with the relative location of the source and receiver, the height of the buildings and the width of the canyon and buildings. 565 configurations with combinations of these parameters were simulated.

The excess attenuation caused by screening and ground effects was proven not to be affected too much by whether the source is a line source or a point source [19]. However, in the case of multiple reflections in a street canyon, small differences might still occur. Therefore, an the time-domain response is multiplied by  $1/\sqrt{ct}$  to approximately translate the line source propagation to point source propagation [20]. In our data post-processing, this technique is used to approximate point source propagation from canyon to canyon.

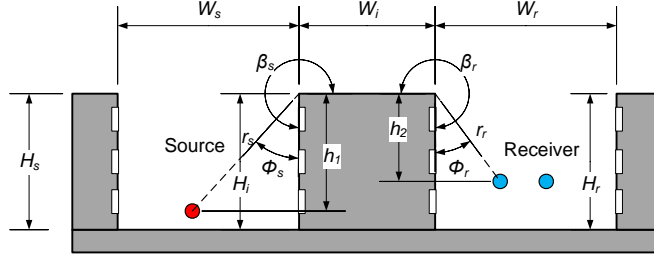


Figure 2: A typical simulation configurations, where  $W_s$ ,  $W_i$  and  $W_r$  are the width of source canyon, intermediate building and receiver canyon;  $H_s$ ,  $H_i$  and  $H_r$  are the height of the left, intermediate and right building;  $h_1$  and  $h_2$  are the distance from the source or receiver to the top of the building;  $\phi_s$  and  $\phi_r$  are the angle between the building façade and the connecting line from the source or receiver to the diffraction edge;  $\beta_s$  and  $\beta_r$  are the outside angle of the building which equals  $3\pi/2$  in this study.

### 3 Analysis of attenuations terms: $A_{bar}$ , $A_{can}$ , and $A_{inter}$

#### 3.1 $A_{bar}$

$A_{bar}$  is the attenuation of a thick barrier including the presence of the ground. In absence of canyons and in case of a flat roof, it is the only remaining term. In this study  $A_{bar} = A_{bar}^f + A_{bar,roof}$ , where,  $A_{bar}^f$  is the attenuation of a rigid barrier with flat roof;  $A_{bar,roof}$  is the correction of the roof shape in dB.

##### 3.1.1 $A_{bar}^f$ : rigid barrier with flat roof

In most noise mapping standards (including CNOSSOS), the ISO9613-2 diffraction formula or similar is used to calculate  $A_{bar}^f$ . By comparing with in situ long term measurement [21] and FDTD simulation, it was found that using the ISO standard to calculate  $A_{bar}$  underestimates the attenuation considerably. According to the literature [22, 23, 24, 25],  $A_{bar}^f$  can be expressed with high accuracy by equation (4):

$$A_{bar,0}^f = -10 \log_{10} \left( \frac{R}{L} \right)^2 ([f^2(X_1) + g^2(X_1)] [f^2(X_2) + g^2(X_2)]) \quad (4)$$

where,  $X_1 = Y_s$  and  $X_2 = B Y_r$  when  $Y_s > Y_r$ ;  $X_1 = B Y_s$  and  $X_2 = Y_r$  when  $Y_s < Y_r$ . Definitions of parameters are shown in figure (2).  $Y_s$  and  $Y_r$  are functions of geometrical positions and diffraction angles.  $Y_s = \gamma_s M_{\nu_s}(\beta_s - \phi_s)$ ,  $Y_r = \gamma_r M_{\nu_r}(\beta_r - \phi_r)$ ,  $\gamma_s = \sqrt{2r_s(W_i + r_r)/(\lambda L)}$ ,  $L = \sqrt{(r_s + r_r + W_i)^2 + (z_s - z_r)^2}$ , ( $z_s = z_r$  in the two dimensional case considered here),  $R$  is the distance between source and receiver,  $B = \sqrt{W_i(W_i + r_s + r_r)/[(W_i + r_s)(W_i + r_r)]}$  and  $M_{\nu_s}(\theta) = \frac{\cos(\nu\pi) - \cos(\nu\theta)}{\nu \sin(\nu\pi)}$ ,  $\nu_s = \pi/\beta_s$  and  $\nu_r = \pi/\beta_r$ .  $f(Y)$  and  $g(Y)$  are functions of Fresnel integrals  $C$  and  $S$  [22]:

$$f(Y) = \left(\frac{1}{2} - S\right) \cos\left(\frac{1}{2}\pi Y^2\right) - \left(\frac{1}{2} - C\right) \sin\left(\frac{1}{2}\pi Y^2\right) \quad (5)$$

$$g(Y) = \left(\frac{1}{2} - C\right) \cos\left(\frac{1}{2}\pi Y^2\right) + \left(\frac{1}{2} - S\right) \sin\left(\frac{1}{2}\pi Y^2\right) \quad (6)$$

The combination  $f^2 + g^2$  needed in equation (4) simplifies since the cosine and sine functions cancel out, reducing the expression to:

$$f^2(Y) + g^2(Y) = C^2(Y) + S^2(Y) - C(Y) - S(Y) + 0.5 \quad (7)$$

where  $Y$  is the input argument;  $C$  and  $S$  are Fresnel integrals. For the noise mapping model, calculating the Fresnel integrals is too computationally costly, so an approximation has to be found.

For this, it is first observed that the distances involved in the diffraction formulas, and in particular  $W_i$ , are generally large compared to the wavelength for diffraction over buildings. Thus  $\gamma$  will be large. Sources and receivers at ground level and realistic building shape,  $\beta - \phi$  will remain larger than  $\pi$  and it can be verified that  $M_\nu$  is not smaller than one. For these cases, the input argument  $Y$  satisfies  $Y \gg 0$ . For large arguments, the Fresnel integrals can be approximated by [26]:

$$C(x) \approx 0.5 + \frac{1}{\pi x} \sin\left(\frac{\pi}{2}x^2\right) \quad (8)$$

$$S(x) \approx 0.5 - \frac{1}{\pi x} \cos\left(\frac{\pi}{2}x^2\right) \quad (9)$$

Introducing equation (8 and (9)) into equation (7) results a very simple form for  $f^2 + g^2$ :

$$f^2(Y) + g^2(Y) = \frac{1}{(\pi Y)^2} \quad (10)$$

However, when the source or observer are in the extension of the plane of the roof, the angle difference  $\beta - \phi$  approaches  $\pi$  and  $M_\nu$  approaches zero which makes  $S(Y)$ ,  $C(Y)$  and  $f^2(Y) + g^2(Y)$  become singular. To avoid this strong singularity while keeping the error at larger  $x$  limited, a small constant is added to the numerator and denominator. Based on an analysis of typical urban situation that will be explicit below, the following approximation of equation (10) is proposed below:

$$f^2(Y) + g^2(Y) = \left(\frac{0.37}{x + 0.37}\right)^2 \quad (11)$$

Thus, equation (4) is simplified to:

$$A_{bar,0}^f \approx -10 \log_{10} \left(\frac{R}{L}\right)^2 \left(\frac{0.37}{X_1 + 0.37}\right)^2 \left(\frac{0.37}{X_2 + 0.37}\right)^2 \quad (12)$$

When  $Y_s > Y_r$ ,  $X_1 = \sqrt{\frac{6r_s(W_i+r_r)}{\lambda(r_s+W_i+r_r)}} |-0.5 + \cos(2/3\phi_s)|$ ,  $X_2 = \sqrt{\frac{6r_r W_i}{\lambda(W_i+r_r)}} |-0.5 + \cos(2/3\phi_r)|$ ;  
when  $Y_s < Y_r$ ,  $X_1 = \sqrt{\frac{6r_s W_i}{\lambda(r_s+W_i)}} |-0.5 + \cos(2/3\phi_s)|$ ,  $X_2 = \sqrt{\frac{6r_r(W_i+r_r)}{\lambda(r_s+W_i+r_r)}} |-0.5 + \cos(2/3\phi_r)|$ .

Figure (3) illustrates how for a typical urban sound propagation case, the large argument approximation and the proposed approximation for the Fresnel Integrals differ from the accurate calculation. Although there is a small increase in inaccuracy for the proposed approximation when  $\phi_r$  is very small, a strong benefit can be observed for  $\phi_r > \pi/3$ . Even when  $\phi_r = \pi/2$ , there is still less than 3dB deviation. Let us now have a closer look at the situation where the approximation of large argument for the Fresnel integral fails. At  $X = 0$  the approximate formula gives 1 while knowing that  $C$  and  $S$  become zero at  $X=0$ , the actual value should be 0.5, which implies a 3dB error. It should however be kept in mind that this situation will only occur for very few of the source receiver

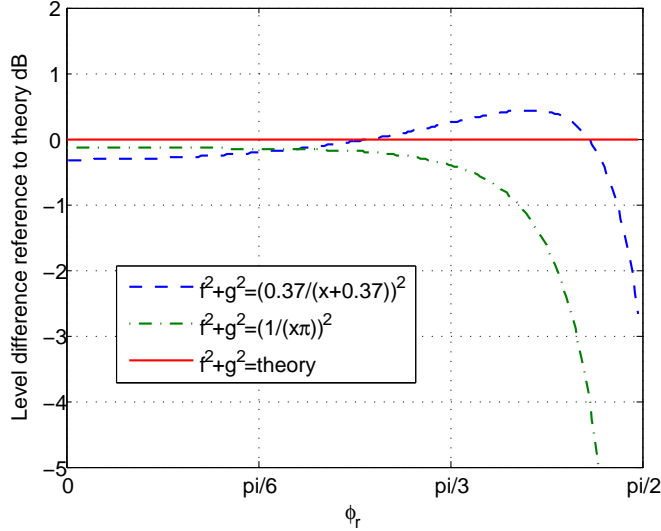


Figure 3: Error estimation of  $f^2 + g^2$  compared with the theoretical values. In this case,  $W_i = 10\lambda$ ,  $r_s = r_r = 10\lambda$ ,  $\beta_s = \beta_r = \frac{3\pi}{2}$ ,  $\phi_s = \frac{\pi}{4}$ ,  $\phi_r$  increases from 0 to  $\pi/2$

paths contributing to the overall noise level. To further illustrate why the proposed approximation is so appropriate for diffraction over buildings, the distribution of the input  $X$  is extracted for the city of Ghent and plotted together with error contours in figure (4). At the X1 and X2 combinations where the distribution peaks, the error introduced by using equation (12) is particularly small and it stays below 1.5 dB for all combinations that have a significant probability of occurring.

With this simplification, the Fresnel integrals are canceled out and a simple function of the geometrical parameters remains, which could reduce computing time considerably and make it easier to implement. It is suggested to include contributions from the image sources explicitly as a rule. However, as the source height is usually very low, the diffraction term does not differ between the path from the original source and from the image source and the calculation can be simplified by assuming that  $A_{bar,1}^f$  for image source is the same as  $A_{bar,0}^f$  for source. The total  $A_{bar}^f$  can be achieved by summing up the contribution of paths “source  $\rightarrow$  receiver”  $A_{bar,0}^f$ , “image source  $\rightarrow$  receiver”  $A_{bar,1}^f$ , “source  $\rightarrow$  image receiver”  $A_{bar,2}^f$  and “image source  $\rightarrow$  image receiver”

Figure (5) shows the comparison between the calculated  $A_{bar}^f$  and the simulation with FDTD including the reflection from a rigid ground. The source is on the ground and 4.8m to the barrier; the receiver is located at height of 4.4m and 4.5m to the barrier; the barrier width varies from 10m to 80m and the barrier height is 11m. The engineering approach  $A_{bar}^f$  matches the full-wave numerical simulation results quite well.

### 3.1.2 $A_{bar,roof}$ : correction of roof shape

In some European city centers, gabled roofs are very common. The sound waves propagating over an idealized gabled roof may be diffracted once, twice or three times. It should be noted that roofs may be more complicated and diffraction may result in a wide range of significantly different sound attenuation [27]. The effect of roof depends on the source and receiver position, the angle of the roof

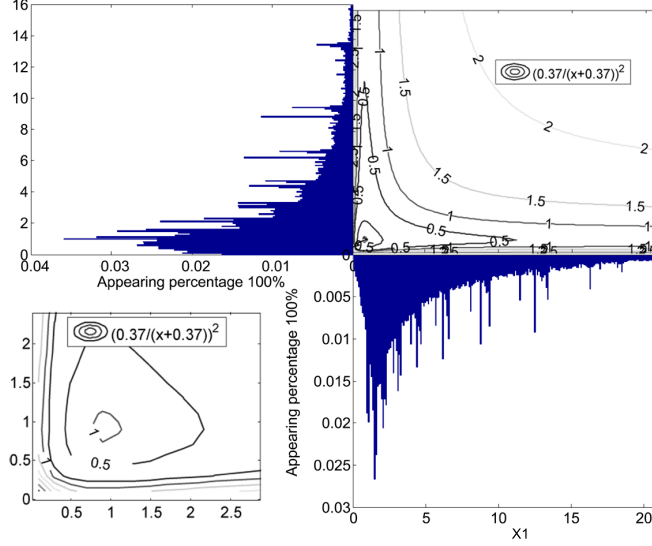


Figure 4: Error estimation reference to the theoretical solution, where “ $\left(\frac{0.37}{x+0.37}\right)^2$ ” indicates the equation (11). Every line indicates 0.5dB difference.

and the building height. According to the statistics for Ghent (as a typical old European city), the most common width of canyons and buildings is 12m and 24m and the mean height of the buildings is 10.9m. If the height of the roof is supposed to be 4.5m, then most of the sources and receivers below 4.5m high would be located inside the shadow region where the sound wave has to diffract three times to reach the receiver at the other side of the building, as shown in figure (9). In most cases, it has to account for the additional loss due to a third diffraction, while the diffraction on the original corners is slightly reduced.

$$A_{bar,roof} = q_0 A_{bar}^f + q_1 \quad (13)$$

Based on fitting on 1788 numerical calculations,  $q_0 = 0.27$  and  $q_1 = 2.9$ , with the mean squared error of the fit equal to 3.0. The fitting database covers building height from 6m to 16m and building width from 10m to 160m. When the source canyon or the receiver canyon exists, the image source or the image receiver would most probably lie outside the three-diffraction region, which means that the effect of roof shape on the multiple-reflection path would probably be much more important. The roof effect in these cases is discussed in detail in section(3.2) as  $A_{can,roof}$ .

### 3.2 $A_{can}$

$A_{can}$  is the attenuation of the sound following a path between source and receiver including at least one reflection in the source and/or receiver canyon.  $A_{can} = A_{can}^f + A_{can,roof}$ , where  $A_{can}^f$  is the extra attenuation in case of a flat roof on the intermediate building;  $A_{can,roof}$  is a correction accounting for a different roof shape in dB.

An analytic formulation for the additional effect of the canyons has to fulfill some requirements: 1) when the height of the outer buildings goes to zero, the term should vanish; 2) when the outer

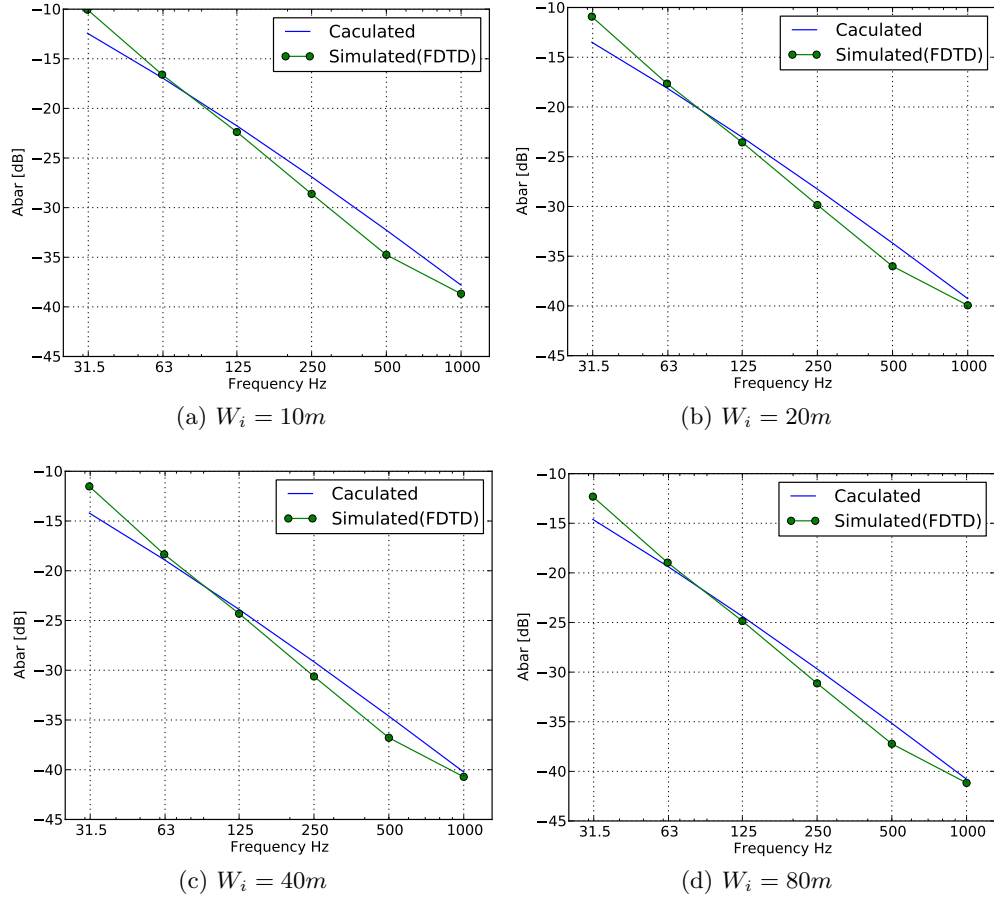


Figure 5: Comparison between  $A_{bar}^f$  and FDTD simulations(rigid thick barrier on rigid ground).

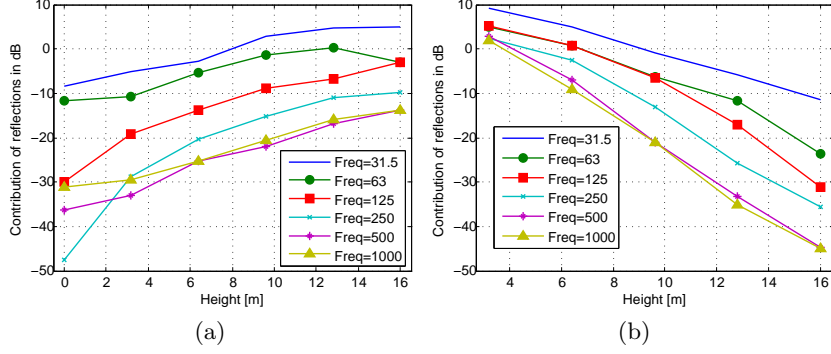


Figure 6: (a)Contribution of reflections caused by increasing  $H_s$  with  $W_s = W_r = 9.6\text{m}$ ,  $W_i = 10\text{m}$ ,  $H_i = H_r = 9.6\text{m}$ , source height ( $Z_s$ )  $0.5\text{m}$ , receiver height ( $Z_r$ )  $4.5\text{m}$ ; (b)Contribution of reflections caused by increasing  $H_i$  with  $H_s = H_r = W_s = W_r = 9.6\text{m}$ ,  $W_i = 10\text{m}$ ,  $Z_s = 0.5\text{m}$ ,  $Z_r = 4.5\text{m}$

buildings becoming much higher than the screening building,  $A_{can}$  should saturate with further increase of the outer building height.

### 3.2.1 Contribution of multiple reflections

Multiple reflections occur at the facades of the outer buildings and intermediate building. However, these buildings influence the canyon-to-canyon propagation in a different way. When  $H_s$  or  $H_r$  increases, the effect of multiple reflections increases monotonically at all frequencies to saturate at a maximum value. Figure (6a) shows the relation between  $H_s$  and the numerical calculation of  $A_{can}^f$ , which is  $10 \log_{10} \left( 10^{0.1L_{pFDTD}} - 10^{-0.1A_{bar}^f} + 10^{0.1A_{free}} \right)$ . A similar trend is observed by changing  $H_r$ . When  $H_i$  increases, the effect of multiple reflections increases at one hand. At the other hand, the shielding of the middle building also increases. When the height of  $H_i$  is lower than a threshold, the effect of multiple reflections is more important than the effect of shielding. However, since the receivers are usually located at  $4\text{m}$  in a noise mapping and the height of a 2-floor building exceeds  $6\text{m}$  in most cases, this effect is not important here. Similar to  $A_{bar}$  term,  $A_{can}^f$  is also frequency dependent.

### 3.2.2 Analytic form for $A_{can}^f$

To derive the general form of the analytic expression that will be fitted to the numerical results, diffraction over the central building from multiple image sources in the source canyon to multiple image receivers in the receiver canyon is studied. The total sound pressure at the receiver caused by all of these propagation paths can be summed incoherently. The total contribution is:

$$\sum_{i=0}^{\infty} \sum_{j=0}^{\infty} |p_{i,j}|^2 = |p_{0,0}|^2 + \sum_{i=1}^{\infty} |p_{i,0}|^2 + \sum_{j=1}^{\infty} |p_{0,j}|^2 + \sum_{i=1}^{\infty} \sum_{j=1}^{\infty} |p_{i,j}|^2 \quad (14)$$

where the subscript indicates the position of the source, the receiver and the image sources and image receivers, i.e.  $i = 0$  indicates the source position and  $j = 0$  indicates the receiver position;

the  $i = 1, 2, 3, \dots$  indicates different image sources; similarly,  $j = 1, 2, 3, \dots$  indicates different image receivers.  $|p_{0,0}|^2$  contains the part of the sound pressure square at the receiver, emitting by the source and diffracted directly over the building. This term is included in  $A_{bar}^f \cdot \sum_{i=1}^{\infty} |p_{i,0}|^2$  indicates the total sound pressure square at the receiver position, emitting by all the image sources.  $\sum_{j=1}^{\infty} |p_{0,j}|^2$  indicates the sound pressure square emitted by the source and received by all the image receivers (i.e. located at the image receiver positions).  $\sum_{i=1}^{\infty} \sum_{j=1}^{\infty} |p_{i,j}|^2$  indicates the total sound pressure square at all the image receiver positions, emitting by all the image sources. For each of these three terms, an analytic expression is now derived.

### 3.2.3 Analytic solutions of $\sum_{i=1}^{\infty} |p_{i,0}|^2$ and $\sum_{j=1}^{\infty} |p_{0,j}|^2$

Image sources will occur in the direction away from the intermediate building and in the direction of this building. Because the diffraction angle is much larger and the distance is comparable for the latter set, it can easily be shown that these can be neglected. Thus the derivation can focus on the image sources away from the intermediate building. A few assumptions are listed before hand: the first assumption is that the buildings are not very low. Accordingly, the decay caused by the finite size of the reflecting surface that could be expressed as a decaying overlap between the surface and the Fresnel zone can be ignored even after many reflections. This decay will be considered in a fitting coefficient later. Second assumption is the building height of the source canyon and receiver canyon are the same. As a result, the image sources can reach to the receiver or image receivers by double diffraction. Afterwards, other conditions such as,  $H_s < H_i$ ,  $H_r < H_i$ ,  $H_s > H_i$  and  $H_r > H_i$  will be studied. With the above assumptions and equation (4), the square of the sound pressure generated by the  $i$ th image source is:  $|p_{i,0}|^2 = \left( \frac{0.37}{X_{i,0,1} + 0.37} \right)^2 \left( \frac{0.37}{X_{i,0,2} + 0.37} \right)^2 |p_{at,L_i}|^2$ . For a point source, the sound pressure at distance  $L_i$  is  $p_{at,L_i} = \frac{A}{4\pi L_i} e^{-jkL_i}$ , where A is the amplitude. Note that in accordance with the diffraction theory  $L_i$  is the shortest path between source and receiver around the diffracting elements. Then the sum of  $p_{i,0}$  is:

$$\sum_{i=1}^{\infty} |p_{i,0}|^2 = \sum_{i=1}^{\infty} \left| \frac{\alpha^i A}{4\pi} \right|^2 \left| \frac{1}{L_{i,0}} \right|^2 \left( \frac{0.37}{X_{1,i,0} + 0.37} \right)^2 \left( \frac{0.37}{X_{2,i,0} + 0.37} \right)^2 \quad (15)$$

In a general case,  $Y_s = M_{\nu s} \gamma_s = \sqrt{\frac{2r_{s,i}(r_r + W_i)}{r_{s,i} + r_r + W_i}} \sqrt{3} (\cos \frac{2}{3} \phi_{s,i} - 0.5)$ . For  $\phi_{s,i}$  in the range between 0 and  $\pi/2$ , which is the shielded area,  $\cos \frac{2}{3} \phi_{s,i} - 0.5$  can be approximated by  $0.5 \cos \phi_{s,i}$  which is calculated as  $0.5h_1/r_{s,i}$ . It can easily be verified that this approximation introduces a very small error,  $std = 0.0056$  in more than 1500 checking samples. As a result,  $Y_s$  and  $Y_r$  can be simplified as:

$$Y_{s,i} \approx \sqrt{\frac{2r_{s,i}(r_r + W_i)}{r_{s,i} + r_r + W_i}} \frac{\sqrt{3}}{2} \cos \phi_{s,i} = \sqrt{\frac{2r_{s,i}(r_r + W_i)}{r_{s,i} + r_r + W_i}} \frac{\sqrt{3}}{2} \frac{h_1}{r_{s,i}}; \quad (16)$$

$$Y_{r,i} \approx \sqrt{\frac{2r_r(r_{s,i} + W_i)}{r_{s,i} + r_r + W_i}} \frac{\sqrt{3}}{2} \cos \phi_{r,i} = \sqrt{\frac{2r_r(r_{s,i} + W_i)}{r_{s,i} + r_r + W_i}} \frac{\sqrt{3}}{2} \frac{h_2}{r_r}; \quad (17)$$

According to the diffraction theory, the factor B has to be multiplied to the smallest of the two Y terms. Therefore we have a closer look at the ratio  $Y_{s,i}/Y_{r,i}$  which is  $\frac{h_1}{h_2} \sqrt{\frac{r_r(r_r + W_i)}{r_{s,i}(r_{s,i} + W_i)}}$ . Considering that the receiver is generally higher than the source and that all façades of buildings or mostly of the same height,  $h_1 > h_2$ . In most cases it can be shown that this ratio is less than 1 after a few

reflections, since  $r_{s,i} \gg r_r$  is expected. For deducing an analytic form for  $A_{can}^f$ , all  $Y_{s,i}$  are supposed to be less than  $Y_r$ . As a result,  $X_{1,i,0} = Y_{s,i}B$  and  $X_{2,i,0} = Y_r$ .

Let us now consider the second term in equation (15) which we call  $C_{1s}$  for convenience:

$$\begin{aligned} C_{1s} &= \left( \frac{0.37}{X_{2,i,0} + 0.37} \right)^2 \approx \left( \frac{0.37}{\sqrt{\frac{2r_r(W_i+r_{s,i})}{\lambda(r_{s,i}+W_i+r_r)}} \frac{\sqrt{3}}{2} \cos \phi_r + 0.37} \right)^2 \\ &\approx \left( \frac{0.37}{\sqrt{\frac{2r_r}{\lambda} \frac{\sqrt{3}}{2} \cos \phi_r} + 0.37} \right)^2 \end{aligned} \quad (18)$$

which becomes independent of  $i$  when it can be assumed that  $W_i + r_{s,i} \gg r_r$ , which is the case for higher order reflections at least. The remaining part of equation (15) can be rewritten as:

$$\begin{aligned} \left| \frac{1}{L_{i,0}} \right|^2 \left( \frac{0.37}{X_{1,i,0} + 0.37} \right)^2 &\approx \left( \frac{0.37}{\sqrt{\frac{2r_{s,i}W_i}{\lambda(W_i+r_{s,i})}} \frac{\sqrt{3}}{2} \cos(\phi_{s,i})L_{i,0} + 0.37L_{i,0}} \right)^2 \\ &= \left( \frac{1}{\sqrt{\frac{2W_i(r_{s,i}+W_i+r_r)}{\lambda(r_{s,i}+W_i)}} \frac{\sqrt{3}}{0.74} h_1 \sqrt{\frac{(r_{s,i}+W_i+r_r)}{r_{s,i}}} + (r_{s,i} + W_i + r_r)} \right)^2 \end{aligned} \quad (19)$$

Again assuming that  $r_{s,i} + W_i \gg r_r$ , the first square root term simplifies and becomes independent of the reflection order  $i$ .  $\sqrt{\frac{(r_{s,i}+W_i+r_r)}{r_{s,i}}}$  is difficult to handle but fortunately assuming that it is close to 1 introduces at most 3dB of error for the  $r_{s,i}$  and  $W_i$  that can be expected in an urban setting. The reader should keep in mind that the purpose of this derivation is to extract an analytic form with coefficients that will be fitted on numerical simulation results. As a result of these approximations, the total sum of equation (15) is reduced to:

$$\sum_{i=1}^{\infty} |p_{i,0}|^2 = C_{1s} \sum_{i=1}^{\infty} \left| \frac{\alpha^i A}{4\pi} \right|^2 \left( \frac{1}{\sqrt{\frac{2W_i}{\lambda} \frac{\sqrt{3}}{0.74} h_1} + r_{s,i} + W_i + r_r} \right)^2 \quad (20)$$

The first term in the denominator is independent of the image source index  $i$ . This implies that the approximations made above boil down to assuming that the effect of increasing distance from the image source to the diffraction edge is neatly compensated by the effect of changing diffraction angle. To simplify the sum further it is now assumed that the source is positioned in the middle of the canyon and that when  $r_{s,i}$  becomes large compared to the height of the canyon above the source  $h_1$ , its value can be approximated by  $r_{s,i} \approx D_i$ , where  $D_i = i * W_s + 0.5W_s$  is the horizontal distance from the  $i$ th image source to the edge of the building façade. In this case, the sum is a special function:

$$\sum_{i=1}^{\infty} |p_{i,0}|^2 = C_{1s} \left| \frac{A}{4\pi} \right|^2 \frac{\alpha^2}{W_s^2} \Phi \left( \alpha^2, 2, \frac{C_{3s} + W_s}{W_s} \right) \quad (21)$$

where  $C_{3s} = \sqrt{\frac{2W_i}{\lambda} \frac{\sqrt{3}}{0.74} h_1} + 0.5W_s + r_r + W_i$ .  $\Phi$  is the Hurwitz-Lerchi transcendent.

Until now it was assumed that the flanking building creating the source street canyon was very

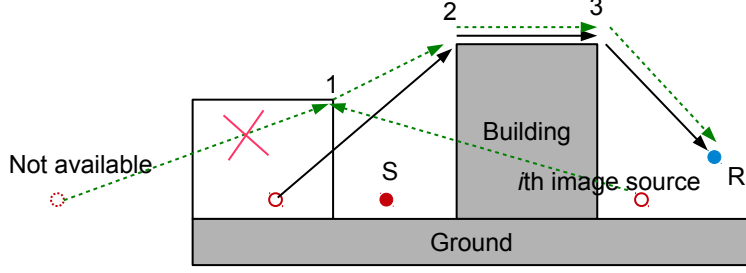


Figure 7: Demonstration of contributed image sources.

high so that all reflections were possible. However, when  $H_s < H_i$ , the sound emitting from some of the left image sources cannot contribute to the receiver and the contribution of the image sources from the right side start becoming stronger. The sound will need to diffract three times to reach the receiver and follows the route “image source  $\rightarrow 1 \rightarrow 2 \rightarrow 3 \rightarrow$ receiver” to reach the receiver position, as shown in figure 7.

After one more diffraction, the sound power decreases significantly, which can be accordingly ignored. When  $H_s$  is not much smaller than  $H_i$ , the sound from first few important images sources can still reach the receiver position by diffracted only twice and follow the routine “image source  $\rightarrow 2 \rightarrow 3 \rightarrow$ receiver”, as shown in figure 7. In this condition and neglecting high order diffraction, the total contribution of the image sources is approximated by:

$$\begin{aligned}
 \sum_{i=1}^N |p_{i,0}|^2 &= \sum_{i=1}^{\infty} |p_{i,0}|^2 - \sum_{i=N+1}^{\infty} |p_{i,0}|^2 \\
 &= C_{1s} \left| \frac{A}{4\pi} \right|^2 \frac{\alpha^2}{W_s^2} \Phi \left( \alpha^2, 2, \frac{C_{3s} + W_s}{W_s} \right) - C_{1s} \left| \frac{A}{4\pi} \right|^2 \frac{\alpha^{2(N+1)}}{W_s^2} \Phi \left( \alpha^2, 2, N + 1 + \frac{C_{3s}}{W_s} \right)
 \end{aligned} \tag{22}$$

where  $N$  is the number of images sources which can reach the receiver by only two diffraction. As expected, the higher  $H_s$  is the larger  $N$  is. When  $H_s = H_i$ ,  $N$  becomes infinite. The number of visible image sources,  $N$ , is the most important parameter to determine the difference between the level calculated using equation (22) and equation (21). Other parameters, such as  $W_s$ ,  $W_i$  and  $\lambda$  can still affect this level difference slightly. To avoid calculating  $N$  for every source position in the canyon,  $N$  is proposed to use the assumption that the source is in the middle of the canyon and categorize situations according to the ratio of  $(H_s - h_s)/(H_i - h_s)$ . The relation can be written as:  $H_s - h_s = \frac{2N-1}{2N+1}(H_i - h_s)$  for a source in the middle of the source canyon. Specifically, when  $N = [1, 2, 3, \dots]$  corresponds to the ratio  $(H_s - h_s)/(H_i - h_s) \leq [1/3, 3/5, 5/7, \dots]$ . When  $(H_s - h_s)/(H_i - h_s) \leq 1/3$ , no image sources are available from the left side and the canyon effect can be neglected, then  $L_{hs}$  is set to  $-\infty$ . When  $1/3 < (H_s - h_s)/(H_i - h_s) \leq 3/5$ , only the first image source from the left side can contribute and  $\sum |p_{i,0}|^2 = 10^{(-0.1A_{bar}^f)}$  with the “source position” being at the first image source; when  $3/5 < (H_s - h_s)/(H_i - h_s)$ , more than one image source from the left side are available, an approximation of the level difference between equation (22) and equation (21) is:  $L_{hs} = -6.17 \left( 1 - \frac{H_s - h_s}{H_i - h_s} \right) \left[ 1 - 1.37 \log_{10} \left( \frac{\sqrt{\lambda W_s}}{W_i} \right) \right]$  dB which is fitted on the condition of  $W_s \in$

[15, 100],  $W_i \in [20, 500]$ ,  $H_i = 18\text{m}$  and Frequency  $\in [60, 8000]\text{Hz}$ . When  $\frac{H_s - h_s}{H_i - h_s} > 1$ ,  $L_{hs} = 0$ .

When  $H_s > H_i$ , in most cases the important contribution comes from the sound from the image sources diffracting twice over the middle building. In some extreme cases, when  $H_s$  is high and  $H_i$  is low and narrow, sound could reach the receiver after only one reflection on the edge of the building of height  $H_s$ . This effect will contribute in the fitting but its importance is negligible in extracting the analytic form of the functions used for fitting. Without the numerical constant, the fitting formula for  $\sum_{i=1}^{\infty} |p_{i,0}|^2$  is:

$$\sum_{i=1}^{\infty} |p_{i,0}|^2 \approx F(1) \left[ C_{1s} \frac{\alpha^2}{W_s^2} \Phi \left( \alpha^2, 2, \frac{C_{3s} + W_s}{W_s} \right) 10^{0.1L_{hs}} \right] \quad \text{if} \quad \frac{3}{5} < \frac{H_s - h_s}{H_i - h_s} \leq 1 \quad (23)$$

where  $F(1)$  is a fitting coefficient. Similarly, the  $\sum_{j=1}^{\infty} |p_{0,j}|^2$  could also be obtained.

$$\sum_{j=1}^{\infty} |p_{0,j}|^2 \approx F(2) \left[ C_{1r} \frac{\beta^2}{W_r^2} \Phi \left( \beta^2, 2, \frac{C_{3r} + W_r}{W_r} \right) 10^{0.1L_{hr}} \right] \quad \text{if} \quad \frac{3}{5} < \frac{H_r - h_r}{H_i - h_r} \leq 1 \quad (24)$$

where  $F(2)$  is the fitting coefficient,  $\beta$  is the average reflection coefficient of the façade in the receiver canyon and other parameters are as follows:

$$\begin{aligned} L_{hr} &= -6.17 \left( 1 - \frac{H_r - h_r}{H_i - h_r} \right) \left[ 1 - 1.37 \log_{10} \left( \frac{\sqrt{\lambda W_r}}{W_i} \right) \right] \\ C_{1r} &\approx \left( \frac{0.37}{\sqrt{\frac{2r_s}{\lambda} \frac{\sqrt{3}}{2} \cos \phi_s} + 0.37} \right)^2 \\ C_{3r} &= \sqrt{\frac{2W_i}{\lambda} \frac{\sqrt{3}}{0.74}} h_2 + 0.5W_r + r_s + W_i \end{aligned}$$

Similarly, when  $\frac{H_r - h_r}{H_i - h_r} < 1/3$ , the canyon effect is neglected and  $L_{hr}$  is set to  $-\infty$ ; when  $1/3 < \frac{H_r - h_r}{H_i - h_r} < 3/5$ ,  $\sum_{j=1}^{\infty} |p_{0,j}|^2 = 10^{-0.1A_{bar}^f}$ . In a special case when  $H_i = h_r$ , the canyon effect is neglected as well.

To quantify the effect of the finite size of an object on the amount of the reflected acoustic energy, the envelope of the object and the Fresnel ellipsoid should be calculated. The source height of a vehicle is often set to 0.05m which implies that half of the section of the ellipsoids is below the building façade. If the ground is considered, its contribution can be treated as an image source. As a result, the Fresnel zone can only cause decay when the radius of the Fresnel ellipsoids is greater than  $H_s$  or  $H_i$ . If the radius  $\sqrt{\lambda D}/2 \leq H_s$ , the sound energy will be totally reflected, where  $D$  equals twice the distance of the image source which is  $D = 2(iW_s + 0.5W_s)$ . If  $H_s = 12\text{m}$  (corresponding to a 3-floors building),  $W_s = 15\text{m}$  (appears frequently in Gent), the Fresnel zone starts to cause decay after 10 and 112 reflection for  $\lambda = 3.4\text{m}$  (corresponding to 100Hz) and  $\lambda = 0.34\text{m}$  (corresponding to 1000Hz) respectively. It can be concluded that the decay speed is much less than the decay caused by the absorption of the façade. which decays by power function and the absorption starts to decay from the first reflection.

For the receiver canyon, it is difficult to make accurate estimation considering the receiver height is often at 4m. Suppose  $H_s = 10\text{m}$ ,  $H_i = 10\text{m}$ ,  $W_s = 12\text{m}$ , The decay starts from 2 for 100Hz and

20 for 1000Hz. Although the decay due to the Fresnel ellipsoid depends differently on the reflection area, it is decided to include its effect by increasing the average contribute of the façade.

### 3.2.4 Approximation of $\sum_{i=1}^{\infty} \sum_{j=1}^{\infty} |p_{i,j}|^2$

The double sum can be written as a sum of single sums for the source canyons for example. It is already known that the sum over all image sources results in the Hurwitz-Lerchi transcendent, but it is not possible to convert the sum over these special functions to a closed form. Then Hurwitz-Lerchi transcendent  $\Phi$  is approximated by  $G(\alpha, x) = K\alpha^2/x^2$ . In the region  $x \in (5, 20]$ ,  $\alpha \in [0.8, 1]$ , this approximation with  $K = 1.59$  results in a mean squared error of 0.0034, which is acceptable. Because the solution of every sum  $\sum_{i=j}^{\infty} |p_{i,j}|^2$  is similar as equation (21). As a result, the double sum can be generally written as:

$$\sum_{i=j}^{\infty} \sum_{i=1}^{\infty} |p_{i,j}|^2 = 10^{L_{hs}} \left| \frac{A}{4\pi} \right|^2 \sum_{j=1}^{\infty} C_{1s,j} \frac{\alpha^2 \beta^{2j}}{W_s^2} \Phi \left( \alpha^2, 2, \frac{C_{3s,j} + W_s}{W_s} \right) \quad (25)$$

where  $C_{3s,j} = \sqrt{\frac{2W_i}{\lambda} \frac{\sqrt{3}}{0.74}} h_1 + 0.5W_s + r_{r,j} + W_i$ . It should be mentioned that while deriving this equation, it was assumed that  $r_{s,i} \gg r_{r,j}$  which may not hold for high order receiver reflections. According to the approximation mentioned in this section, equation (25) changes to:

$$\sum_{i=j}^{\infty} \sum_{i=1}^{\infty} |p_{i,j}|^2 = 1.59\alpha^2 L_{hs} \left| \frac{A}{4\pi} \right|^2 \sum_{j=1}^{\infty} \left( \frac{0.37}{\sqrt{\frac{2r_{r,j}}{\lambda} \frac{\sqrt{3}}{2}} \cos \phi_{r,j} + 0.37} \right)^2 \left( \frac{1}{C_{3s,j} + W_s} \right)^2 \quad (26)$$

For high order image receivers,  $\left( \frac{0.37}{\sqrt{\frac{2r_{r,j}}{\lambda} \frac{\sqrt{3}}{2}} \cos \phi_{r,j} + 0.37} \right)^2 = \left( \frac{0.37}{3.31h_1/\sqrt{\lambda r_{r,j}} + 0.37} \right)^2 \rightarrow 1$ . As a result, the above equation approximates to:

$$\begin{aligned} \sum_{i=j}^{\infty} \sum_{i=1}^{\infty} |p_{i,j}|^2 &< 1.59\alpha^2 \left| \frac{A}{4\pi} \right|^2 \sum_{j=1}^{\infty} \left( \frac{1}{C_{3s,j} + W_s} \right)^2 \\ &= \left| \frac{A}{4\pi} \right|^2 1.59\alpha^2 \frac{\beta^2}{W_r^2} \Phi \left( \beta^2, 2, \frac{3.31h_1/\sqrt{\lambda} + 1.5W_s + W_i + 1.5W_r}{W_r} \right) \\ &\approx \left| \frac{A}{4\pi} \right|^2 \left( \frac{1.59\alpha\beta}{3.31h_1/\sqrt{\lambda} + 1.5W_s + W_i + 1.5W_r} \right)^2 \end{aligned} \quad (27)$$

The asymmetry is caused by the above assumption. If we calculate the double sum from the receiver canyon, a similar form could be achieved only replacing “ $h_1$ ” by “ $h_2$ ”. To moderate the assuming error, the average of the two calculations is used to approximate the double sum by:

$$\sum_{i=j}^{\infty} \sum_{i=1}^{\infty} |p_{i,j}|^2 \approx \left| \frac{A}{4\pi} \right|^2 \frac{(1.59\alpha\beta)^2}{(3.31h_1/\sqrt{\lambda} + 1.5W_s + W_i + 1.5W_r)(3.31h_2/\sqrt{\lambda} + 1.5W_s + W_i + 1.5W_r)} \quad (28)$$

### 3.2.5 Formulation of $A_{can}^f$

In the previous discussion, an analytic form for  $A_{can}^f$  is derived based on image source theory. By putting coefficients  $F(0)$ ,  $F(1)$ ,  $F(2)$  and  $F(3)$  to different contributing parts and approximating Hurwitz-Lerchi transcendent with  $K\alpha^2/x^2$ , the fitting formula is:

$$A_{can}^f \approx -F(0)10 \log_{10} \left( F(1) \frac{C_{1s}\alpha^2 R^2}{(C_{3s} + W_s)^2} 10^{0.1L_{hs}} + F(2) \frac{C_{1r}\beta^2 R^2}{(C_{3r} + W_r)^2} 10^{0.1L_{hr}} \right. \\ \left. + F(3) \frac{\alpha^2 \beta^2 R^2}{(3.31h_1/\sqrt{\lambda} + C)(3.31h_2/\sqrt{\lambda} + C)} 10^{0.1L_{hs}} 10^{0.1L_{hr}} \right) \quad (29)$$

where  $C = 1.5W_s + W_i + 1.5W_r$ , other parameters can be found in the previous sections.

The  $F(1)$  term expresses reverberate source canyon field diffracted into receiver canyon. As such  $1/\left(3.31h_1\sqrt{W_i/\lambda} + 1.5W_s + W_i + r_r\right)^2$  expresses mainly the amplification due to the source canyon reverberation. When  $W_i$  becomes very large, the whole  $F(1)$ ,  $F(2)$  and  $F(3)$  term will approach to  $F(1)C_{1s}\alpha^2 10^{0.1L_{hs}}$ ,  $F(2)C_{1r}\beta^2 10^{0.1L_{hr}}$  and  $F(2)\alpha^2\beta^2 10^{0.1L_{hs}} 10^{0.1L_{hr}}$ , which implies that the contribution of the source and receiver canyon becomes independent with each other and only related to the receiver or source canyon dimension. This is also verified by numerical simulation as shown in [15]. When  $W_s$  becomes very big, the source canyon effect will vanish and similar situation can be found for the receiver canyon when  $W_r$  becomes big. When  $h_2 \rightarrow 0$ ,  $L_{hr}$  becomes meaningless because of  $(H_r - h_r)/(H_i - h_r)$  tends to  $\infty$ . This condition implies that the receiver is at the same height as the top of the shielding building and the canyon effect can be neglected. As a result,  $F(2)$  term is set to zero. Since the source position is almost close to the ground in most cases,  $h_1$  is expected not tending to zero.

After fitting to our database (44766 observations) by equation (29) with  $\alpha = \beta = 0.97$ ,  $F(0) = 1.05$ ,  $F(1) = 12.46$ ,  $F(2) = 22.24$  and  $F(3) = 0.05$ . The standard deviation between  $A_{can,L}^f$  and the simulation is 2.8dB. When both  $H_s$  and  $H_r$  are very large,  $A_{can}^f$  tends to a constant.

The comparison between the fitted equation and several common cases calculated by full-wave method are shown in figure (8). Four typical configurations are compared, which have good agreement between the fitted equation and the simulations.

### 3.2.6 $A_{can,roof}$

When canyons are present, the sound reflects in the canyons and the  $A_{can,roof}$  can be considered as the extra attenuation of the sum of different  $A_{bar}^f$  with different powers and positions of image sources and receivers. However, the image sources could reach the receivers or image receivers by only one diffraction from the roof top which will significantly increase the sound power at the receiver positions, as show in figure (9). Additionally, this effect depends strongly on the geometrical configuration of the buildings and canyons which also differs significantly from one to another. In this study,  $A_{can,roof}$  is qualified by the literature [27] where a extensive set of roof shapes were studied and the general contribution of a gabled roof was around 5dB. In this paper,  $A_{can,roof} = 5\text{dB}$  if both source and receiver canyons exist;  $A_{can,roof} = 2.5\text{dB}$  if only one canyon exists.

Although there could be more than one building between source and receiver, the contribution of a single source propagating over one building is larger than the one propagating over several buildings.

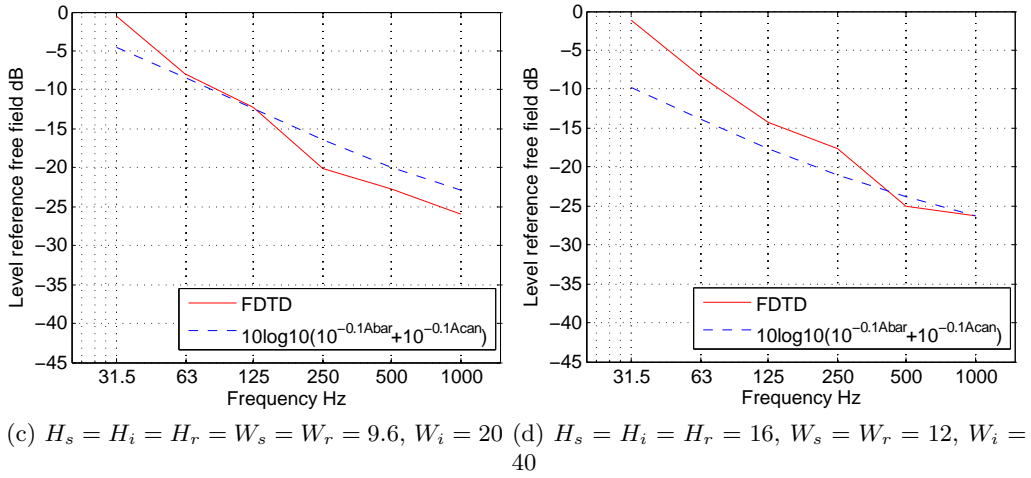
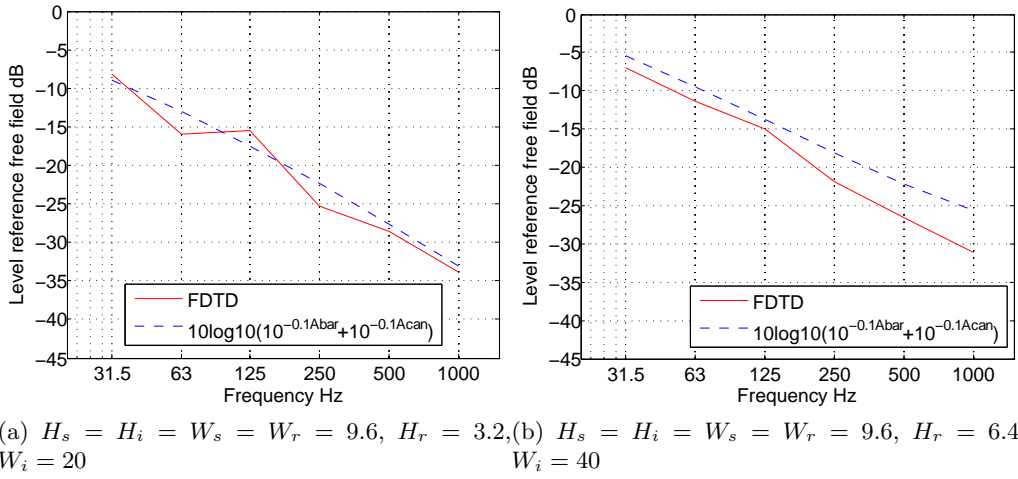


Figure 8: Comparison between  $A_{diff}$  and FDTD simulations.

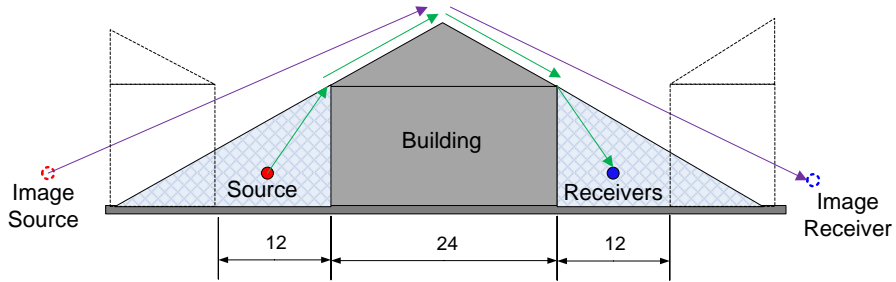


Figure 9: Effect of roof shape.

As a result,  $A_{bar, roof}$  and  $A_{can, roof}$  are considered as acceptable even they were discussed based on only one building existing between the source and receiver.

### 3.3 $A_{inter}$

The presence of intermediate canyons could lead to additional attenuation of sound. Since  $A_{can}$  is fitted based on only thick barrier simulations, an extra correction term,  $A_{inter}$ , is necessary. According to the FDTD simulations,  $A_{inter}$  will saturate after propagating approximately over 9 canyons (figure (10)). Similar findings were reported based on the measurement data from Soder in Stockholm [28]. In realistic cases, the heights of the buildings in successive canyons differ from each other, which could bring more variety than assuming the buildings have the same height. To quantify this effect some cases were simulated, as show in (figure (11)). In this figure, “H” indicates the height of the intermediate building-block equals to 9.6m; “L” indicates 6.4m; the combination of “H” and “L” indicates the positions of the building-blocks. For example “HLLHLH” means that the source propagates over → a higher building → two lower buildings → a higher building → a lower building → a higher building, then to the receiver. According to the simulations, the attenuations become smaller when the heights of the intermediate buildings decrease on the condition that the height of the buildings adjacent to the source and receiver do not change (solid lines in figure 11). However the situation becomes complicated when the heights of the buildings adjacent to the source or receiver decrease (dashed lines in figure 11). The attenuation decreases in low frequencies and increases in high frequencies. Both of these cases would cancel out in practice. The overall numerical average over the range of frequencies considered, relative to the equal-building simulation case “HHHHHH” is 1.1dB. As a result, the effect caused by the height difference is neglected in this model avoid unnecessary complexity. According to the geometrical data of Ghent Belgium and Soder Sweden [29], one canyon per 100 meters appears most frequently. Based on the calculations shown in figure 10, an attenuation of 1dB/100m could be an efficient but still reasonably accurate approach for  $A_{inter}$ . According to simulations,  $A_{inter}$  could accumulated to 10dB. However compare with rigid roofs, there is no attenuation for vegetated roofs. As a result, for canyon terrain in cities, the suggested broadband (and frequency independent) attenuation is 1 dB per 100 m, up to a maximum 5dB in this model.

## 4 Comparison with measurement

An inner city noise measurement network in Ghent (Belgium) with microphone nodes [30] placed at both shielded and directly exposed locations is used as a first validation of the current methodology. At these locations, road traffic noise was the main source of environmental noise exposure. The officially approved noise maps made for the agglomeration of Ghent in the framework of the Environmental Noise Directive were used as the basic noise map. The same traffic intensity and composition database (i.e. a combination of traffic counts and traffic flow modeling) as used for the END map was used for the background noise mapping calculations. The building coordinates and the heights are extracted from a GIS system. The mean height of the buildings in the calculation zone is 10.9m with std= 4.50. Measured data during 90 days lead to convergence of the energetically averaged  $L_{day}$  noise exposure indicator at all locations considered. All the sources up to 1500m from

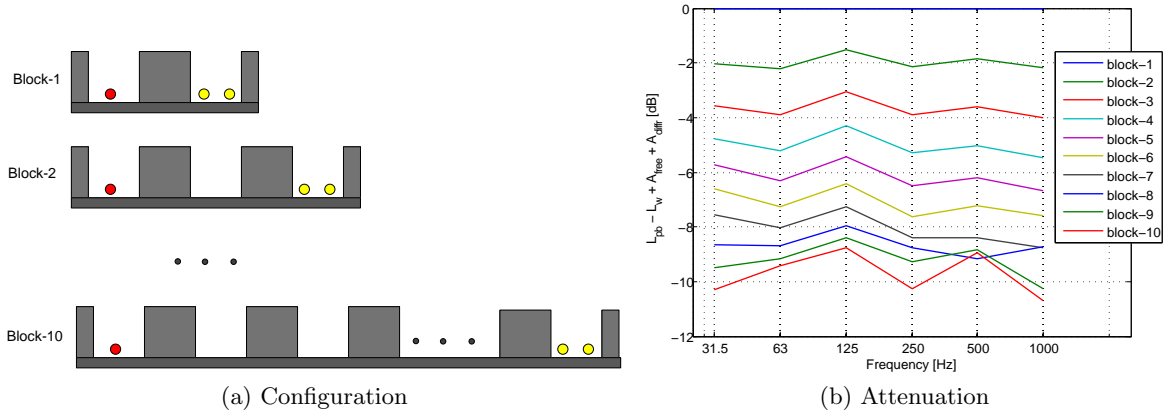


Figure 10: Attenuation caused by multiple intermediate buildings of equal height, with  $W_s = W_r = W_i = 10m, H_s = H_i = H_r = 9.6m$ .

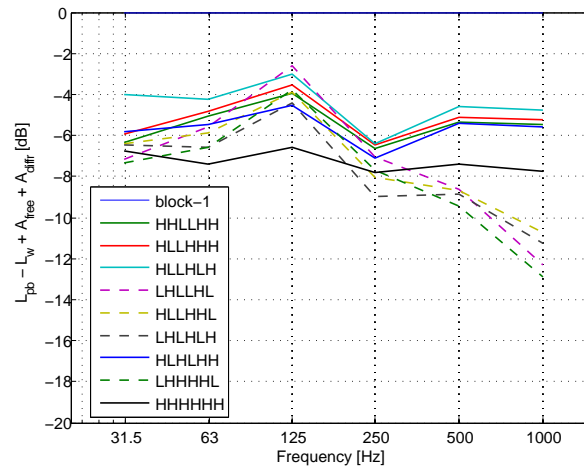


Figure 11: Intermediate canyon effect for different variations in the sequence of heights of intermediate buildings between source and receiver. See Fig. 10 for a description of Block-1. “HHHHH” is considered as the equal-building height reference

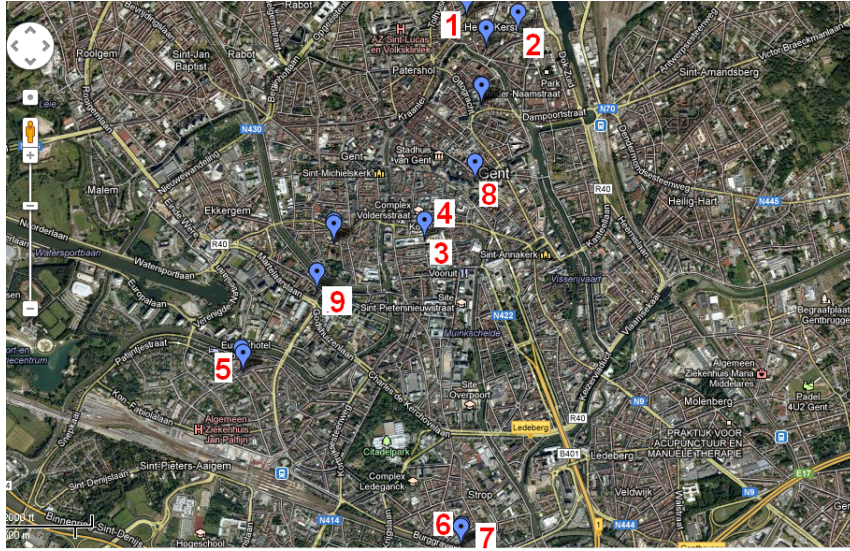


Figure 12: Measurement positions of Ghent city Belgium.

the receiver were considered. 9 measurement positions are available and their locations are shown in figure (12). The comparisons between the measurements and the END-reported noise levels, and the predicted levels based on the background noise mapping concept are shown in figure (13). Since the distance from the measurement microphones to the wall is in most cases less than 20cm, 3dB is subtracted from the measurement to remove the expected standing wave effect. Position 6, position 8, and position 9 are inside an enclosed yard and other positions are at the directly exposed façades. The spectrum of the totally shielded positions are shown in figure (14, 15, 16). The results show that the noise levels of  $L_{day}$  calculated by the END noise map are close to the measured levels in the directly exposed facades, but clearly underestimate levels at the shielded façades. In position 9, this difference can exceed 14dBA. At the most exposed façades the level of  $L_{day}$  mainly comes from the contribution of direct sound. At shielded locations, the  $A_{can}$  term improves the noise level in low frequencies very well, but it poorly predicts the high frequencies. As a result, adding a turbulent scattering contribution, by using the engineering model as described in detail in [12], further improves in modifying the spectrum properties can be observed. The poor underestimation in position 8 may be because of the insufficient estimation of the traffic flow. This position locates inside the city and almost far away from all the major roads. Although we have model to simulate the traffic flow in minor roads, it may still not considered quite well.

At the most exposed façades, some difference between the measurements and the calculated levels by the Environment Noise Directive could be attributed to e.g. inaccuracies in traffic data. Also the measurement error should be mentioned, which is expected to be below 2 dBA for road traffic dominated environmental noise exposure [30].

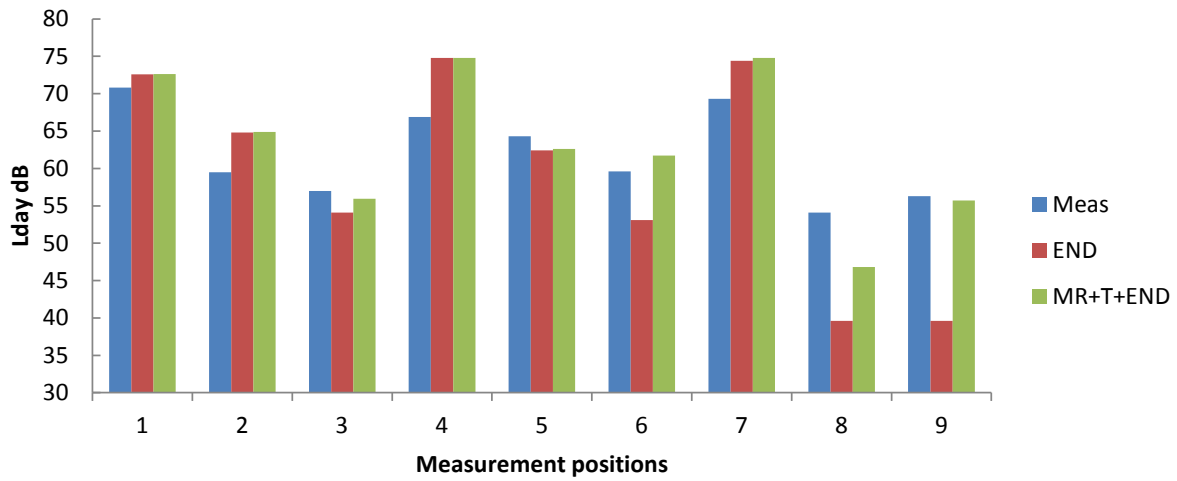


Figure 13: Comparison of predicted level and measurement. The legends “Meas” is the measurement value of  $L_{day}$ ; “END” is the  $L_{day}$  calculated by Environment Noise Directive of Europe; “MR+T+END” is the  $L_{pb}$  by adding the extra bonus by multiple reflections and the turbulence scattering model [12] to END.

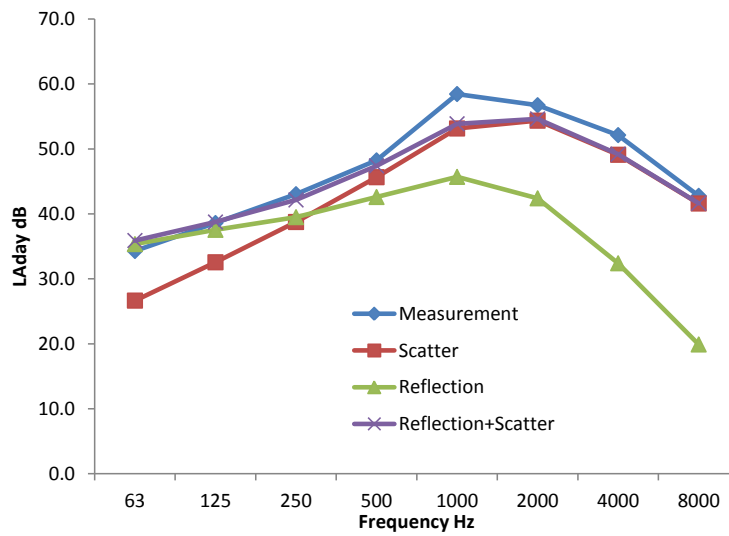


Figure 14: Spectrum of position 6. Legend “Scatter” is calculated by the model in [12]; “Reflection” is calculated by equation (2); “Reflection+Scatter” is calculated by equation (1).

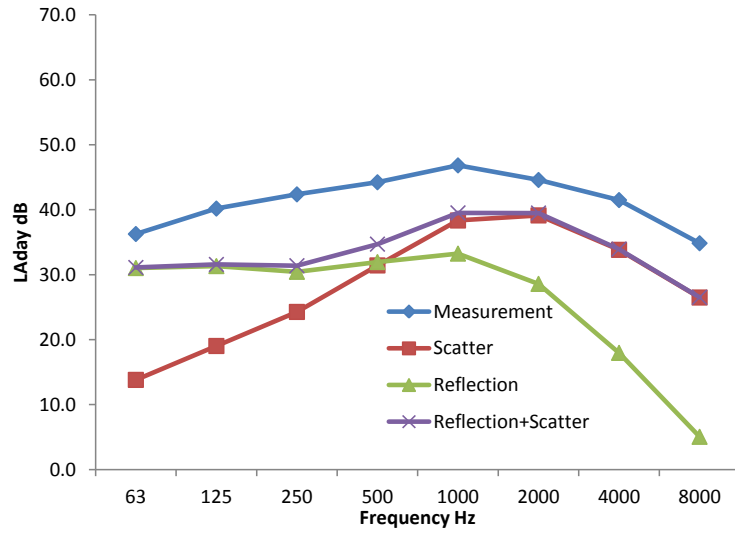


Figure 15: Spectrum of position 8.

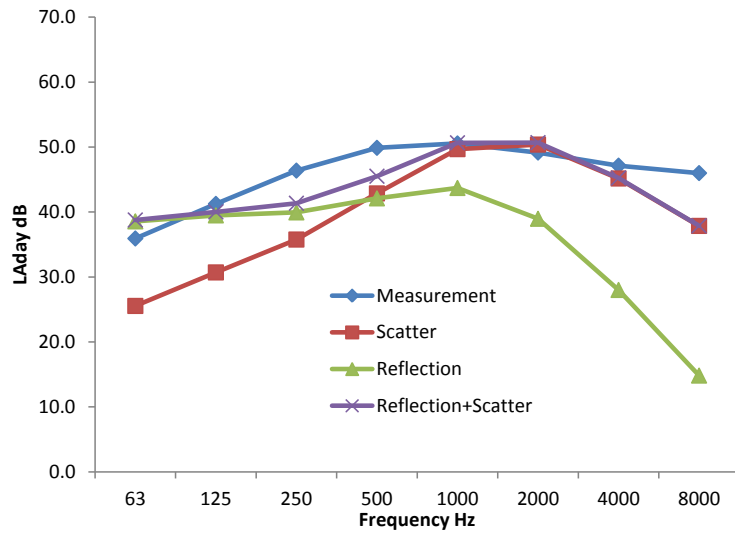


Figure 16: Spectrum of position 9.

## 5 Conclusions

An engineering model to improve predictions at shielded locations in an urban noise map is presented, based on a large set of 2-D full-wave numerical calculations of canyon to canyon propagation. The engineering model of background noise mapping proposed here can be used to correct existing noise maps with a poor prediction at shielded zones. In this model, different attenuation terms,  $A_{bar}$ ,  $A_{can}$ , and  $A_{inter}$  are quantified separately, which opens possibilities to add more correction terms, such as refraction by wind and temperature gradients and turbulent scattering [12]. Another advantage is that the inputs of the model are only geometrical parameters of the canyons, buildings, sources and receivers. Such parameters are easily derived from common GIS systems. A comparison between predicted levels and measurements shows that the model performs well in total  $L_{day}$  and the compatibility of the background noise mapping concept to existing noise maps is illustrated. Especially at shielded building facades, predictions are strongly improved.

## Acknowledge

We gratefully appreciate the financial support of Life+ program of the European Community (project QSIDE, LIFE09 ENV/NL/000423).

## References

- [1] E. Öhrström, A. Skånberg, H. Svensson, and A. Gidlöf-Gunnarsson. Effects of road traffic noise and the benefit of access to quietness. *J. Sound Vib.*, 295:40–59, 2005.
- [2] E. Öhrström. Psycho-social effects of traffic noise exposure. *J. Sound Vib.*, 151(3):513–517, 1991.
- [3] Yvonne de Kluzenaar, Erik M. Salomons, Sabine A. Janssen, Frank J. van Lenthe, Henk Vos, Han Zhou, Henk M. E. Miedema, and Johan P. Mackenbach. Urban road traffic noise and annoyance: The effect of a quiet facade. *J. Acoust. Soc. Am.*, 130(4):1936–1942, 2011.
- [4] Timothy Van Renterghem and Dick Botteldooren. Focused study on the quiet side effect in dwellings highly exposed to road traffic noise. *International Journal of Environmental Research and Public Health*, 9(12):4292–4310, November 2012.
- [5] The environmental noise directive: <http://ec.europa.eu/environment/noise/directive.htm>, October 2010.
- [6] Frits Van den Berg, Carlo Schoonebeek, and Menno Hillebregt. On the definitions of quiet faades and quiet urban areas. In *Proc. of Euronoise 2012, Prague, Prague, Czech*, August 2012.
- [7] Environmental noise and the crossoos-eu initiative, 2012.
- [8] Mikael Ögren and Jens Forssén. Modelling of a city canyon problem in a turbulent atmosphere using an equivalent sources approach. *Appl. Acoust.*, 65:629–642, 2004.
- [9] Maarten Hornikx and Jens Forssén. The 2.5-dimensional equivalent sources method for directly exposed and shielded urban canyons. *J. Acoust. Soc. Am.*, 122:2532–2541, 2007.

- [10] Timothy Van Renterghem and Dick Botteldooren. Prediction-step staggered-in-time fdtd: An efficient numerical scheme to solve the linearised equations of fluid dynamics in outdoor sound propagation. *Appl. Acoust.*, 68:201–216, 2007.
- [11] Dick Botteldooren. Finite-difference time-domain simulation of low-frequency room acoustic problems. *J. Acoust. Soc. Am.*, 98:3302–3308, 1995.
- [12] Jens Forssén, Maarten Hornikx, T. Van Renterghem, W. Wei, D. Botteldooren, and M. Ögren. Urban background noise mapping: the turbulence scattering model. *Manuscript in preparation for submission to Acta Acust. United Ac*, 2013.
- [13] Jérôme Defrance, Erik Salomons, Ingrid Noordhoek, Dietrich Heimann, Birger Plovsing, Greg Watts, Hans Jonasson, Xuetao Zhang, Eric Premat, Isabelle Schmich, François Aballea, Marine Baulac, and Foort de Roo. Outdoor sound propagation reference model developed in the european harmonoise project. *Acta Acust. Acust.*, 93:213–227, 2007.
- [14] Timothy Van Renterghem, Erik Salomons, and Dick Botteldooren. Parameter study of sound propagation between city canyons with coupled fdtd-pe model. *Appl. Acoust.*, 67(9):487–510, 2006.
- [15] Maarten Hornikx, Jens Forssén, T. Van Renterghem, D. Botteldooren, W. Wei, M. Ögren, and Erik Salomons. Urban background noise mapping: the multiple-reflection correction term. *Manuscript in preparation for submission to Acta Acust. United Ac*, 2013.
- [16] International Organization for Standardization. Iso 9613-2:1996 acoustics attenuation of sound during propagation outdoors - part 2. 1996.
- [17] Christopher Torrence and Gilbert P. Compo. A practical guide to wavelet analysis. *B. Am. Meteorol. Soc.*, 79:61–78, 1998.
- [18] Maarten Hornikx and Jens Forssén. A scalemodel study of parallel urban canyons. *Acta Acust. Acust.*, 94:265–281, 2008.
- [19] Timothy Van Renterghem, Erik Salomons, and Dick Botteldooren. Efficient fdtd-pe model for sound propagation in situations with complex obstacles and wind profiles. *Acta Acust. Acust.*, 91:671–679, 2005.
- [20] Kurt Heutschi. Calculation of reflections in an urban environment. *Acta Acust. Acust.*, 95:644–652, 2009.
- [21] Timothy Van Renterghem and Dick Botteldooren. Meteorological influence on sound propagation between adjacent city canyons: A real-life experiment. *J. Acoust. Soc. Am.*, 127(6):3335–3346, 2010.
- [22] Allan D. Pierce. Diffraction of sound around corners and over wide barriers. *J. Acoust. Soc. Am.*, 55(5):941–955, 1974.
- [23] Allan D. Pierce. *Acoustics: An Introduction to Its Physical Principles and Applications*. Acoustical Society of America, New York, USA, 1989.
- [24] T. Kawai. Sound diffraction by a many-sided barrier or pillar. *J. Sound Vib.*, 79(2):229–242, 1981.
- [25] Hyun-Sil Kim, Jae-Sueng Kim, Hyun-Ju Kang, Bong-Ki Kim, and Sang-Ryul Kim. Sound diffraction by multiple wedges and thin screens. *Applied Acoustics*, 66(9):1102–1119, September 2005.

- [26] N.N. Lebedev. *Special Functions and their Applications*. Dover Publications, Inc., 1972.
- [27] Timothy Van Renterghem and Dick Botteldooren. The importance of roof shape for road traffic noise shielding in the urban environment. *J. Sound Vib.*, 329(9):1422–1434, 2010.
- [28] Mikael Ögren and Jens Forssén. Road traffic noise propagation between two dimensional city canyons using an equivalent source approach. *Acta Acust. Acust.*, 90:293–300, 2004.
- [29] Pontus J. Thorsson, Mikael Ögren, and Wolfgang Kropp. Noise levels on the shielded side in cities using a flat city model. *Appl. Acoust.*, 65:313–323, 2004.
- [30] Timothy Van Renterghem, Pieter Thomas, Frederico Dominguez, Samuel Dauwe, Abdellah Touhafi, Bart Dhoedt, and Dick Botteldooren. On the ability of consumer electronics microphones for environmental noise monitoring. *Journal of environmental monitoring: JEM*, 13(3):544–552, March 2011. PMID: 21157618.



## Appendix C

This is the author's version of a manuscript submitted to Acta Acustica united with Acustica

# A model of sound scattering by atmospheric turbulence for use in noise mapping calculations

Jens Forssén<sup>1</sup>, Maarten Hornikx<sup>1,2</sup>, Dick Botteldooren<sup>3</sup>, Weigang Wei<sup>3</sup>,  
Timothy Van Renterghem<sup>3</sup> and Mikael Ögren<sup>4</sup>

<sup>1</sup>*Department of Civil and Environmental Engineering, Division of Applied Acoustics,  
Chalmers University of Technology, SE-41296 Göteborg, Sweden.*

<sup>2</sup>*Building Physics and Services, Eindhoven University of Technology, Eindhoven, the  
Netherlands*

<sup>3</sup>*Department of Information Technology, Ghent University, Ghent, Belgium*

<sup>4</sup>*Department of Environmental and Traffic Analysis, VTI, Gothenburg, Sweden*

---

---

## 1. Introduction

When acoustic shadow regions appear, creating areas with sound much weaker than the free field level, the sound scattering by turbulence grows in importance. The shadow regions of interest here are those caused by shielding objects such as buildings and other noise barriers. Acoustic shadows caused by upward refraction are similarly affected but not focus of the current study. The turbulence of the atmospheric surface layer has previously been shown to increase the noise level behind barriers, mainly at higher sound frequencies (e.g. [1]). In first estimates, the turbulent flow actually caused by a noise barrier itself, has been shown to lead to less significant scattering [2]. Previous studies have shown that models using energy based single scattering approximations are well applicable to the problem (e.g. [3, 4]). Even though a higher precision is expected by using wave-based models, as the parabolic equation method (e.g. [5]), the finite-difference time-domain method (e.g. [7]) or the equivalent sources method [8], the single scattering approximation is concluded to be accurate enough to serve as basis for an engineering model; in addition, having large benefits in computational cost. The scattering model developed in [4], based on theory known from literature (e.g. [9, 10, 11]), has been used, in simplified forms, in engineering models for noise mapping purpose [12, 13]. In the present paper the aim is to present an engineering model that is more generally applicable, i.e. for a single screen

*August 19, 2013*

on ground as well as for more built up areas with street canyons and inner yards. Below, we describe the underlying scattering cross section model, the development of a numerically efficient model for non-canyon situations, a parameter study for canyon situations and the suggested engineering model for general urban situations, followed by conclusions.

## 2. Model development

### 2.1. Underlying scattering cross section model

Using the scattering cross section by Tatarskii [9], Daigle [3] created a model for the total scattering into the shadow region created by a noise barrier, as briefly described here for convenience. The scattered intensity, or here rather the mean square acoustic pressure,  $\tilde{p}^2$ , can be written as an integral over a volume  $V$ , as

$$\tilde{p}^2 = \int_V \tilde{p}_0^2 \frac{\sigma(\theta)}{r^2} dV, \quad (1)$$

where  $p_0$  is the incoming, undisturbed pressure from the source,  $\sigma(\theta)$  the scattering cross section as a function of the scattering angle  $\theta$ , and  $r$  the distance from the point in volume  $V$  to the receiver, where  $V$  is defined as all points above the lines of sight from both the source and the receiver to the barrier top (see [3] for further details). Ostashev describes the derivation of the scattering cross section as well as different turbulence models [11]. For the work made here, an isotropic von Kármán turbulence model has been used as a starting point. Within the inertial range of the turbulence, the scattering cross section is identical to the one for the more simplified Kolmogorov model, which can be written

$$\sigma(\theta) = Ak^{1/3} \frac{\cos^2 \theta}{\sin(\theta/2)^{11/3}} \left( \frac{C_v^2}{c_0^2} \cos^2 \frac{\theta}{2} + 0.14 \frac{C_T^2}{T_0^2} \right), \quad (2)$$

where  $A = 0.0330$ ,  $k$  is the acoustic wave-number ( $k = 2\pi f/c_0$ , with  $f$  the sound frequency and  $c_0$  the mean sound speed),  $C_v$  and  $C_T$  the structure parameters of velocity and temperature fluctuations, respectively, describing their partial turbulence strengths, and  $T_0$  the mean temperature in Kelvin.

## 2.2. Development of a turbulence scattering model for non-canyon situations

Inherent in the above described modelling is the assumption of a single scattering approximation. In an improved model the incoming pressure,  $\tilde{p}_0$ , in Eq. (1), would be altered due to multiple scattering as well as due to the barrier diffraction. A first order correction for multiple scattering would be to remove intensity from the incoming field according to that already lost due to scattering by volume elements closer to the source. Here, however, a slightly different approach has been taken, where the scattering is limited by a saturation determined by an assumed smallest value of turbulence strength, as further described below. In addition, for use in a noise mapping model, the scattering should be limited so that scattered plus diffracted intensity does not exceed that of the open field, i.e. without barrier.

To reduce the numerical cost for evaluating the integral of Eq. (1), the integration is made analytically for constant  $\theta$ -values, i.e. in the azimuthal direction to the source–receiver line, as described previously [14]. Furthermore, since the integrand is a relatively slow-varying function of space, not a very fine discretization is needed. Here a grid spacing of 1 m has been used, and the height and length of the integration domain is limited to about the size of the source–receiver distance.

It is evident from Eqs. (1-2) that, if the two terms corresponding to temperature and velocity fluctuations are kept separate, the integrals can be calculated for a given geometry, and the dependence on the factors  $k^{1/3}$ ,  $C_v^2$  and  $C_T^2$  can be inferred later.

Since the used scattering model is based on a single scattering approximation, a saturation of the scattering is modelled. This is done by multiplying the scattered energy by  $\exp(-2xk^2J_{\text{vonK}})$ , where  $x$  is the horizontal range of propagation and  $J_{\text{vonK}} = 10^{-8}$  m. Here,  $k^2J_{\text{vonK}}$  is the total extinction coefficient according to the von Kármán model, and the value of  $J_{\text{vonK}}$  has been estimated from assuming a rather small outer length scale of  $L_0 = 10$  m and small values of the structure parameters, such that  $C_v^2/c_0^2$  and  $C_T^2/T_0^2$  approximately equals  $10^{-8} \text{ m}^{-2/3}$  in the expression

$$J_{\text{vonK}} = \frac{3}{10}\pi^2 AK_0^{-5/3} \left( 4\frac{C_v^2}{c_0^2} + \frac{C_T^2}{T_0^2} \right), \quad (3)$$

where  $K_0 = 2\pi/L_0$  [11].

Furthermore, the effect of air attenuation is taken into account, with a level reduction in proportion to the horizontal range,  $x$ , using standardized

attenuation rates <sup>1</sup>. The effects of varying the sound frequency and the strengths of temperature and velocity turbulence as well as modelling the air attenuation and the scattering saturation are studied at a later stage. First, the total scattered level is estimated, relative to free field, for a set of geometries and for unit turbulence strengths ( $C_v^2 = 1 \text{ m}^{4/3}/\text{s}^2$  respectively  $C_T^2 = 1 \text{ K}^2/\text{m}^{2/3}$ ). In the set of geometries, the screen height,  $h$ , is varied in  $M = 20$  logarithmic steps from 4 to 80 m. The distances to the screen, from the source,  $d_S$ , as well as from the receiver,  $d_R$ , are each varied in  $N = 25$  logarithmic steps from 10 to 500 m. Thereby a dataset of  $M \times N \times N = 12500$  cases is created (the actual number of calculations is 6500 since only the upper triangle of each  $N \times N$  matrix needs to be calculated, due to symmetry).

For each source–screen distance, a planar fit is made to the scattered level as function of the  $M \times N$  points of varying screen height and screen–receiver distance (in log coordinates). Since a plane can be described by a  $3 \times 1$  vector of coefficients, these vectors are computed and stored for each of the  $N$  planes of source–screen distances. Their values are appended in Tables A.3 and A.4, for velocity and temperature turbulence, respectively, where the geometric variables have been normalized by  $d_S$ , which turns out to be preferable for later use. When the result for a new geometry is to be calculated, an interpolation between the set of vectors can be made for the wanted source–screen distance, and the found  $3 \times 1$  vector of plane coefficients can be used to estimate the scattered level for the wanted screen height and screen–receiver distance. If the source and the receiver are not on the same height, the input geometry to the model is first rotated. (The geometry is shown in Fig. 1.) An example estimate of scattered levels were calculated assuming a source–screen distance of  $d_S = 40$  m. The interpolation then uses values at  $d_S = 36.8$  and  $43.4$  m, which are the two nearest  $d_S$  values used in the precalculation of the data set. The results are compared with those of a direct calculation for  $d_S = 40$  m, as shown in Figs. 2-3. The maximum errors for these results are less than 3 dB for screen heights varying between 5 and 40 m, and screen–receiver distances varying between 10 and 100 m, for both velocity and temperature turbulence. The mean error is within  $\pm 0.2$  dB and the standard deviation of the error (i.e. the standard error) is about 1 dB. Hence, the model based on this precalculated dataset can be used for

---

<sup>1</sup>Applying values from ISO 9613, part 1, for standard atmospheric conditions with a relative humidity of 70 %, a temperature of 20° C and a static pressure of 101325 Pa.

calculating the amount of turbulence scattering in non-canyon cases, i.e. with a single obstacle (a building or other noise barrier) and no further reflecting façades.

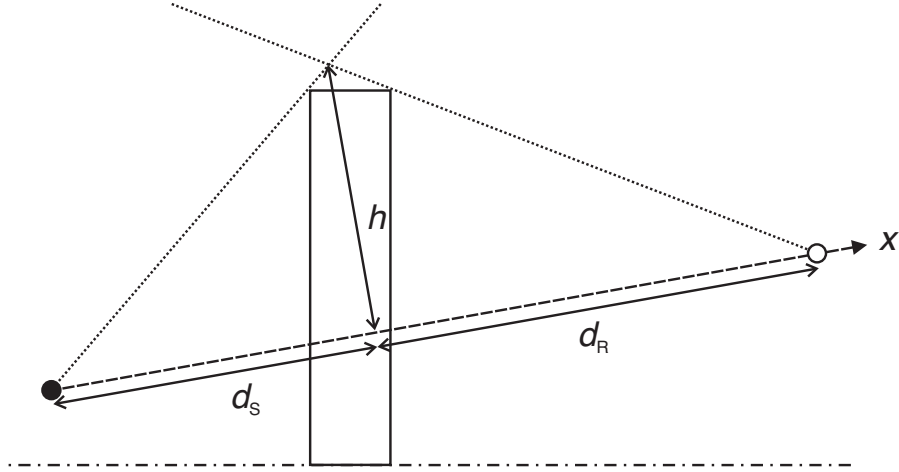


Figure 1: Geometric set-up for single noise barrier.

### 2.3. Parameter study for urban canyon situations

For the canyon situations, flat roofs have been assumed and the default cases have equal roof height. Looking at Fig. 4, where the geometric parameters are explained, the default double canyon cases have  $H_S = H_R = H_I$ , whereas for single canyon cases either  $H_S$  or  $H_R$  is zero, and for cases without canyon, both  $H_S$  and  $H_R$  are zero. In the parameter study, geometric parameters and the sound frequency were varied. The number of parameters, their range of values and other input data are shown in Table 1.

Entirely, the set of calculations consisted of 225792 separate cases, including the 8 frequencies. To calculate the scattered level, relative to free field, for each case, the scattering is added energy wise for the different reflection orders. Reflection order zero means that the sound has not been reflected in any façade; reflection order one means one façade reflection, in either source or receiver canyon; etc. The reflections are reduced by assuming an energy absorption coefficient of the façades of  $\alpha = 0.2$ , independent of frequency. An additional cause for energy reduction at reflection is modelled by a Fresnel number criterion, which reduces the reflections that are sufficiently close to the edge between façade and roof. For this model, the Nord2000

Table 1: Input data to parameter study of turbulence scattering for urban canyon situations. The geometric parameters are explained in Fig. 4. The last five parameters are the maximum reflection order,  $M$ , the façade's energy absorption coefficient,  $\alpha$ , the sound speed,  $c_0$ , the octave band centre frequencies,  $f$ , and the air attenuation,  $\beta$ .

$H_I$	=	5	10	20	40					[m]
$H_S, H_R$	=	0	$H_I$							[m]
$W_I$	=	.1	1	10	20	40	200			[m]
$W_S, W_R$	=	5	10	20	40	80	160	320		[m]
$x_S$	=	$.5W_S$								[m]
$x_R$	=	$.05W_R$	$.5W_R$	$.95W_R$						[m]
$y_S$	=	.5								[m]
$y_R$	=	1.5								[m]
$M$	=	15								[-]
$\alpha$	=	.2								[-]
$c_0$	=	340								[m/s]
$f$	=	31.5	63	125	250	500	1k	2k	4k	[Hz]
$\beta$	=	.023	.090	.34	1.1	2.8	5.0	9.0	23	[dB/km]

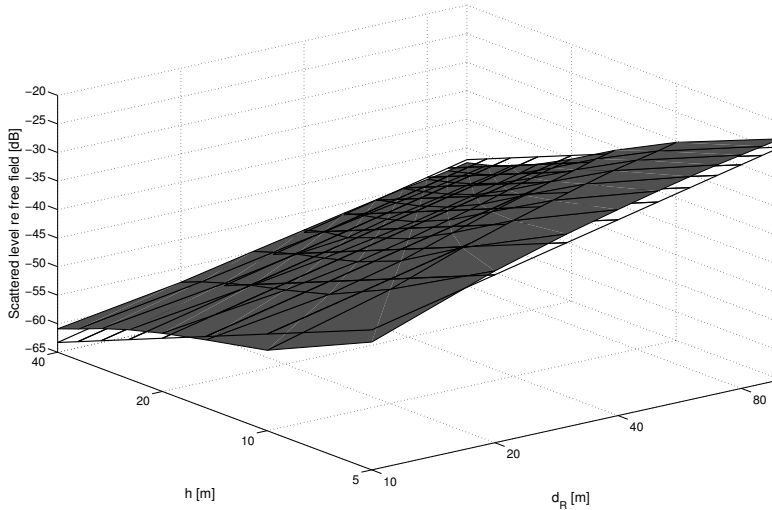


Figure 2: Comparison between originally calculated results (grayscale surface) and the best fit plane (black grid) for  $f_0 = 1000$  Hz,  $C_v^2 = 1 \text{ m}^4/\text{s}^2$  and  $C_T^2 = 0$ .

methodology for vertical surfaces has been used [12, Section 5.20], except an adaptation to an energy scattering based model (by using  $10 \log_{10}(S)$  instead of  $20 \log_{10}(S)$ , where  $S$  is the effective surface within the Fresnel-zone). Also air attenuation and scattering saturation are included, as described above for the non-canyon situations. The effect of ground is modelled as a doubling of energy both at the source side and at the receiver side. The used receiver height is  $y_R = 1.5$  m and can be seen as an approximation also for a receiver at 4 m height. In the calculations, reflections up to order  $M = 15$  were used, which, for these settings, was shown by numerical tests to give converging results.

#### 2.4. Engineering turbulence scattering model for general urban situations

For the engineering models, the results from the parameter study are first energy averaged over the three horizontally separated receiver positions. One quarter of the cases are for no canyon. It turns out that these 18816 cases are well approximated by a linear fit of variables  $\log_{10} \frac{h}{d_0}$  and  $\log_{10} \frac{d_S d_R}{h^2}$ , in addition to  $\frac{10}{3} \log_{10} \frac{f}{f_0}$ , where  $d_0 = 10$  m and  $f_0 = 1000$  Hz have been used and where the geometrical distances now are interpreted as the effective distances

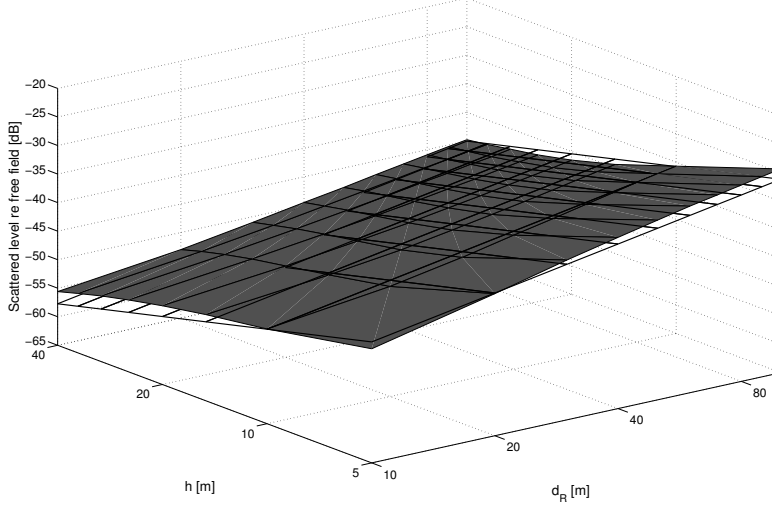


Figure 3: Comparison between originally calculated results (grayscale surface) and the best fit plane (black grid) for  $f = 1000$  Hz,  $C_v^2 = 0$  and  $C_T^2 = 1 \text{ K}^2/\text{m}^{2/3}$ .

from the source to the mid receiver position over a thin screen as depicted in Figure 1. The resulting model can be written as follows.

$$L_{p, \text{scat, no canyon}} = b_1 + b_2 \log_{10} \frac{h}{d_0} + b_3 \log_{10} \left( \frac{h^2}{d_S d_R} + \epsilon \right) + \frac{10}{3} \log_{10} \frac{f}{f_0} \text{ dB}, \quad (4)$$

where the values of  $b_i$  ( $i = 1, 2, 3$ ) are given in Table 2 and where  $\epsilon$  is inserted, with a value of 0.0012, in order to make the scattering saturate outside the boundaries of the parameter study, i.e.  $d_S, d_R = 500$  m. The standard error of the model without canyons is about 2 dB for both velocity and temperature turbulence.

The derived model of the scattered level in the canyon case,  $L_{p, \text{scat, canyon}}$ , is given as a correction term to the level for the non-canyon case,  $L_{p, \text{scat, no canyon}}$ :

$$L_{p, \text{scat, canyon}} = L_{p, \text{scat, no canyon}} + \Delta L_\gamma. \quad (5)$$

The correction term  $\Delta L_\gamma$  is estimated as follows (with  $H_0 = 10$  m).

$$\Delta L_\gamma = \gamma_1 + \gamma_2 \log_{10} \frac{H_I}{H_0}, \quad (6)$$

$$\gamma_1 = \begin{cases} 7, & \text{if single canyon} \\ 14, & \text{if double canyon} \end{cases}, \quad (7)$$

$$\gamma_2 = \begin{cases} 2H_I/W_S, & \text{if single canyon, on source side} \\ 2H_I/W_R, & \text{if single canyon, on receiver side} \\ 2H_I(1/W_S + 1/W_R), & \text{if double canyon} \end{cases}. \quad (8)$$

Table 2: Linear fit coefficients for velocity and temperature turbulence.

	<i>Velocity turbulence</i>	<i>Temperature turbulence</i>
$b_1 =$	$-52.8 + 10 \log_{10} C_v^2$	$-49.6 + 10 \log_{10} C_T^2$
$b_2 =$	11.3	11.5
$b_3 =$	-17.1	-13.1

For the above model, the standard errors are about 6 dB, for both the velocity and temperature turbulence scattering. Even though further accuracy improvements of the model are possible, the balance between simplicity and accuracy is deemed appropriate for the purpose of engineering noise map calculation models.

For an intermediate height of  $H_s$  or  $H_r$ , i.e. between 0 and  $H_i$ , it is suggested that a linear interpolation of the level is used. Calculated results (not presented here) have shown that the scattered level is a monotonically increasing function with the height of  $H_s$  or  $H_r$ . The rate of increase is higher closer to  $H_i$ , whereby the linear interpolation corresponds to a conservative estimate in the sense of rather overestimating than underestimating the scattered level. Furthermore, as  $H_s$  or  $H_r$  approaches  $H_i$ , the level converges, whereby results for values of  $H_s$  or  $H_r$  larger than  $H_i$  can be taken as those at  $H_i$ .

Suggested starting values of the structure parameters for fairly strong turbulence are  $C_v^2 = 1.2 \text{ m}^{4/3}/\text{s}^2$  and  $C_T^2 = 0.4 \text{ K}^2/\text{m}^{2/3}$ . It should be emphasized that the underlying turbulence model assumes a finite value of the

outer length scale,  $L_0$ , i.e. in analogy with a von Kármán turbulence model, here chosen as  $L_0 = 10$  m. It could be noted that, in relation to typical values in literature, the values suggested here for the structure parameters are relatively large. The values are motivated by previous results [4], where measured values of the structure parameters in a setting with a thick noise barrier were used as input to scattering predictions of the sound field, which were compared with measured acoustic data. Furthermore, the relatively small value of the outer length scale used here is linked to a weaker total strength of the turbulence, considering e.g. the total scattering cross section. The suggested values are also in the same order as those found in a more recent study [15]. Also, to repeat, for a later use in a noise mapping model, the scattering should be limited so that the total level does not exceed that predicted for open field.

Furthermore, this model assumes a point source in a domain that varies only in two dimensions. Thereby it is suggested that a so-called 2.5D approach is used for sources further down the road, and the width of the intermediate building is taken as the length of the source–receiver line occupied by the building.

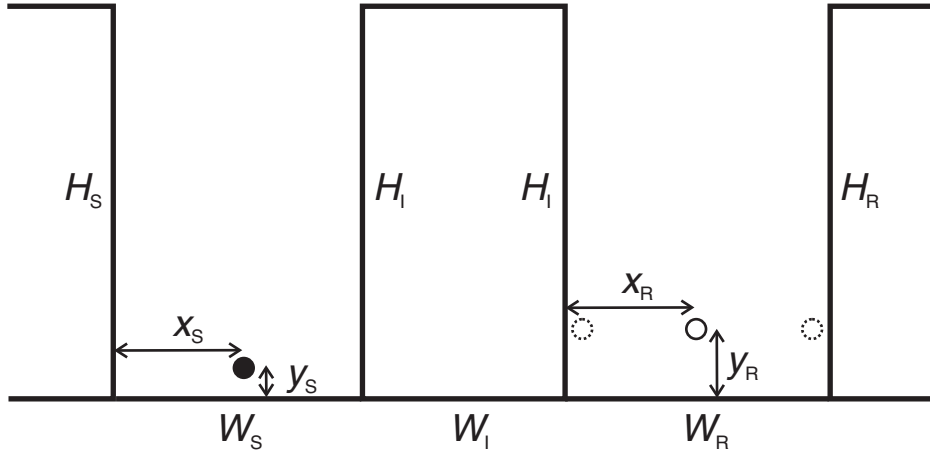


Figure 4: Geometric set-up for urban canyon situations.

### 3. Conclusion

A previously established turbulence scattering cross section model for a single noise screen has been used to develop an engineering model for a gen-

eral urban situation with the possibility to account for a street canyon and an inner yard. As an intermediate step, a numerically efficient model was developed, which was also made to account for multiple facade reflections, and then used for a parameter study. Using the results of the parameter study, the engineering model was developed with the aim to balance computational cost and accuracy. Studying the error for the case without canyons, the engineering model showed an overall standard error of about 2 dB in relation to the intermediate model, which in turn showed a standard error of about 1 dB in relation to the starting model. Hence, by assuming additivity of the variances, the total standard error can be estimated to less than 3 dB. With canyons the error increases further, up to about 6 dB.

#### 4. Acknowledgements

Part of this work was financially supported by the Life+ program of the European Community (project QSIDE, LIFE09 ENV/NL/000423).

#### References

- [1] Sound shielding in the presence of turbulence (Special issue). *Applied Acoustics*, Vol. 65, Issue 6, 2004, pp. 559-642.
- [2] Heimann, D. and Blumrich, R. Time-domain simulations of sound propagation through screen-induced turbulence. *Applied Acoustics*, Vol. 65, 2004, pp. 561-582.
- [3] Daigle GA. Diffraction of sound by a noise barrier in the presence of atmospheric turbulence. *J. Acoust. Soc. Am.* 1982, Vol. 71, pp. 847-54.
- [4] Forssén J. and Ögren, M. Barrier noise-reduction in the presence of atmospheric turbulence: Measurements and numerical modelling. *Applied Acoustics*, Vol. 63, 2002, pp. 173-187.
- [5] Gauvreau, B., Brengier, M., Blanc-Benon, Ph., and Depollier, C. Traffic noise prediction with the parabolic equation method: Validation of a split-step Pad approach in complex environments. *J. Acoust. Soc. Am.* 112, 2680 (2002).
- [6] Forssén J. Calculation of sound reduction by a screen in a turbulent atmosphere using the parabolic equation method. *Acustica-Acta Acustica* 1998, Vol. 84, pp. 599-606.

- [7] Van Renterghem, T., Salomons, E. and Botteldooren, D. Parameter study of sound propagation between city canyons with coupled FDTD-PE model. *Applied Acoustics*, 67 (6), p. 487-510, 2006.
- [8] Ögren, M. and Forssén J. Modelling of a city canyon problem in a turbulent atmosphere using an equivalent sources approach. *Applied Acoustics*, Vol. 65, 2004, pp. 629-642.
- [9] Tatarskii VI The effects of the turbulent atmosphere on wave propagation. Keter Press, Jerusalem, 1971.
- [10] Ishimaru, A. Wave propagation and scattering in random media. IEEE Press (and Oxford University Press, Oxford), New York, 1997.
- [11] Ostashev VE. Acoustics in moving inhomogeneous media. E & FN Spon (an imprint of Thomson Professional), London, 1997.
- [12] Plovsing B. Proposal for Nordtest Method: Nord2000 – Prediction of Outdoor Sound Propagation. Nordtest Proposal AV 1106/07. 2007, Hørsholm, Denmark: Delta.
- [13] van Maercke, D. and Defrance, J. Development of an Analytical Model for Outdoor Sound Propagation Within the Harmonoise Project *Acustica-Acta Acustica*, Vol. 93, 2007 , pp. 201-212.
- [14] Forssén J. Forssén, J. Influence of Atmospheric Turbulence on Sound Reduction by a Thin, Hard Screen: A Parameter Study Using the Sound Scattering Cross-Section. Proc. 8th Int. Symp. on Long-Range Sound Propagation, The Pennsylvania State University, USA, pp. 352-364 (1998).
- [15] T. Van Renterghem, W. Wei, J. Forssén, M. Hornikx, M. Ogren, D. Botteldooren, E. Salomons. Improving the accuracy of engineering models at shielded building facades : experimental analysis of turbulence scattering. Proceedings of the 42nd international congress and exposition on noise control engineering (Internoise 2013), Innsbruck, Austria.

## Appendix A. Tabulated coefficients used for parameter study

Table A.3: Values of coefficients to define the planes of scattered levels for a unit strength of velocity turbulence, i.e.  $C_v^2 = 1 \text{ m}^{4/3}/\text{s}^2$  and  $C_T^2 = 0$ , at  $f = 1000 \text{ Hz}$ , for varying values of the source–screen distance,  $d_S$ . The scattered level relative to free field is  $L_{p,\text{scat}} = a_1 + a_2 \log_{10}(d_R/d_S) + a_3 \log_{10}(h/d_S)$  dB, where  $d_R$  is the screen–receiver distance and  $h$  is the screen height. For intermediate values of  $d_S$ , interpolation is used.

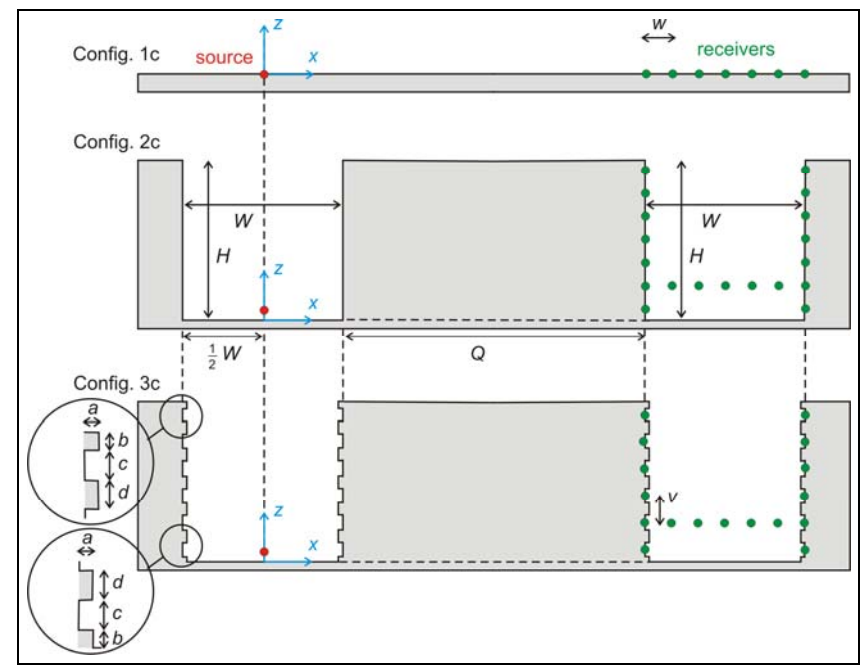
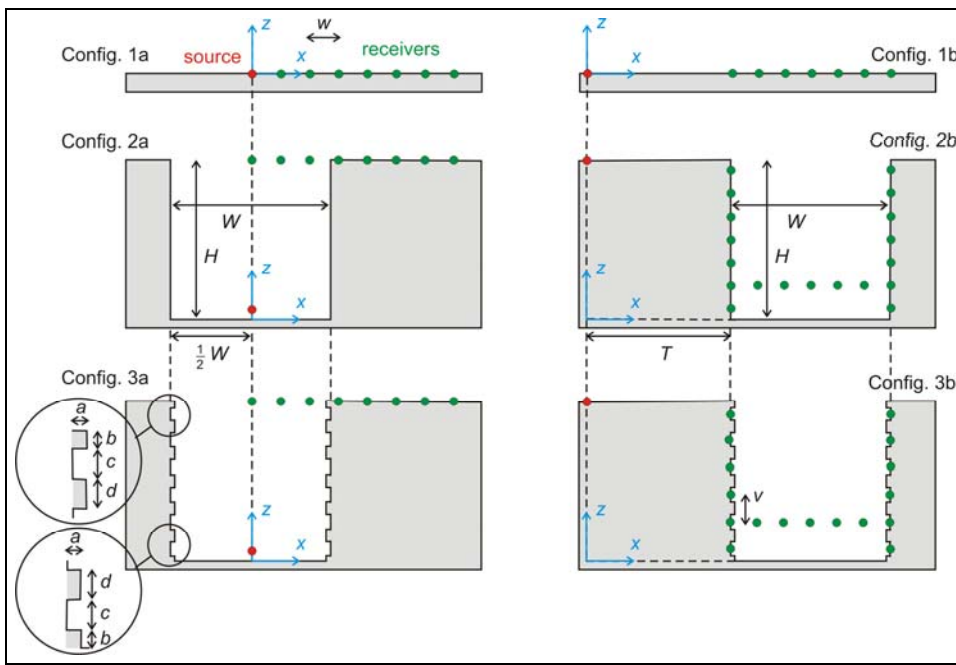
$d_S$ [m]	$a_1$ [dB]	$a_2$ [dB]	$a_3$ [dB]
10.0	-61.6	17.9	-19.5
11.8	-60.2	17.6	-20.5
13.9	-59.0	17.3	-21.4
16.3	-57.9	17.1	-22.4
19.2	-56.9	16.8	-23.2
22.6	-56.0	16.6	-23.9
26.6	-55.3	16.4	-24.5
31.3	-54.5	16.3	-24.9
36.8	-53.9	16.2	-25.2
43.4	-53.2	16.2	-25.3
51.0	-52.5	16.2	-25.3
60.1	-51.8	16.3	-25.2
70.7	-51.0	16.4	-25.0
83.2	-50.1	16.6	-24.7
98.0	-49.1	16.7	-24.3
115	-48.0	16.9	-23.8
136	-46.8	17.1	-23.3
160	-45.5	17.3	-22.7
188	-44.2	17.4	-22.2
221	-42.9	17.6	-21.7
261	-41.5	17.7	-21.2
307	-40.2	17.8	-20.7
361	-38.9	17.9	-20.3
425	-37.6	17.9	-19.9
500	-36.3	18.0	-19.5

Table A.4: Same as in Table A.3 except for a unit strength of temperature turbulence, i.e.  $C_T^2 = 1 \text{ K}^2/\text{m}^{2/3}$  and  $C_v^2 = 0$ .

$d_S$ [m]	$a_1$ [dB]	$a_2$ [dB]	$a_3$ [dB]
10.0	-58.3	14.9	-11.6
11.8	-57.1	14.5	-12.0
13.9	-56.0	14.2	-12.5
16.3	-54.9	13.9	-13.0
19.2	-53.8	13.6	-13.5
22.6	-52.9	13.3	-14.0
26.6	-52.0	13.1	-14.5
31.3	-51.2	12.9	-14.9
36.8	-50.5	12.8	-15.3
43.4	-49.7	12.6	-15.6
51.0	-49.1	12.6	-15.8
60.1	-48.4	12.5	-16.0
70.7	-47.7	12.5	-16.1
83.2	-47.0	12.5	-16.1
98.0	-46.2	12.5	-16.1
115	-45.4	12.6	-16.0
136	-44.6	12.6	-15.8
160	-43.6	12.7	-15.6
188	-42.7	12.8	-15.4
221	-41.7	12.8	-15.2
261	-40.6	12.9	-14.9
307	-39.6	12.9	-14.7
361	-38.5	13.0	-14.4
425	-37.4	13.0	-14.2
500	-36.4	13.0	-13.9



## Appendix D



We choose  $a = 0.16$ ,  $b = 0.64$ ,  $c = 1.92$ ,  $d = 1.28$ ,  $w = 1.6$ ,  $v = c + d = 3.2$  (all dimensions in meters).

We define  $x_m = mw$  and  $z_n = b + \frac{1}{2}c + nv = 1.5 + 3.2n$ , with  $m, n = (0), 1, 2, \dots$

Config	Source	Receivers
1a	(0,0)	$(x_m, 0)$
2a	$(0, z_s)$	$(x_m, H)$
3a	$(0, z_s)$	$(x_m, H)$

Config	Source	Receivers
1b	(0,0)	$(T + x_m, 0)$
2b	$(0, H)$	$(T + x_m, z_n)$
3b	$(0, H)$	$(T + x_m, z_n)$

Config	Source	Receivers
1c	(0,0)	$(\frac{1}{2}W + Q + x_m, 0)$
2c	$(0, z_s)$	$(\frac{1}{2}W + Q + x_m, z_n)$
3c	$(0, z_s)$	$(\frac{1}{2}W + Q + x_m, z_n)$

Source height  $z_s = 0.5$   
 Canyon dimensions  $H = 9.6$  and  $19.2$   
 $W/H = 0.5, 1, 2, 4, 8, 16, 32$   
 $T = 10$  and  $200$   
 $Q = 10$  and  $200$

Surface types Configs 1, 2: horizontal surfaces are rigid, vertical surfaces (facades) have  $Z = 10$ .

Config 3: idem, except façade segments with sizes  $a$ ,  $b$ , and  $d$  have  $Z = 10$ , and segments with size  $c$  (windows) have  $Z = 77$ .

Frequencies Four frequencies per 1/3-octave band:  $f_j = f_k 10^{j/80}$  with  $j = -3, -1, 1, 3$  and center frequencies  $f_k = 10^{k/10}$  with  $k = 14, \dots, 32$  (25 – 1600 Hz).

Source spectrum A-weighted sound power levels 63, 75, 87, 93, 97, 104 dB for six octave bands 32-1000Hz (for broadband analysis).

Air absorption Neglected.

Air parameters  $c = 340$  m/s,  $\rho = 1.2$  kg/m<sup>3</sup>.



## **Appendix E**

This is the author's version of a manuscript submitted to Internoise 2013, Innsbruck, Austria

# Improving the accuracy of engineering models at shielded building facades: experimental analysis of turbulence scattering

Timothy Van Renterghem<sup>1</sup>, Weigang Wei<sup>2</sup>, Jens Forssén<sup>3</sup>, Maarten Hornikx<sup>4</sup>, Mikael Ögren<sup>5</sup>, Dick Botteldooren<sup>6</sup>, Erik Salomons<sup>7</sup>

<sup>1,2,6</sup> Ghent University, Department of Information Technology, Sint-Pietersnieuwstraat 41, B-9000 Gent, Belgium

<sup>3,4</sup> Applied Acoustics, Chalmers University of Technology, Gothenburg, Sweden

<sup>4</sup> Building Physics and Services, Eindhoven University of Technology, P.O. box 513, 5600 MB Eindhoven, The Netherlands

<sup>5</sup> Department of Environmental and Traffic Analysis, VTI, Gothenburg, Sweden

<sup>7</sup> TNO Urban Environment and Health, Delft, The Netherlands

## ABSTRACT

Noise mapping models are able to accurately predict directly exposed facade levels near busy roads on condition that sufficiently detailed traffic data is available. At the non-directly exposed side of the building, however, common practice application of standard methods strongly underpredicts sound pressure levels, potentially leading to an incorrect assessment of noise annoyance and sleep disturbance. The concept of background noise mapping was proposed before, which has the important advantage that it can increase the accuracy of existing noise maps at a limited computational cost. In this study, long-term meteorological and noise data showed that turbulence scattering contributes significantly to the noise level at shielded facades, already at sound frequencies below 1 kHz. Periods with strong atmospheric turbulence are dominant for long-term equivalent noise levels as typically used in strategic noise maps. A comparison between predictions and measurements show that rather high turbulence strengths should be used when producing noise maps.

Keywords: urban sound propagation, quiet sides, atmospheric turbulence

## 1. INTRODUCTION

Preserving or promoting a quiet side near a dwelling helps to reduce noise annoyance and sleep disturbance in the urban environment. This was shown by small-scale and large-scale surveys in different countries [1][2][3]. The presence of the bedroom at the quiet facade was shown to be an important aspect, not only to reduce noise-induced sleep disturbance, but also to limit the self-reported noise annoyance at home in general [3].

While street-side predictions are typically reasonably accurate on condition that detailed traffic data is available, level estimates at shielded locations are usually problematic as shown with long-term measurements in Ref. [4]. The main reason is the need to fully consider the complex physics of sound propagation in street canyons like the multiple specular and diffuse reflections, in combination with diffraction over (complexly shaped) roofs. Although accurate calculation methodologies are available for such sound propagation problems, these cannot be directly used to produce noise maps due to the large computational cost. The concept of background noise mapping has been introduced in Ref. [4] to overcome this problem, allowing to correct levels at shielded facades “a posteriori”.

In addition, turbulence scattering of sound in the urban atmospheric boundary layer influences noise shielding to an important degree [5] and further complicates predictions. It was shown in Ref. [4] that by just relying on multiple reflections and diffractions, accurate predictions above roughly 1 kHz are not possible.

---

<sup>1</sup> timothy.van.renterghem@intec.ugent.be

<sup>2</sup> weigang.wei@intec.ugent.be

<sup>3</sup> jens.forssen@chalmers.se

<sup>4</sup> m.c.j.hornikx@tue.nl

<sup>5</sup> mikael.ogren@vti.se

<sup>6</sup> dick.botteldooren@intec.ugent.be

<sup>7</sup> erik.salomons@tno.nl

The main purpose of this paper is assessing the variability in the sound level measured at highly shielded locations in a dense urban setting, and to what degree this can be linked to meteorological data. The effect of atmospheric turbulence on long-term equivalent levels as commonly used in noise maps is studied as well.

## 2. DATA

### 2.1 Meteorological data

Wind speed, wind direction, relative humidity, rainfall intensity, air temperature, and atmospheric pressure were available as hourly averages from an inner city meteorological observation point above roof level. Direct solar irradiation (in  $\text{W}/\text{m}^2$ ) was available from a location near the city border.

### 2.2 Noise data

IDEA-noise nodes [6] measured 1-s equivalent sound pressure levels in 1/3-octave bands. The concept behind the IDEA-project is using (cheap) consumer-electronics microphones for environmental noise monitoring. It was shown by long-term outdoor testing that differences relative to type 1 reference equipment stay below 1-2 dBA for road traffic noise monitoring [6].

Focus in this paper is on a single location (see Figure 1) with simultaneous measurements at both the directly exposed and shielded building side. As the noise levels were gathered as part of a research project aiming at developing and testing the noise nodes and network aspects, there are missing periods.



Figure 1 – Areal photograph indicating the front (red dot) and back (green dot) facade noise nodes and surroundings.

## 3. TURBULENCE STRENGTH PREDICTION

The Harmonoise meteorological classification framework [7] has been used to estimate values of turbulence related parameters  $u^*$  (friction velocity),  $T^*$  (temperature scale) and  $1/L$  (inverse Monin-Obukhov length). Estimates of these are provided [7] based on common meteorological observations like wind speed, cloudiness, and time of the day. Cloudiness during daytime (in octas) was estimated based on solar insolation. The temperature and velocity structure constants ( $C_T^2$  and  $C_v^2$ ) are estimated following Ref. [8], although these formulas were not specifically designed to take into account the influence of the urban structure on atmospheric turbulence. The largest values predicted are  $C_v^2=1.00 \text{ m}^{4/3}/\text{s}^2$  and  $C_T^2=0.03 \text{ K}^2/\text{m}^{2/3}$ .

## 4. NOISE LEVEL VARIABILITY

In Figures 2 and 3, the measured hourly equivalent noise level distribution (during daytime, between 7 h and 19 h) is shown at the directly exposed and shielded facade. The data is split up in “weak” ( $C_v^2+C_T^2<0.1$ ) and “strong” ( $C_v^2+C_T^2>0.3$ ) turbulence by using the Harmonoise turbulence prediction framework as described in Section 3. Hours with rainfall were not retained in the dataset.

At the most exposed facade, a very similar distribution is observed under both atmospheric conditions. A small offset is observed between the two categories. No normalization has been performed for the variation in traffic intensity during the day, although the occurrence of weak and strong turbulence will typically depend on the time of the day. Similar distributions are found over the full frequency range.

At the shielded side, strong turbulence gives rise to a large variation in hourly equivalent sound pressure levels, and this variation increases with frequency. The difference in sound pressure level between the first and third quartile can be as large as 15 dB at 4 kHz under strong turbulence. At very low frequencies a similar distribution is found as at the front facade. The median of the noise levels under weak turbulence are clearly lower than at high turbulence, already at rather low sound frequencies.

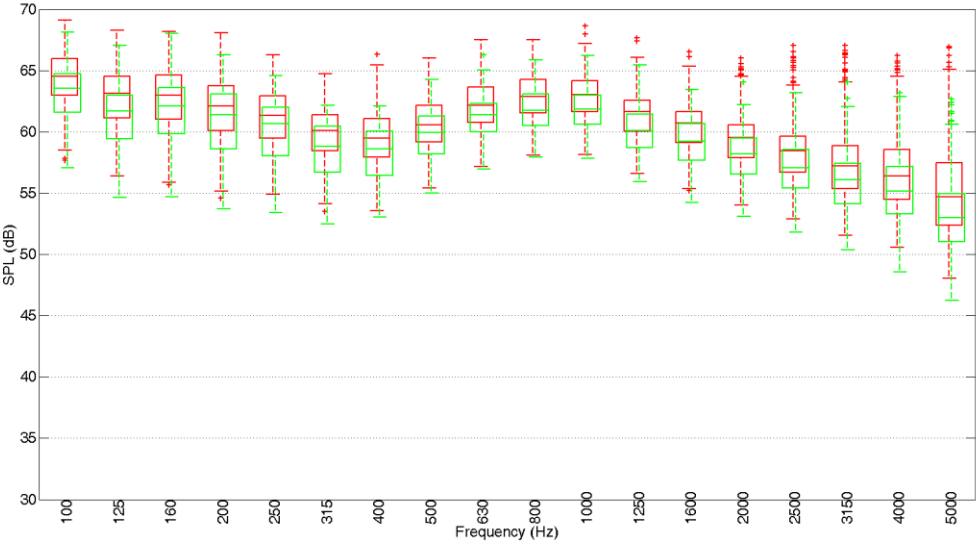


Figure 2 – Boxplots showing the (measured) level variation over time in 1/3-octave bands (hourly averaged, non-weighted, equivalent sound pressure levels) at the directly exposed facade. The distinction is made between weak turbulence (*green*) and strong turbulence (*red*). The (middle) horizontal line in the box indicates the median of the data. The box is closed by the first and third quartile. The whiskers extend to 1.5 times the interquartile distance above the maximum value inside the box, and to 1.5 times the interquartile distance below the minimum value inside the box. Data points that fall outside these limits are indicated with the plus-signs.

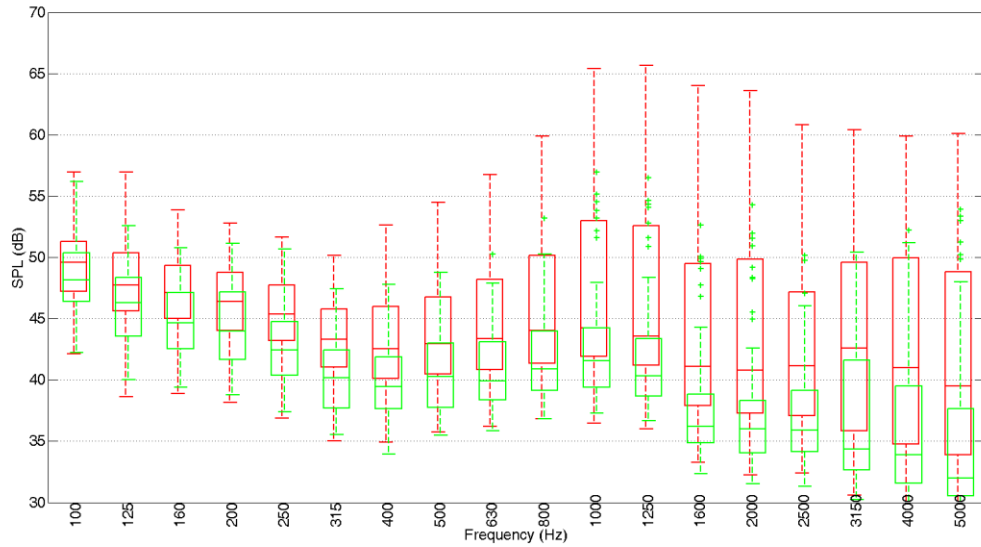


Figure 3 – See caption of Figure 2, but now for the shielded facade.

## 5. LONG-TERM NOISE LEVEL PREDICTION

Measured  $L_{day}$ , over the full period considered at hours where both noise and meteorological data were available, are depicted in Figure 4, averaged separately over weak and strong turbulence moments. Predictions with the background noise mapping model [4], applied to the location under study, are shown as well. The traffic data from the approved noise maps for the agglomeration of Ghent (following the Environmental Noise Directive 2002/49/EC) was used. Calculations are provided taking into account diffraction and multiple reflections between building facades [4], and a turbulence scattering engineering model [9] using the turbulence structure values close to the largest ones as estimated before in both the weak and strong turbulence class (see Section 3).

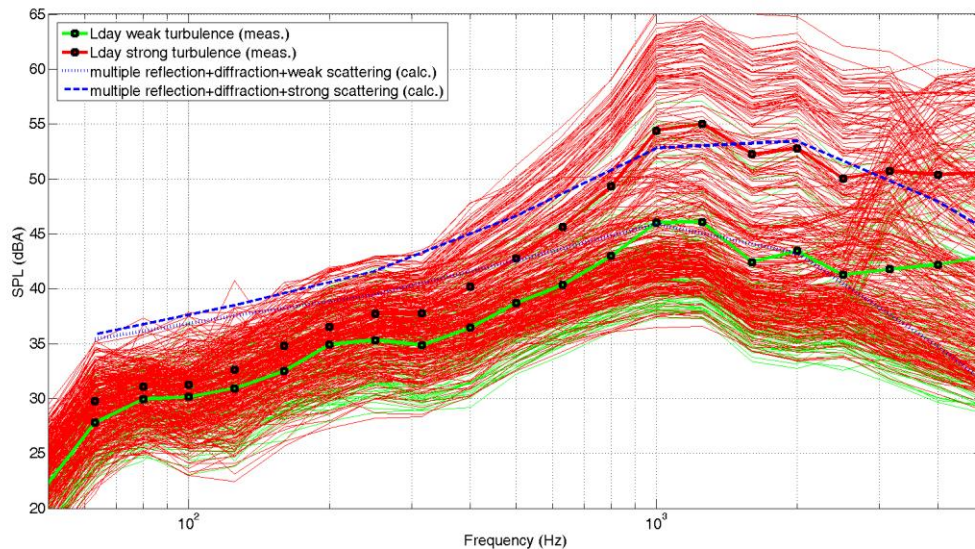


Figure 4 – Measured and calculated spectra at the shielded location. All hourly equivalent sound pressure level spectra are shown as well (thin green and red lines) that form the basis for the energetically averaged values  $L_{day}$ .

The measurements show that at low sound frequencies the difference between weak and strong turbulence is limited. Above 1 kHz, this difference can be near 10 dB for long-term equivalent noise levels. Turbulence scattering is therefore essential for accurate predictions at shielded locations in a city. The background noise mapping model shows good agreement near the maxima in the spectra. There is a tendency to overpredict the low frequency content at the current location.

Other sounds like e.g. the rustling of leaves might be present in the measurements at the shielded side, especially during moments of strong turbulence, often characterized by high wind speeds. In addition, there is a railway track parallel to the road at the front facade (see Figure 1) while the calculations only take into account road traffic noise sources.

Refraction by wind from the dominant road at the front facade is not expected due to the small distance relative to the microphone. However, long-distance refraction from other roads and highways could not be excluded, although specific wind directions could not be linked to increased or decreased sound levels at the current site.

## 6. CONCLUSIONS

Including turbulence scattering when predicting sound levels at shielded locations in a city showed to be essential. Atmospheric turbulence leads to a strong variation in (hourly) equivalent sound pressure levels, yielding both low and high values. Periods with strong turbulence scattering become dominant for long-term equivalent noise levels. In noise mapping efforts, reasonably high values for the turbulence strength are therefore needed.

## ACKNOWLEDGEMENT

The research leading to these results has received funding from the LIFE+ program of the European Community (project QSIDE, LIFE09 ENV/NL/000423).

## REFERENCES

- [1] E. Öhrström, A. Skånberg, H. Svensson, A. Gidlöf-Gunnarsson, "Effects of road traffic noise and the benefit of access to quietness," *Journal of Sound and Vibration*, 295, 40-59 (2006).
- [2] Y. de Kluizenaar, E. Salomons, S. Janssen, F. van Lenthe, H. Vos, H. Zhou, H. Miedema, J. Mackenbach, "Urban road traffic noise and annoyance: The effect of a quiet façade," *Journal of the Acoustical Society of America*, 130, 1936-1942 (2011).
- [3] T. Van Renterghem, D. Botteldooren, "Focused study on the quiet side effect at dwellings highly exposed by road traffic noise," *International Journal of Environmental Research and Public Health*, 9, 4292-4310 (2012).
- [4] W. Wei, T. Van Renterghem, D. Botteldooren, M. Hornikx, J. Forssén, E. Salomons, M. Ögren, "Urban background noise mapping: general model," *submitted to Acta Acustica united with Acustica* (2013).
- [5] J. Forssén, M. Ögren, "Thick barrier noise-reduction in the presence of atmospheric turbulence: measurements and numerical modelling," *Applied Acoustics*, 63, 173-187 (2002).
- [6] T. Van Renterghem, P. Thomas, F. Dominguez, S. Dauwe, A. Touhafi, B. Dhoedt, D. Botteldooren, "On the ability of consumer electronics microphones for environmental noise monitoring," *Journal of Environmental Monitoring*, 13, 544-552 (2011).
- [7] J. Defrance, E. Salomons, I. Noordhoek, D. Heimann, B. Plovsing, G. Watts, H. Jonasson, X. Zhang, E. Premat, I. Schmich, F. Aballea, M. Baulac, F. de Roo, "Outdoor sound propagation reference model developed in the European Harmonoise project," *Acta Acustica united with Acustica*, 93, 213-227 (2007).
- [8] K. Wilson, V. Ostashev, "A reexamination of acoustic scattering in the atmosphere using an improved model for the turbulence spectrum," *Technical report AD-A388573* (1998).
- [9] J. Forssén, M. Hornikx, D. Botteldooren, W. Wei, T. Van Renterghem, M. Ögren, "A model of sound scattering by atmospheric turbulence for use in noise mapping calculations," *in preparation for submission to Acta Acustica united with Acustica* (2013).